

1 Reconciling the total carbon budget for boreal forest wildfire emissions using airborne  
2 observations

3  
4 Katherine L. Hayden<sup>1\*</sup>, Shao-Meng Li<sup>2</sup>, John Liggio<sup>1</sup>, Michael J. Wheeler<sup>1</sup>, Jeremy J.B. Wentzell<sup>1</sup>, Amy  
5 Leithead<sup>1</sup>, Peter Brickell<sup>1</sup>, Richard L. Mittermeier<sup>1</sup>, Zachary Oldham<sup>1,6</sup>, Cris Mihele<sup>1</sup>, Ralf M. Staebler<sup>1</sup>,  
6 Samar G. Moussa<sup>1</sup>, Andrea Darlington<sup>1</sup>, Mengistu Wolde<sup>3</sup>, Daniel Thompson<sup>4</sup>, Jack Chen<sup>1</sup>, Debora  
7 Griffin<sup>1</sup>, Ellen Eckert<sup>1</sup>, Jenna C. Ditto<sup>5</sup>, Megan He<sup>5</sup> and Drew R. Gentner<sup>5</sup>

8 [1]{Air Quality Research Division, Environment Canada, Toronto, ON, Canada}  
9 [2]{College of Environmental Sciences and Engineering, Peking University, Beijing, China}  
10 [3]{National Research Council of Canada, Ottawa, ON, Canada}  
11 [4]{Canadian Forest Service, Natural Resources Canada, Edmonton, AB, Canada}  
12 [5]{Yale University, New Haven, CT, USA}  
13 [6]{University of Waterloo, Waterloo, ON, Canada}

14  
15 \*Correspondence to: Katherine Hayden (katherine.hayden@ec.gc.ca)  
16

17 **Abstract**

18 Wildfire impacts on air quality and climate are expected to be exacerbated by climate change with the  
19 most pronounced impacts in the boreal biome. Despite the large geographic coverage, there is ~~a lack~~  
20 ~~of~~limited information on boreal forest wildfire emissions, particularly for organic compounds, which are  
21 critical inputs for air quality model predictions of downwind impacts. In this study, airborne  
22 measurements of ~~193 250~~compounds from 15 instruments, including ~~173228~~ non-methane organics  
23 compounds (NMOG), were used to provide the most detailed characterization, to date, of boreal forest  
24 wildfire emissions. Highly speciated measurements showed a large diversity of chemical classes  
25 highlighting the complexity of emissions. Using measurements of the total NMOG carbon (NMOG<sub>T</sub>), the  
26 ΣNMOG was found to be ~~46.250±3~~ to ~~53±3~~ % of NMOG<sub>T</sub>, of which, the intermediate- and semi-volatile  
27 organic compounds (I/SVOCs) were estimated to account for ~~7.47~~ to ~~10~~ %. These estimates of I/SVOC  
28 emission factors expand the volatility range of NMOG typically reported. Despite extensive speciation, a  
29 substantial portion of NMOG<sub>T</sub> remained unidentified (~~46.447±15~~ to ~~50±15~~ %), with expected

30 contributions from more highly-functionalized VOCs and I/SVOCs. The emission factors derived in this  
31 study improve wildfire chemical speciation profiles and are especially relevant for air quality modelling  
32 of boreal forest wildfires. These aircraft-derived emission estimates were further linked with those  
33 derived from satellite observations demonstrating their combined value in assessing variability in  
34 modelled emissions. These results contribute to the verification and improvement of models that are  
35 essential for reliable predictions of near-source and downwind pollution resulting from boreal forest  
36 wildfires.

37

38

39

40

41

42

## 43 **1 Introduction**

44 Wildfires play a natural role in maintaining forest health and diversity through the release of  
45 nutrients, seed germination, removal of aging vegetation, and reducing the spread of forest diseases.  
46 Wildfires are, however, one of the largest global sources of trace gases and aerosols to the atmosphere  
47 (Andreae, 2019; Yu et al., 2019) and can have deleterious impacts on human health (Cascio, 2018; Cherry  
48 and Haynes, 2017; Reid et al., 2016; Finlay et al., 2012), air quality (Landis et al., 2018; Miller et al.,  
49 2011; Rogers et al., 2020), ecosystems (Kou-Giesbrecht et al., 2019; Campos et al., 2019; Kallenborn et  
50 al., 2012; Johnstone et al., 2010) and climate (Randerson et al., 2006). Not only can wildfire pollutants  
51 fumigate local source areas, they can be transported over long distances resulting in degraded air quality  
52 in locations far from fire sources (Miller et al., 2011; Rogers et al., 2020), and pose threats to downwind  
53 ecosystems through wet and dry deposition processes (Kou-Giesbrecht et al., 2019; Kallenborn et al.,  
54 2012; Campos et al., 2019).

55 The severity and frequency of wildfires is expected to increase in response to climate change  
56 (Bush and Lemmen, 2019; Seidl et al., 2017; Whitman et al., 2019) with evidence to suggest that ~~Wildfire~~  
57 ~~impacts on air quality and climate are expected to be exacerbated by climate change (Bush and Lemmen,~~  
58 ~~2019; Seidl et al., 2017; Whitman et al., 2019)~~ and such impacts are expected to be most pronounced in  
59 the boreal biome (Seidl et al., 2017; Whitman et al., 2019). The boreal forest zone is the most northerly  
60 of all forest biomes accounting for 1.2 billion ha of mostly coniferous forest and comprising about  
61 ~~3033~~ % of the global forest area, or ~~11-14~~ % of the earth's land surface ([https://www.nrcan.gc.ca/our-](https://www.nrcan.gc.ca/our-natural-resources/forests/sustainable-forest-management/boreal-forest/8-facts-about-canadas-boreal-forest/17394)  
62 [natural-resources/forests/sustainable-forest-management/boreal-forest/8-facts-about-canadas-boreal-](https://www.nrcan.gc.ca/our-natural-resources/forests/sustainable-forest-management/boreal-forest/8-facts-about-canadas-boreal-forest/17394)  
63 [forest/17394](https://www.nrcan.gc.ca/our-natural-resources/forests/sustainable-forest-management/boreal-forest/8-facts-about-canadas-boreal-forest/17394)). On a global basis, boreal forest wildfires are responsible for an estimated 20 % of yearly  
64 global biomass burning emissions (van der Werf et al., 2006). Canada's boreal forests account for  
65 ~~~2830~~ % of the global boreal zone area and encompasses 75 % of Canada's 347 million ha of forested  
66 land (Fig. S1) ([https://www.nrcan.gc.ca/our-natural-resources/forests/sustainable-forest-](https://www.nrcan.gc.ca/our-natural-resources/forests/sustainable-forest-management/boreal-forest/8-facts-about-canadas-boreal-forest/17394)  
67 [management/boreal-forest/8-facts-about-canadas-boreal-forest/17394](https://www.nrcan.gc.ca/our-natural-resources/forests/sustainable-forest-management/boreal-forest/8-facts-about-canadas-boreal-forest/17394)). In the past decade, Canada has

68 experienced unprecedented fire seasons, with large numbers of evacuations, major property damage, poor  
69 air quality and significant economic impacts (NRCan, 2018; Landis et al., 2018; McGee et al., 2015).  
70 Model predictions have suggested that Canadian fire occurrences will increase by 25 % by 2030 from a  
71 1975 to 1990 baseline scenario (Wotton et al., 2010).

72 To adequately assess and mitigate the risks of wildfire emissions to human and ecosystem health,  
73 reliable pollutant predictions are required which depend on accurate and detailed fire emissions data.

74 Such emissions data are developed by multiplying emission factors ~~and ratios~~ with the mass of biomass  
75 burned (Chen et al., 2019). In Canada, Environment and Climate Change Canada (ECCC) provides  
76 predictions of particulate matter (PM) (<2.5 µm in diameter) from wildfire smoke to the public using the  
77 FireWork modelling system that combines forecast meteorology, emissions inputs (e.g. emission factors),  
78 forest fire and fuel data (e.g. fuel maps, plume height parameterization), and a regional air quality model,  
79 GEM-MACH (details in Chen et al., 2019). FireWork is also used for air quality research studies with  
80 significantly more complex chemical mechanisms for emissions characterization and detailed physical  
81 processes. Wildfire field studies, as well as prescribed burns and laboratory work, have resulted in  
82 valuable global databases of fire emission factors covering a broad range of ecosystems and geographic  
83 areas (e.g. Andreae, 2019; Akagi et al., 2011), however, they are primarily concentrated on the temperate  
84 forests of the American mid-west and savannah/grasslands of Africa (e.g. Andreae 2019; Permar et al.,  
85 2021; Palm et al., 2020; Lindaas et al., 2020; Roberts et al., 2020; Juncosa-Calaharrano et al., 2021;  
86 Coggon et al., 2019; Koss et al., 2018; Hatch et al., 2017). ~~Until now, the most complete characterization~~  
87 ~~of boreal forest wildfire emissions in Canada was provided by Simpson et al. (2011) which relied on~~  
88 ~~whole air canisters with offline analysis for organic compounds. Due to a lack of limited comprehensive~~  
89 emission data specific for boreal wildfires, air quality models for northern regions face significant  
90 challenges resulting in uncertain predictions of emissions, exposure and associated impacts.

91 In the summer 2018, a research aircraft was deployed to measure emissions and subsequent  
92 transformation processes from ~~an active~~ boreal forest wildfire in western Canada (Fig. 1; Fig. S1). In this  
93 paper, ~~measurements of a comprehensive suite of detailed emissions information is provided from an~~

94 ~~active, near field boreal forest wildfire using a detailed measurement suite of over 200 gas- and particle-~~  
95 ~~phase compounds are used to. Emissions of highly speciated non-methane organic gases (NMOG) are~~  
96 ~~provide a detailed characterization of smoldering wildfire emissions. The highly speciated non-~~  
97 ~~methane organic gas (NMOG) measurements are described by broad chemical classes and across a range~~  
98 ~~of volatilities extending from VOCs to SVOCs. The wide range of measured Speciated-NMOGs, along~~  
99 ~~with concurrent total NMOG carbon (NMOG<sub>T</sub>) measurements, provides a unique opportunity to reconcile~~  
100 ~~the total carbon budget. Emission factors are derived for all-measured 193 compounds which represents~~  
101 ~~the most extensive chemical speciation of wildfire emissions to date, almost tripling the number of~~  
102 ~~reported values for the boreal forest ecosystem in the Andreae (2019) compilation paper. Emission~~  
103 ~~estimates are also combined resulting in more relevant emissions information for boreal forest wildfires~~  
104 ~~and improved emission quantification and chemical speciation representations in air quality models.~~  
105 ~~Combining aircraft derived emissions with those from satellite observations demonstrates usefulness to~~  
106 ~~evaluate modelled emissions-diurnal variability. The purpose of this work is to provide relevant The~~  
107 ~~emissions information for boreal forest wildfires to ultimately in this work will contribute towards~~  
108 ~~improved emissions quantification and chemical speciation representations in air quality models.~~  
109 ~~verification and improvements of models that are essential for reliable predictions of boreal forest~~  
110 ~~wildfires pollutants.~~

## 112 2 Methods

### 113 2.1 Aircraft measurements

114 The NRC's Convair-580 research aircraft was deployed on June 25, 2018 to sample a wildfire  
115 detected to the east of the Alberta/Saskatchewan border (56.4°N, 109.7°W) (Fig. 1). Measurements of a  
116 comprehensive suite of trace gases, particles and meteorology were made with high time resolution.  
117 Meteorological measurements including relative humidity, temperature, wind direction and speed, as well  
118 as aircraft state parameters such as altitude (masl) and geographic coordinates were conducted at 1 sec  
119 ~~interval~~ time resolution. A detailed description of the various measurements methods with references is

120 provided in the supporting information (SI Sect. 21.1, Table S1, S2), with only a brief description  
121 provided here.

122 **2.1.1 Trace gas measurements** In-situ measurements of NO, NO<sub>2</sub>, NO<sub>y</sub>, O<sub>3</sub> and SO<sub>2</sub> were conducted  
123 using commercial instruments (Thermo Scientific Inc.) modified to measure at 1 sec time resolution.

124 Ammonia (NH<sub>3</sub>) measurements were made at 1 sec time resolution using a Los Gatos Research (LGR)

125 NH<sub>3</sub>/H<sub>2</sub>S Analyzer, model 911-0039. ~~Calibrations were conducted periodically throughout the~~

126 ~~measurement study using NIST certified standards. Instrument zeros were performed for all these~~

127 ~~instruments 3-5 times per flight for a duration of ~3-5 minutes each time at the beginning, during and~~

128 ~~after each flight.~~ Gas phase elemental Hg (GEM) was measured with a Tekran 237X instrument (Tekran

129 Instruments Corporation) modified to allow a reduced sampling time of 2 min (McLagan et al., 2021;

130 Cole et al., 2014). CO, CO<sub>2</sub> and CH<sub>4</sub> were measured with a Cavity Ring Down spectroscopy instrument

131 (Picarro G2401-m). A second Picarro G2401-m instrument was used to measure Total Carbon (TC, in

132 units of ppm C) by passing the sample air ~~through a catalyst to convert all carbon species to CO<sub>2</sub>. through~~

133 ~~a platinum catalyst (Shimadzu) which was placed at the external rear facing inlet assembly and~~

134 ~~maintained at 650 °C, adapted from Stockwell et al. (2018) and Veres et al., (2010)~~ Total non-methane

135 organic gases (NMOG<sub>T</sub>), in mixing ratios units of ppm C, ~~were was~~ quantified by subtracting the ambient

136 CH<sub>4</sub>, CO and CO<sub>2</sub> measurements (instrument without the ~~upstream~~-catalyst) from the TC measurements

137 (see SI Methods for more details).

138 Individually speciated NMOGs (as well as some inorganic species) were measured with a

139 Chemical Ionization Mass Spectrometer (CIMS), a Proton Transfer Time-of-Flight Mass Spectrometer

140 (PTRMS), and through whole air sampling using canisters (Advanced Whole Air Sampler; AWAS). In

141 addition, integrated cartridge-based samples were taken. The CIMS (a modified ToFwerk/Aerodyne Api-

142 ToF) was operated using iodide as the reagent ion providing 1 sec time resolved measurements for 30

143 compounds (Table S2). The PTRMS (Ionicon Analytik GmbH, Austria) used chemical ionization with

144 H<sub>3</sub>O<sup>+</sup> as the primary reagent ion providing 1 sec measurements for a suite of organic compounds. For

145 those compounds with no available gas standard, a relative response factor was calculated with reaction

146 rate constants using the method described in Sekimoto et al. (2017) and guided by the work of Koss et al.  
147 (2018) ('calculated' compounds). Integrated 'grab' samples (20-30 sec) were collected from the aircraft  
148 using the Advanced Whole Air Sampler (AWAS) with offline analysis. The AWAS provided speciated  
149 measurements of hydrocarbons ( $\leq C_{10}$ ), but no oxygenates. Overlapping compounds/isomers that were  
150 measured by both the PTRMS and AWAS, as well as between the PTRMS and CIMS, were handled as  
151 described in SI Sect. 12.1.4. Integrated gas phase samples were collected using an automated adsorbent  
152 tube (i.e. cartridge) sampling assembly with offline analysis (Ditto et al., 2021; Sheu et al., 2018; Khare et  
153 al., 2019). These samples provided targeted measurements of gas-phase compounds ranging in volatility  
154 from  $C_{10}$  volatile organic compounds (VOCs) to  $C_{25}$  semivolatile organic compounds (SVOCs) including  
155 hydrocarbons (CH), and functionalized compounds containing 1 oxygen atom ( $CHO_1$ ), and 1 sulfur atom  
156 ( $CHS_1$ ).

### 157 **2.1.2 Particle measurements**

158 Particle chemistry was obtained with a high resolution aerosol mass spectrometer (AMS)  
159 (Aerodyne) providing mass concentrations of particle species including total organics (OA),  $NO_3$ ,  $SO_4$   
160 and  $NH_4$  for particles less than  $\sim 1 \mu m$ . Particle size distributions were measured between 60 and 1000  
161 nm at 1 sec time resolution using the Ultra High Sensitivity Aerosol Spectrometer (UHSAS; Droplet  
162 Measurement Technologies). Refractory black carbon (rBC) was measured using a single particle soot  
163 photometer (SP2; Droplet Measurement Technologies).

164

### 165 **2.2 Flight and fire description**

166 A wildfire located near Lac La Loche in Saskatchewan ( $56.40^\circ N$   $109.90^\circ W$ ) was detected by  
167 satellite on June 23 (Fig. 1; Fig. S1). The fire was ignited by lightning on June 23, 2018 at 19:45 UTC  
168 and lasted 50 hrs to June 25 21:41 UTC burning an estimated 10,000 ha before being extinguished by  
169 rain. The area burned was mostly mature Jack pine and boreal spruce forest with a smaller fraction of  
170 boreal mixed-wood forest. Satellite images from the VIIRS spectroradiometer on the Suomi NPP and  
171 NOAA-20 satellites taken on June 25 showed merged fire hot spots with a visible smoke plume moving

172 in a north-westerly direction (Fig. 1; see SI Sect. 2.02 for more details). Lagrangian flight tracks were  
173 flown downwind of the wildfire to follow the fire plumes. Multiple horizontal transects, vertically  
174 stacked and perpendicular to the plume direction were made at different altitudes from 640 to 1460 m asl  
175 (~220 – 1040 m agl, based on 420 m asl at Lac La Loche) forming virtual screens. Five screens were  
176 completed over two flights with the closest screen ~10 km and the farthest screen 164 km downwind of  
177 the fire, with the screens spaced such that the instruments sampled the same air parcels as they were  
178 transported downwind. A vertical profile which typically reached ~2500 m asl was conducted in the  
179 plume at each screen to gather information on its vertical structure and the height of the plume. As  
180 demonstrated by the elevated CO mixing ratios in Fig. 2, two distinct plumes were identified - a south  
181 plume (SP) and north plume (NP), that were transported in parallel in a northwesterly direction. The SP  
182 is estimated to be ~42 min old based on the measured wind speed at Screen 1 and the distance from the  
183 closest edge of the VIIRS fire hot spots (~10 km). The NP is estimated to be an additional 30 min older  
184 than the SP (further details in SI Sect. 2.02). For the purposes of this investigation, only data from Screen  
185 1 are used to characterize the direct emissions from this fire. ~~Evaluation of emissions of photolabile~~  
186 ~~species could be influenced by photochemical and depositional losses that may take place between the~~  
187 ~~time of emission and the time of measurement. - primary at 10 km (<1 hr) away from the fire source,~~  
188 ~~Screen 1 measurements represent some of the freshest emissions ever measured under wildfire conditions.~~  
189 There ~~are~~ were no ~~other~~ significant anthropogenic sources like upwind urban or industrial areas,  
190 impacting the Screen 1 measurements. Plume evolution during transport from Screen 1 to downwind  
191 Screens 2 to 5 is discussed in other papers (Liu et al., 2022; Ditto et al., 2021; McLagan et al., 2021).

192

### 193 ~~2.3 Emission ratios, emission factors and combustion efficiency~~

#### 194 **2.3 Emission ratios**

195 Emission ratios (ERs) were calculated using an integration method (e.g. Yokelson et al., 2009;  
196 Garofalo et al., 2019) ~~with~~ using the in-plume measurements for the SP and NP. The integration method  
197 was carried out ~~for the real-time measurements~~ by first subtracting a background from the in-plume



198 measurements. Background measurements were defined as the average over short time segments (~30  
199 sec) outside and at the same altitude as inside the plume, and typically selected at the ends of the  
200 horizontal transects. The background-subtracted plume measurements yielded enhanced plume values  
201 (e.g.  $\Delta X(t)$ ) which were then integrated using the plume start and end times guided by when CO mixing  
202 ratios were above the CO background. Nominal plume time periods are indicated by the vertical grey  
203 bars in Fig. 3 which shows time series for CO, NMOG, OA and acetonitrile for the first 4 of 5 transects  
204 on Screen 1. Integrated pollutant values were subsequently normalized by the integrated values of CO  
205 (Eq. 1) to account for changes due to dilution producing emission ratios (ER) for the SP and NP for each  
206 transect on Screen 1.

$$ER = \frac{\int_{start}^{end} \Delta X(t) (dt)}{\int_{start}^{end} \Delta CO(t) (dt)} \quad (1)$$

207  
208  
209  
210 CO is known to be a suitable dilution tracer as it has a long atmospheric lifetime of 1-4 months (Seinfeld  
211 and Pandis, 1998), is unreactive on the time scale of the measurements. ~~, and is a particularly good tracer  
212 for smoldering fires (e.g. Simpson et al., 2011).~~ In this study, ERs were calculated using CO as it was  
213 ~~well-enhanced~~ above a background of  $\sim 0.119 \pm 0.005$  ppmv for the plumes measured, there were no other  
214 significant CO sources in the study area, ~~and CO is a particularly good tracer for smoldering fires (e.g.  
215 Simpson et al., 2011), and co-varied well with the majority of measurements.~~

216 ERs for the AWAS compounds were determined using the average mixing ratio of 3 samples  
217 taken in the SP and two in the NP, and the average mixing ratio of two background samples. CO mixing  
218 ratios were averaged across the AWAS sample time period. For the integrated cartridges, samples were  
219 collected over the lower set of aircraft transects ('LOW') and higher set of transects ('HIGH'), resulting  
220 in two integrated cartridge samples for each screen. The HIGH sample was used as the background. The  
221 HIGH sample was collected largely outside the wildfire plume, but may have been influenced to some  
222 extent from emissions. However, this impact is expected to be minimal as average CO mixing ratios

223 during the HIGH sample were at background levels (~0.14 ppmv). Nevertheless, to address the potential  
 224 for influence of the plume in the HIGH sample, the ERs are presented as ranges with the lower estimates  
 225 derived by subtracting the HIGH background sample, and the upper estimates without subtracting the  
 226 HIGH sample. This calculation is described in Eq. 2 where  $Cartridge_{LOW}$  represents the LOW cartridge  
 227 sample measurements,  $Cartridge_{BKGD}$  is the background derived from the HIGH cartridge sample  
 228 measurements, and  $CO_{LOW}$ ,  $CO_{BKGD}$  are the average CO concentrations during the respective LOW and  
 229 HIGH cartridge integration time periods. The uncertainty with this bounding analysis is acknowledged,  
 230 but the I/SVOCs ERs within a plume are likely to vary similar to other work (Hatch et al., 2018).

$$231 \quad ER = \frac{Cartridge_{LOW} - Cartridge_{BKGD}}{CO_{LOW} - CO_{BKGD}} \text{ to } \frac{Cartridge_{LOW} - 0}{CO_{LOW} - CO_{BKGD}} \quad (2)$$

## 233 2.4 Emission factors

234 Emission factors (EFs) were determined as the mass of species X emitted per unit mass of dry  
 235 fuel burned in  $\text{g kg}^{-1}$  assuming that all of the carbon in the fuel was released into the atmosphere and  
 236 measured (Ward and Radke, 1993; Yokelson et al., 2007), and that the mass fraction of carbon in the fuel  
 237 is constant. EFs were determined using Eq. 32 where  $F_c$  is the mass fraction of carbon in the fuel and  
 238 estimated to be 0.5 (de Groot et al., 2009 and references therein),  $mm_x$  is the molar mass of the compound  
 239 of interest, and  $mm_c$  is the molar mass of carbon,  $12 \text{ g mol}^{-1}$ ,  $\Delta X$  is the **integrated** background-subtracted  
 240 mixing ratio or concentration of the species of interest,  $\Delta TC$  is the **integrated** background-subtracted ~~total~~  
 241 ~~carbon~~TC. ~~TC~~ ~~total Carbon~~ (TC) (see Sect. 2.1) was directly measured and includes all the carbon mass in  
 242  $\text{CO}_2$ ,  $\text{CO}$ ,  $\text{CH}_4$ , and  $\text{NMOG}_T$ , as well as that from particulate black carbon (rBC) and particulate organic  
 243 carbon (OC) (which were added to the TC), for a complete accounting of all the emitted carbon. For  
 244 species measured in mass concentration units, Eq. 32 was modified by converting TC to mass  
 245 concentrations using the measured temperature and pressure, and removing the molar mass ratio term.  
 246 The EFs for the AWAS and the cartridge samples were derived using the average measurements as  
 247 discussed for the ER, but with TC as the denominator.

248

249

$$EF \left( \frac{g}{kg} \right) = F_c \times 1000 \left( \frac{g}{kg} \right) \times \frac{mm_x}{mm_c} \times \frac{\int_{start}^{end} \Delta X(t) (dt) \Delta X}{\int_{start}^{end} \Delta TC(t) (dt) \Delta TC} \quad (32)$$

250

251

EFs were determined for the SP and NP for each transect, and then averaged to obtain screen-averaged

252

EFs for the SP and the NP, as well as for both plumes together. ~~There is a potential for inherent~~

253

~~uncertainties with this approach for calculating EFs and ERs as the ratios derived this way represent the~~

254

~~average plume composition and ignore the spatial heterogeneity in wildfire plumes (Liu et al., 2022;~~

255

~~Decker et al., 2021; Peng et al., 2020; Garofalo et al., 2019), chemical transformation processes, and can~~

256

~~also be affected by changing background levels.~~

257

## 2.5 Emissions Uncertainties

258

There is the potential for inherent uncertainties using a plume integration method for calculating

259

EFs and ERs as the ratios derived this way represent the average plume composition and ignore the

260

spatial heterogeneity in wildfire plumes (Palm et al., 2021; Decker et al., 2021; Garofalo et al., 2019),

261

chemical transformation processes, and can also be affected by changing background levels. Pollutants

262

released by wildfires can be influenced by photochemical and physical changes that may take place

263

between the time of emission and the time of measurement, particularly for more reactive compounds

264

(e.g. Palm et al., 2021; Lindaas et al., 2020; Peng et al., 2020; Akagi et al., 2011). Although controlled

265

laboratory studies are well suited to examine direct emissions with minimal aging, they cannot reproduce

266

realistic burning conditions. Field measurements are critical to understand emissions that are impacted by

267

factors such as complex burning dynamics, fuel moisture, temperature and winds (Andreae 2019).

268

Recognizing the challenges of measuring primary emissions by aircraft, at 10 km (<1 hr) away from the

269

fire source, Screen 1 measurements represent some of the freshest emissions measured under wildfire

270

conditions, thus providing best estimates of initial conditions.

271

Uncertainties in the EFs and ERs are estimated by summing in quadrature the standard error of

272

the average EF (or ER) and the propagated measurement uncertainties. The standard error is used as

273 description of the uncertainty on the average EF (and ER) characterizing repeated transects across the SP  
274 and NP for a total of 20 min of in-plume sampling. The standard error is expected to at least partially  
275 capture uncertainties associated with plume aging and vertical plume heterogeneity. As many compounds  
276 exhibited significant in-plume enhancements above background levels, uncertainties in the integrated  $\Delta X$ ,  
277  $\Delta CO$  and  $\Delta TC$  values were assumed to be dominated by instrumental (measurement) uncertainties (Table  
278 S1, S2). Emissions are not reported for compounds where the average mixing ratios were within  $1\sigma$  of  
279 the background average. The low and high I/SVOCs EFs (and ERs) are provided as estimates of their  
280 uncertainties (as described in Sect. 2.3). The derivation of AWAS and cartridge EFs (and ERs) may have  
281 potential limitations as they rely on a limited number of samples, with the potential of the AWAS discrete  
282 samples capturing only part of a plume.

## 284 **2.6 Combustion efficiency**

285 Combustion efficiency (CE) is a useful indicator of the relative proportion of flaming vs  
286 smoldering stages of combustion which has a significant influence on the chemical composition of the  
287 smoke (see SI Sect. 3.04 for further details). Flaming fires have  $CE > 0.90$  (Yokelson et al., 1996) and  
288 smoldering fires are typically  $\sim 0.8$  with a range of 0.65 to 0.85 reported in the literature (Akagi et al.,  
289 2011; Yokelson et al., 2003). A modified combustion efficiency (MCE) is commonly calculated  
290 assuming that  $CO_2 + CO$  adequately represents all of the fuel carbon that has been volatilized and detected  
291 in ambient air. Here, as the TC in the plume was directly measured,  $\Delta TC$  was used in Eq. 43 to improve  
292 on the estimation of the CE by accounting for all the sources of carbon.  $\Delta CO_2$  and  $\Delta TC$  in Eq. 43 are the  
293 integrated, background-subtracted mixing ratios.

$$295 \quad CE = \frac{\Delta CO_2}{\Delta TC} \quad (43)$$

## 297 **3 Results and Discussion**

### 298 3.1 Fire combustion state

299 The plume-averaged CE for the SP (transects 1 to 4) was  $0.84 \pm 0.04$  and for the NP (transects 1 to  
300 3)  $0.82 \pm 0.01$ . Transect 4 was excluded from the calculations for the NP because only a portion of the  
301 plume was detectable at this altitude (Fig. 3). The derived CE indicates that the fire was predominantly in  
302 a **low intensity** smoldering phase which is consistent with the satellite-derived fire intensities during the  
303 flight (see Fig. 10) and ground-based meteorological observations, and may reflect some residual  
304 smoldering combustion (RSC). It is estimated that emissions from this fire were sampled 14 hrs post  
305 flaming. Other chemical measurements from this flight also support that the fire was largely smoldering  
306 including the detection of elevated  $C_2H_4O_2^+$  (levoglucosan fragment from the AMS), **low  $NO_x$  levels**  
307 **(Lapina et al., 2008) (Fig. S32)**, and no detectable  $K^+$  (from the AMS) (Lee et al., 2010). Significant  
308 spatial variability in the concentrations of many of the measured species were observed closest to the fire  
309 source, while the plumes became more well-mixed as they were transported downwind (Fig. S63). This  
310 highlights the complexities of assessing wildfire combustion processes (Ward and Radke, 1993), and in  
311 particular, boreal forests have been observed to exhibit greater variability in combustion efficiencies than  
312 for other vegetation types (Urbanski et al., 2009).

### 313 3.2 General plume features

314 ~~Most pollutants were strongly concentrated in the fire plumes~~ Table A1 shows mixing ratios (or  
315 concentrations) and background levels of 193200 pollutants that were enhanced in the fire plumes. ~~with~~  
316 ~~the exception of s~~The quantification of this suite of compounds provides new and additional emission  
317 estimates to those reported in Simpson et al. (2011) and compiled in Andreae (2019) for the boreal forest  
318 ecosystem. Several sulphur-containing compounds and a few other VOCs **were not detected** (Table S6),  
319 and although not part of the measurement suite in the present study, Simpson et al. (2011) did not observe  
320 emissions of anthropogenic halocarbons from wildfires in the same boreal forest ecosystem. In Fig. 3, the  
321 in-plume portions are highlighted by the grey vertical bars and the SP and NP are indicated as the aircraft  
322 flew at increasing altitudes to complete five horizontal transects. The lowest 4 transects showed enhanced  
323 pollutant levels while the 5<sup>th</sup> transect (not shown) was predominantly above the height of the plumes.

324 Higher concentrations were generally observed in the SP compared to the NP, possibly because of some  
325 plume dilution in the NP resulting from a change in wind direction prior to sampling. The SP and NP  
326 were distinctly separated from each other, with pollutants typically dropping to background levels  
327 between the plumes. NMOG<sub>T</sub> mixing ratios varied between ~~background levels of ~400-375~~ ppbv to near  
328 10 ppmv in-plume. CO and acetonitrile, often used as tracers of biomass burning (e.g. Wiggins et al.,  
329 2021; Landis et al., 2018; Simpson et al., 2011; de Gouw et al., 2006), reached 6.6 ppmv and 20 ppbv,  
330 respectively in the SP, while maximum OA concentrations reached 276  $\mu\text{g m}^{-3}$ , above a background level  
331 of ~~~912.5±0.83~~  $\mu\text{g m}^{-3}$ . OA was the largest contributor to particulate mass (PM) comprising over 90 % of  
332 the measured submicron mass with remaining portion comprised of BC, NO<sub>3</sub>, NH<sub>4</sub>, and SO<sub>4</sub> (Fig. S64).  
333 Integrated filter samples taken from the aircraft across Screen 1 also showed the presence of a diverse set  
334 of functionalized particle-phase organic compounds (Ditto et al., 2021).

335 The most abundant reactive nitrogen compounds (N<sub>r</sub>) were in the forms of reduced nitrogen (~~85-79~~  
336 %) with NH<sub>3</sub> comprising ~~421.7~~ % of  $\Sigma\text{N}_r$  (Fig. 4) and substantially lower nitrogen oxides i.e. NO<sub>x</sub> < 1  
337 ppbv. ~~A large portion of unmeasured nitrogen-containing compounds found in these plumes was likely~~  
338 ~~dominated by peroxyacetyl nitrate (PAN) (Liu et al., 2022). These observations are consistent with~~  
339 ~~emissions from smoldering fires (Burling et al., 2011; Goode et al., 2000; McMeeking et al., 2009;~~  
340 ~~Yokelson et al., 1996).~~ Dominant proportions of reduced nitrogen in biomass burning emissions were  
341 also reported previously (Lindaas et al., 2020; Burling et al., 2011; Yokelson et al., 1996). ~~Nitrogen-~~  
342 ~~containing organics were detected in the present study totalling 3.9 ppbv and 18 % of  $\Sigma\text{N}_r$  (Fig. 4),~~  
343 ~~however, other such compounds that were not included with the instrument suite used in this study were~~  
344 ~~also likely emitted. Such compounds could include organic nitrates, amines, amides, heterocyclic~~  
345 ~~compounds, nitriles and nitro compounds that have been found in biomass burning emissions (Roberts et~~  
346 ~~al., 2020; Lindaas et al., 2020; Andreae 2019; Koss et al., 2018; Tomaz et al., 2018; Stockwell et al.,~~  
347 ~~2015).~~ Alkyl nitrates have been identified in biomass burning emissions, but their contributions to total N<sub>r</sub>  
348 appeared to be small (Juncosa-Calahorrano et al., 2021; Roberts et al., 2020; Lindaas et al., 2020;  
349 ~~Simpson et al., 2011; Alvarado et al., 2010; Singh et al., 2010).~~

### 350 3.3 Total carbon budget

#### 351 3.3.1 NMOG chemical classes – PTRMS, CIMS, AWAS

352 In-plume mixing ratios and the relative contribution of individually measured NMOG species to  
353 the sum of those species ( $\Sigma$ NMOG) are shown for 13 chemical classes in Fig. 5. (See Fig. S75 for  
354 separate SP and NP chemical classes). The largest chemical classes include carbonyls (acids, aldehydes  
355 and ketones), alcohols, hydrocarbons (alkanes, alkenes, alkynes), aromatics (including furans, phenol,  
356 benzene and toluene), and nitriles. Hydrocarbons (i.e.  $C_xH_y$ , including some aromatics) were responsible  
357 for just over half of the  $\Sigma$ NMOG (52.853 %) (Fig. S86), with 27.229 % identified as alkenes such as  
358 ethene, propadiene, and propene, 19.319 % alkanes, predominantly ethane, and 3.13 % alkynes, almost  
359 entirely acetylene. Non-aromatic oxygenates accounted for an additional 36.236 % of the  $\Sigma$ NMOG with  
360 roughly equal contributions (10.1 to 11.09 to 12 %) from acids, aldehydes and alcohols, and a smaller  
361 fraction from ketones (4.85 %). Including other oxygenated compounds such as furanoids and  
362 phenol/phenol derivatives, all oxygenates ( $C_xH_yO_z$ ) comprised 41.442 % (Fig. S86), of the  $\Sigma$ NMOG.

363 A similar range of compound classes has been observed in previous field and laboratory studies,  
364 noting that the measured compound suite between studies varies to some extent. For example, Simpson  
365 et al. (2011) found a similar distribution of compound classes with 57 measured NMOG species, based on  
366 discrete canister samples, in boreal forest wildfires. In that study, oxygenates (non-aromatic) comprised a  
367 smaller portion of NMOG (29 %) as major emitted species like acetaldehyde and acetic acid (Fig. 8) were  
368 not included. ~~For example, some hydrocarbons, like 1-butene, ethane, propane, and isobutene measured~~  
369 ~~in the present study were not included in Koss et al., (2018) results.~~ Other studies have also found  
370 oxygenates to be a large portion of NMOG emissions across multiple fuel types, including those similar  
371 to the current study, ranging from 51 – 68 % (Permar et al., 2021; Koss et al., 2018; Gilman et al., 2015;  
372 Akagi et al., 2011) with a range of 25 – 55 % reported in Hatch et al. (2017). ~~Comparisons between~~  
373 ~~studies are influenced by differences in study measurement suites and variations in fuel composition.~~ The  
374 fraction of NMOG oxygenates in the present study (41.442 %) was closer to those reported in Hatch et al.  
375 (2017) when only the most relevant fuel types of pine and spruce were considered (55 % and 43 %,

376 respectively). Similar to previous work (Koss et al., 2018, Stockwell et al., 2015; Hatch et al., 2015),  
377 emissions of substituted oxygenates like furanoids (furans+derivatives) and phenolic compounds were  
378 observed. Furanoids contributed 4 % of the  $\Sigma$ NMOG mostly due to furfural, furan and methyl furan  
379 while phenolic compounds eg. guaiacol, methyl guaiacol, contributed 0.5 % of the  $\Sigma$ NMOG (Fig. S97).  
380 Although ~~their~~ these emissions were less abundant in the present study, they represent important OH  
381 reactants (Coggon et al., 2019; Koss et al., 2018; Gilman et al., 2015) with phenols being implicated as  
382 precursors to brown carbon formation in secondary organic aerosol (SOA) (Palm et al., 2020).

383 Biogenic emissions of terpenoids including isoprene, monoterpenes, carvone, sesquiterpenes,  
384 camphor/isomers and terpine-4-ol/cineole/isomers were elevated in the plumes collectively reaching ~2.4  
385 ppbv, and contributing ~~~1~~2 % to the  $\Sigma$ NMOGs (Fig. S97). Isoprene was ~~~70~~66 % of these compounds  
386 with an additional ~~29~~32 % from monoterpenes. Emissions of isoprene from biomass burning has been  
387 observed from a wide range of fuel types (Hatch et al., 2019). As isoprene is not stored by plants and the  
388 measurements were taken ~14 hrs post flaming, it was likely emitted as a combustion product.

389 In this study, furfural was the most abundant oxygenated aromatic compound and a factor of 5  
390 times higher than that of phenol. ~~, whereas Hatch et al. (2015) and~~ Although Koss et al. (2018) found  
391 that phenol and furfural emissions were ~~slightly larger than that of furfural~~ similar for ~~all~~most fuels tested  
392 in the laboratory, furfural emissions derived from multiple wildfires sampled in Permar et al. (2021) were  
393 similar to those in the present study, and a factor of 1.6 higher for phenol. As phenol emissions are  
394 associated with lignin pyrolysis (Stockwell et al., 2015; Simoneit et al., 1999), the lower emissions in the  
395 current study could be because the lignin content in the fuel mixture was lower than fuels used in previous  
396 laboratory studies or that most of the phenolic compounds were emitted during the earlier phases of the  
397 fire. Several modelling studies have indicated that aromatics and terpenes are insufficient to explain SOA  
398 formation in biomass burning plumes (e.g. Hodshire et al., 2019) suggesting the importance of inclusion  
399 of other aromatic species such as phenolics and furanoid compounds. However, models typically do not  
400 include reactions involving phenolic and furanoids species, especially substituted compounds like  
401 furfural, guaiacol, and methyl guaiacol. Box model simulations have also shown that incorporation of



402 OH oxidation of furan, 2-methylfuran, 2,5-dimethylfuran, furfural, 5-methylfurfural, and guaiacol, leads to  
403 10 % more O<sub>3</sub> formed (Coggon et al., 2019).

### 404 3.3.2 Intermediate-volatility and semivolatile organic compounds (I/SVOCs)

405 Offline analysis of cartridge samples showed a wider range of hydrocarbons and functionalized  
406 gas-phase organic compounds not observed in the PTRMS, CIMS, and AWAS measurements, including  
407 I/SVOC compounds in the wildfire plume. ERs (Table S7) for species containing carbon ~~and~~ hydrogen,  
408 ~~and with either~~ sulfur ~~and-or~~ oxygen (i.e. CH (hydrocarbons), CHS<sub>1</sub> and CHO<sub>1</sub> type molecules))  
409 accounted for a sizeable fraction of carbon in ~~the~~ C<sub>10</sub> to C<sub>25</sub> range. ~~, -with-expected-~~ Additional  
410 ~~c~~Contributions ~~are expected~~ from more highly functionalized organics in the gas (and particle) phase not  
411 reflected in the CH, CHO<sub>1</sub>, and CHS<sub>1</sub> compound classes (e.g., gas-phase species with multiple oxygen  
412 atoms like vanillic acid or acetovanillone, and gas-phase species containing combinations of oxygen and  
413 nitrogen atoms (CHON) (Ditto et al., 2021; 2022)). ERs in the plume varied across the carbon number  
414 range; in general, the highest ratios were observed for the complex mixture of hydrocarbons (i.e. CH  
415 compounds) broadly peaking at C<sub>200</sub>-C<sub>235</sub> in the SVOC range, with a larger contribution from C<sub>10</sub>  
416 compounds including monoterpenes. By comparison, the complex mixture of CHO<sub>1</sub> compounds was  
417 slightly lower in abundance than CH with contributions from C<sub>10</sub> monoterpene emissions or  
418 ~~monoterpene~~ oxidation products. CHS<sub>1</sub> IVOC-SVOCs were the lowest abundance species quantified.  
419 CHN<sub>1</sub> compounds represent another observed contributor of IVOCs-SVOCs; the sum of all CHN<sub>1</sub>  
420 compound ion abundances was two orders of magnitude smaller than the sum of all CHO<sub>1</sub> species. We  
421 note that for CHN<sub>1</sub>, this qualitative comparison is in terms of ion abundances only, given a lack of  
422 appropriate standards to calibrate for the ~~mass spectrometer's response to the~~ complex mixture of reduced  
423 nitrogen-containing I/SVOCs.

424 ~~EFs were estimated for CH, CHO<sub>1</sub>, and CHS<sub>1</sub> I/SVOCs based on Table S7 ERs (to CO) and the~~  
425 ~~average EF of CO (115.7 ± 7.5 g kg<sup>-1</sup>, Appendix A). It was not possible to directly calculate EFs due to~~  
426 ~~the lack of a background sample upwind of the fire.~~ EFs were estimated to be 1.4±0.037 – 2.4±0.063 g  
427 kg<sup>-1</sup> for CH, 0.81±0.078 – 0.81±0.079 g kg<sup>-1</sup> for CHO<sub>1</sub>, and 0.21 ±0.0033 – 0.22±0.0060 g kg<sup>-1</sup> for CHS<sub>1</sub>

428 species, for a total EF of  $2.4 \pm 0.12 - 3.5 \pm 0.15 \text{ g kg}^{-1}$  (Table A1). ~~EFs were estimated to be  $1.6 \pm 0.04 \text{ g kg}^{-1}$~~   
429 ~~for CH,  $0.9 \pm 0.09 \text{ g kg}^{-1}$  for CHO<sub>1</sub>, and  $0.1 \pm 0.003 \text{ g kg}^{-1}$  for CHS<sub>1</sub> species, for a total EF of  $2.6 \pm 0.14 \text{ g kg}^{-1}$~~   
430 ~~(Table A1)~~. Here, the uncertainty represents measurement uncertainty associated with the conversion  
431 from signal to mass, and the reported ranges show lower and upper limit EF values that account for a  
432 contaminated background and that assume no background concentrations, respectively (as described  
433 above). These estimates accounted for C<sub>11</sub>-C<sub>25</sub> species and focused on I/SVOCs to avoid double counting  
434 the monoterpenes and C<sub>10</sub> monoterpene species, as they were already accounted for in the PTRMS data.  
435 It is noted that the concentrations estimated for the cartridge samples may be sensitive to variations in  
436 sampling efficiency within the under-wing sampling pod across C<sub>10</sub>-C<sub>25</sub> though these effects are expected  
437 to be minimal for the adsorbent tubes used in this study (Ditto et al., 2021; Sheu et al. 2018). These  
438 emission estimates expanded the characterized spectrum of organic species to include IVOC/SVOCs in  
439 boreal forest fire emissions, which until now, had only been available from laboratory measurements  
440 (Hatch et al., 2018). However, the observed emissions of the complex mixture of hydrocarbons and  
441 functionalized species may include contributions from the re-volatilization of compounds previously  
442 emitted from upwind oil sands operations and deposited in the forest ecosystem, as noted in Ditto et al.  
443 (2021).

444

### 445 3.3.3 Accounting for the observed carbon

446 Measurements of TC, along with the speciated measurements from the PTRMS, CIMS, AWAS  
447 and cartridges, provided a unique opportunity to reconcile the TC budget in a wildfire. Fig. 6 shows the  
448 TC partitioning based on derived EFs (Sect. 3.5); overlapping compounds from the individual  
449 measurement methods were handled as described in SI Sect. 12.1.4. The total EF for all carbon-  
450 containing compounds was  $1652 \text{ g-C kg}^{-1}$  and, as expected, CO<sub>2</sub> was the dominant contributor comprising  
451 >90 % of TC. CO contributed 7.0 % followed by a contribution from NMOG<sub>T</sub> of 1.9 % with even  
452 smaller contributions observed from CH<sub>4</sub> (0.5 %) followed by OC and BC (not shown) at <0.5 %. The  
453 ~~magnified pie chart (right side) displays the two magnified pie charts (right side), representing the low~~

454 and high I/SVOC EF estimates, show the percent breakdown of the measured NMOGs, and the remaining  
455 unidentified portion of NMOG<sub>T</sub>. The EF values (g C kg<sup>-1</sup>) are identified in the box below. The ΣNMOG  
456 EFs (for PTRMS+CIMS+AWAS measurements), totalling ~~14.413.6±3.20.9~~ g C kg<sup>-1</sup>, ~~which~~ accounted  
457 for ~~46.243±3~~ % of the NMOG<sub>T</sub> EF of 31.2±4.73.8 g C kg<sup>-1</sup> (refer to Fig. S108 for the individual SP and  
458 NP breakdowns). The ΣNMOG uncertainties were estimated by summing in quadrature the individual  
459 compound EF uncertainties for the SP and NP separately, with these uncertainties subsequently summed  
460 in quadrature to derive the average ΣNMOG uncertainty (Fig. 6). The cartridge data showed the presence  
461 of a range of larger molecular weight I/SVOC compounds between C<sub>10</sub> and C<sub>25</sub> ~~representing with an~~  
462 additional 2.1 to 3.0 ~~3±0.08~~ g C kg<sup>-1</sup> ~~representing and 7.47~~ to 10 % of NMOG<sub>T</sub>. Together, all of the  
463 speciated NMOG measurements in this study accounted for ~~53.650±3~~ % to 53±3 % of NMOG<sub>T</sub>. The  
464 remaining carbon mass was unidentified comprising ~~46.447±15~~ % to 50±15 % of NMOG<sub>T</sub>. Despite using  
465 four state-of-the-art measurement techniques resulting in an extensive measurement suite, almost half of  
466 NMOG<sub>T</sub> remained unidentified. This is consistent with previous work estimating ~50 % of NMOG<sub>T</sub> by  
467 mass as unidentified (Akagi et al., 2011). It is noted, however, that the magnitude of the unidentified  
468 portion is partly affected by uncertainties in the speciated measurements. For example, many of the  
469 ‘calculated’ PTRMS compounds are uncertain by an ~~estimated~~ factor of ~2 (SI Sect. 21.1.1, Table S1).  
470 Nevertheless, a portion of the unidentified species likely consisted of challenging-to-measure-VOCs and  
471 larger I/SVOCs that were highly functionalized or contained molecular features like reduced nitrogen  
472 groups (e.g. amines) that have been observed in the gas and particle phase at various sites (Ditto et al.,  
473 2020; Ditto et al., 2022). ~~While a complex mixture of I/SVOCs were observed from this fire (Table S7);~~  
474 ~~it is likely that other functionalized gas phase species containing nitrogen and/or multiple oxygens (e.g.~~  
475 ~~CHO<sub>n</sub>, CHON, CHN) were also emitted, similar to particle phase observations in the fire plume via~~  
476 ~~tandem MS in Ditto et al. (2021).~~The presence of I/SVOCs in biomass burning emissions has been  
477 previously observed in laboratory experiments (e.g. Koss et al., 2018; Hatch et al., 2018; Hatch et al.,  
478 2017; Bruns et al., 2016) with smoldering more likely to emit a higher fraction of compounds with low  
479 volatility than higher temperature processes (Koss et al., 2018). The unidentified portion may also have

480 been comprised of nitrogen-containing organics (Sect. 3.1). Studies that included measurements of a  
481 larger range of nitrogen-containing organics in biomass burning emissions estimated that they comprised  
482 < 5-6 % of the total nitrogen budget (Lindaas et al. 2020; Gilman et al., 2015), and thus, an even smaller  
483 fraction of NMOG<sub>T</sub>. Advancing analytical techniques to expand the suite of NMOG speciation will  
484 enable further reconciliation of the TC budget which is important for assessing secondary formation  
485 processes in the atmosphere.

### 486 3.3.4 Volatility distribution of NMOG

487 Volatility distributions can help track the full range of organic species to assess their partitioning  
488 between the condensed and gas phases (Donahue et al., 2011). Fig. 7 shows the fractional sum of all  
489 NMOG EFs within each volatility bin in terms of saturation concentration ranges ( $\log_{10}C_o$ ,  $\mu\text{g m}^{-3}$ ) for the  
490 low I/SVOC EF estimate.  $C_o$  values were estimated using the parameterization developed by Li et al.  
491 (2016). NMOG emissions from this fire spanned a large range of volatilities from  $\log_{10}C_o$  of -2 to 10  $\mu\text{g}$   
492  $\text{m}^{-3}$  across SVOCs to VOCs categories. The bin-averaged O/C ratio based on the measurements increased  
493 with reduced volatility reflecting the presence of compounds with additional oxygen-containing  
494 functional groups. The highest fraction of emissions was present as VOCs with ~~63.381~~ % having  $\log_{10}C_o$   
495  $> 6 \mu\text{g m}^{-3}$ , ~~and 11.69~~ % as IVOCs having  $4 < \log_{10}C_o \mu\text{g m}^{-3} < 6 \mu\text{g m}^{-3}$  and ~~107.9~~ % as SVOCs having  
496  $\log_{10}C_o < 3 \mu\text{g m}^{-3}$ . These results align with laboratory studies showing that oxygenates comprised more  
497 than > 75 % of IVOCs across a range of biomass types with IVOCs accounting for ~11 % of the  $\Sigma\text{NMOG}$   
498 (Hatch et al.; 2018). Fig. 7 encompasses the range of volatilities based on all the identified NMOGs in  
499 this study that is expected to represent initial emission conditions for modelling downwind chemistry.  
500 However, improved speciation, particularly of lower volatility compounds, ~~are~~ is needed to further  
501 expand the range of volatilities and advance knowledge in gas to particle partitioning processes.

502

### 503 3.4 Emission factors and comparisons with other studies

504 ~~Emission factors (EFs)~~ (and ~~emission ratios (ERs)~~) in this study are derived for ~~250-193~~  
505 compounds from 15 instruments of which ~~228-173~~ are NMOG species (Table A1). This dataset

506 represents the most extensive range of field-based EFs ever determined for a wildfire in the boreal forest  
507 ecosystem. In Fig. 8 average EFs are shown for compounds grouped by a) particles, b) gas-phase  
508 inorganics, and c) gas-phase organics. Separate EFs and ERs for the SP and NP are shown in the SI  
509 (Figs. S119 to S134). In Fig. 9a-c, EFs are compared with those from other relevant studies. Fig. 9a  
510 shows a comparison with boreal forest field measurements largely taken from a compilation by Andreae  
511 (2019) referred to as BFF19, as well as values from Akagi et al. (2011) and Liu et al. (2017). This results  
512 in a comparison for 50 compounds (35 organics and 15 inorganics/particulate species) with the largest  
513 suite of EFs from one study conducted in a similar boreal region as the present study (Simpson et al.,  
514 2011). EFs are also compared with laboratory-derived EFs for lodgepole pine Koss et al. (2018; referred  
515 to as LAB18) (Fig. 9b), a ~~dominant fuel~~ similar fuel type in the current study, with a total of 99 NMOGs  
516 and 3 inorganics in common. In Fig. 9c, EFs are compared with those recently reported in Permar et al.  
517 (2021) (referred to as TFF21) based on aircraft measurements of temperate forest wildfires in areas  
518 mostly dominated by pine, fir and spruce trees, which provides the closest suitable comparison with  
519 similar speciated NMOGs under wildfire conditions. Comparisons include 111 NMOGs, and 4  
520 inorganics/black carbon. While the Permar et al. (2021) study was conducted in a temperate forest  
521 region, it was at high elevation locations with similar vegetation types as the current study.

522

523 **3.4.1 Particle species** The  $PM_1$  EF ( $6.8 \pm 0.84$  g  $kg^{-1}$ ) represents the total of all particle component  
524 species as measured by the AMS. The  $PM_1$  EF of  $6.8 \pm 1.1$  g  $kg^{-1}$  (Fig. 8a) (accounting for estimated mass  
525 differences due to particle diameters (SI Sect. 1.1.2)) falls in the lower end of the large range previously  
526 observed for boreal forest wildfires ( $18.7 \pm 15.9$  g  $kg^{-1}$ ; Fig. 9b). The few PM EFs for BFF19 (n=5) over a  
527 limited range of MCEs (i.e. 0.89 to 0.93) shows significant variability consistent with previous work  
528 (Jolleys et al., 2015; Akagi et al., 2011; Cubison et al., 2011; Hosseini et al., 2013). OA, accounting for  
529 90 % of  $PM_1$ , has the largest EF, ~~accounting for 90 % of  $PM_1$~~ , with comparatively lower EFs for  $pNO_3$ ,  
530  $pBC$ ,  $pNH_4$ , and  $pSO_4$  (Fig. 8a, Fig. S64). This reflects the dominant particle-phase organic carbon  
531 content of the burned fuel and correspondingly lower fractions of nitrogen and sulphur-containing

532 compounds. Similar high organic fractions have been previously observed in biomass burning emissions  
533 (Liu et al., 2017; May et al., 2014; Hecobian et al., 2011). ERs similarly highlight the dominant OA  
534 emissions. ~~Although the magnitude of EFs and ERs are generally similar~~ between the SP and NP ~~are~~  
535 ~~within their derived uncertainties, the ERs showed differences by up to 70 % for NH<sub>4</sub> (Fig. S12)~~  
536 ~~suggesting some differences in photochemistry between the two plumes.~~ EFs and ERs for ~~chemically-~~  
537 ~~speciated~~ particle species derived in this study represent the first such measurements under boreal forest  
538 wildfire conditions. ~~In Fig. 9a,~~ EFs for chemically speciated compounds are not found in BFF19 (~~except~~  
539 ~~BC~~), but when compared with available values for U.S. temperate forest wildfires (Liu et al., 2017) are  
540 found to be lower for OA (Fig. 9a), SO<sub>4</sub>, NO<sub>3</sub> and NH<sub>4</sub> by factors of ~~32.7, 5.0, 5.3, and 3.04,~~ respectively.  
541 ~~Although differences in fuel type burned between the present study (mature Jack pine, boreal spruce,~~  
542 ~~boreal mixed-wood) and Liu et al. (2017) (mixed conifer, grass, brush and chaparral) may influence the~~  
543 ~~chemical composition of emissions, these large differences suggest the importance of other factors in~~  
544 ~~controlling OA emissions. The lower OA emissions under smoldering conditions in the current study~~  
545 ~~compared to Liu et al. (2017) with higher combustion efficiencies (0.877 to 0.935) conflicts with some~~  
546 ~~findings showing increased OA emissions with lower fire intensities (Liu et al., 2017, Burling et al.,~~  
547 ~~2011). However, the relationship between EF<sub>OA</sub> and combustion efficiency can be impacted by multiple~~  
548 ~~factors such as OA loading, gas-particle partitioning related to dilution, and fuel moisture content (May et~~  
549 ~~al., 2014). The EF<sub>OA</sub> in the current study (6.6±2.6 g kg<sup>-1</sup>) lies in the range of EF<sub>OA</sub> reported for prescribed~~  
550 ~~burns across three temperate ecosystems (2.8±1.6 to 11.2±2.7 g kg<sup>-1</sup>) (May et al., 2014). This may imply~~  
551 ~~that the low intensity, surface, smoldering wildfire conditions in the present study (Sect. 3.1) may be~~  
552 ~~similar to prescribed burn conditions which are typically low intensity fires that are restricted to the forest~~  
553 ~~floor and understory, and conducted under controlled and consistent meteorological and fuel moisture~~  
554 ~~conditions (Yokelson et al., 2013; Carter and Foster, 2004). The lower inorganic particulate-PM~~  
555 ~~emissions, however, are likely more dependent in the present study may reflect differences in fuel~~  
556 ~~elemental composition between temperate and boreal forest ecosystems than combustion efficiency (Liu et~~  
557 ~~al., 2017). Differences in fuel composition between boreal and temperate forest ecosystems are inferred~~

558 through comparisons of NO<sub>x</sub> and SO<sub>2</sub> emissions. For example, the average NO<sub>x</sub> and SO<sub>2</sub> EFs for boreal  
559 forests, are lower than the average EFs for temperate forests by factors of 2.5 and 3.0, respectively. The  
560 lower NO<sub>x</sub> and SO<sub>2</sub> emissions from boreal vs temperate forest wildfires are likely reflective of the  
561 reduced S and N content in boreal biomass (Bond-Lamberty et al., 2006) relative to conifer (Misel, 2012)  
562 fuels in the western U.S., as well as the possible influence of lower anthropogenic sources of nitrogen and  
563 sulphur atmospheric deposition in boreal forests (Jia et al., 2016). ~~The PM<sub>1</sub> EF of 6.85±1.09 g kg<sup>-1</sup>  
564 derived in the present study is a factor of 2.8 lower than the PM<sub>2.5</sub> EF of 18.76±15.90 g kg<sup>-1</sup> that is  
565 available for BFF19 (Fig. 9b). The lower PM emissions in the present study, despite accounting for  
566 particle diameter differences (Sect. 2.1.2), PM EFs for BFF19 (n=5) over a limited range of MCEs (i.e.  
567 0.89 to 0.93) show significant variability. is somewhat surprising given emissions of PM are typically  
568 higher from smoldering compared to flaming fires (Liu et al., 2017; Akagi et al., 2012). ~~However, there  
569 are few PM EFs for BFF19 (n=5) over a limited range of MCEs (i.e. 0.89 to 0.93) showing significant  
570 variability. The PM<sub>1</sub> EF derived in the present study falls within the range previously observed for boreal  
571 forest wildfires and underscores the significant variability in PM emissions.~~~~

572

573 **3.4.2 Gas-phase inorganic species** The largest average EFs for inorganic gases (Fig. 8b; ~~separate NP~~  
574 ~~and SP Fig. S11~~) were from reduced nitrogen compounds dominated by NH<sub>3</sub> (0.63±0.149 g kg<sup>-1</sup>) and  
575 followed by HCN (0.31±0.07 g kg<sup>-1</sup>), with lower EFs for oxidized nitrogen compounds such as NO<sub>2</sub>  
576 (0.154±0.0437 g kg<sup>-1</sup>) and HONO (0.024±0.012 g kg<sup>-1</sup>). This is consistent with previous work  
577 identifying elevated emissions of NH<sub>3</sub> and HCN during smoldering conditions, whereas emissions of  
578 HONO and NO<sub>x</sub> are primarily associated with flaming combustion (e.g. Roberts et al., 2020; Akagi et al.,  
579 2013; Yokelson et al., 1997; Griffith et al., 1991). The EFs for CO<sub>2</sub> and CO from the present study are  
580 ~~very close comparable within uncertainties of~~ that previously reported for BFF19 (Table A1). However,  
581 EFs for most other gaseous inorganic species were lower than the BFF19 EF average including NH<sub>3</sub>,  
582 HONO, ~~SO<sub>2</sub> (n=2)~~ and NO<sub>x</sub> ~~(n=11)~~, by factors of 4.03-9, 2041, 4.7 and 7.114-9, respectively (Fig.  
583 9a). ~~(Fig. 9a).~~ There are only a limited number of studies reporting EFs for these compounds in the

584 BFF19 category. For example, ~~the HONO EF can only be compared with one other BFF19 study, but is~~  
585 ~~also lower compared to LAB18 (Fig. 9b).~~ There are ~~also~~ only 4 previously reported BFF19 EFs for NH<sub>3</sub>  
586 ( $2.56 \pm 1.87$  g kg<sup>-1</sup>) showing a large range of values. ~~Although these comparisons are limited by the few~~  
587 ~~reported values in the literature, -the differences indicate~~ing a strong sensitivity towards factors like fire  
588 intensity, ~~and~~ chemical reactivity, ~~fuel type and moisture, and meteorology.~~ In contrast, EFs for HCN  
589 derived in the current study ( $0.31 \pm 0.0728$  g kg<sup>-1</sup>) ~~compare fairly well with~~ lie within the range of BFF19,  
590 LAB18 and TFF21 values ( $0.28 \pm 0.06$  to  $0.53 \pm 0.30$  g kg<sup>-1</sup>), (Figs 9a, b, c, respectively) and does not vary  
591 widely suggesting that HCN may be less sensitive to burning characteristics. HCN is of concern due to  
592 its impacts on human health particularly since biomass burning emissions are responsible for the majority  
593 of the global HCN (Moussa et al., 2016 and references therein).

594

595 **3.4.3 Gas-phase organic species** In Fig. 8c, the top 25 average EFs for gas-phase organic species are  
596 shown in decreasing order of magnitude. The most abundant emissions were from the lower molecular  
597 weight compounds; such trends are generally in agreement with previous field-based measurements for a  
598 range of fuel types (e.g. Permar et al., 2021; Andreae, 2019; Liu et al., 2017; Simpson et al., 2011;  
599 Urbanski et al., 2009). Excluding CH<sub>4</sub>, the largest EFs were associated with methanol, followed by  
600 ethene, ethane, acetic acid, ~~C<sub>5</sub>-oxo-carboxylic acids,~~ acetaldehyde, formaldehyde, and acetone ranging  
601 from  $1.9 \pm 0.45$  g kg<sup>-1</sup> to  $0.82 \pm 0.22$  g kg<sup>-1</sup> for these compounds. Noting some variations related to  
602 differences in measurement methods, other studies have identified many of these same species as  
603 dominating biomass burning emissions (e.g. Permar et al., 2021; Simpson et al., 2011; Akagi et al., 2011).  
604 For example, Simpson et al. (2011) found that 5 of the same compounds in the present study including  
605 formaldehyde, methanol, ethene, ethane and acetone were in the top 10 NMOG EFs from aircraft-based  
606 measurements made of boreal forest wildfires in northern Saskatchewan, Canada, and within ~300 km of  
607 the current study. In the present study, the top 24 NMOG compounds accounted for ~~just over half (57~~  
608 ~~%)~~81 % of the ΣNMOG by total molecular mass with lower ~~lower~~ emissions from the remaining 149



609 measured compounds. In western U.S. wildfires, small emissions from 151 species were found to  
610 account for almost half of  $\Sigma$ NMOG (Permar et al., 2021).

611 EFs for the NP and SP generally agreed within their uncertainties with larger differences for some of the  
612 more reactive species like isoprene, monoterpenes, and furan. For example, the SP EF for isoprene was a  
613 factor of 3.4 lower than that for the NP ( $0.64 \pm 0.34 \text{ g kg}^{-1}$ ) (Fig. S13). Although the reasons for these  
614 differences are not yet known, observations of higher  $\text{O}_3$  in the SP ( $52.4 \pm 3.0 \text{ ppbv}$ ) compared to the NP  
615 ( $44.7 \pm 3.6 \text{ ppbv}$ ) suggest the influence of higher oxidant chemistry in the SP emissions compared to the  
616 NP.

617 To compare the total NMOG derived in the present study with those from previous studies that  
618 typically sum up their speciated measurements i.e.  $\Sigma$ NMOG, estimates were made using two methods: 1.  
619 increasing the  $\Sigma$ NMOG to account for the unidentified portion of  $\text{NMOG}_T$ ; and 2. adjusting the  $\text{NMOG}_T$   
620 to reflect the total molecular mass (not just the carbon portion). For method 1, the  $\Sigma$ NMOG EF  
621 (including the I/SVOCs) in this study ( $25.8 \pm 3.2$  to  $24.5 \pm 1.6$  to  $25.6 \pm 1.6 \text{ g kg}^{-1}$ ) was increased by 46.450 and  
622 47 % (Fig. 6), respectively, equalling  $37.8$  to  $36.8 \pm 11.3$  to  $37.6 \pm 12.2 \text{ g kg}^{-1}$ . This estimate assumes that the  
623 carbon distribution is the same as the identified, speciated measurements. For method 2, based on the  
624 speciated measurements, the average molecular mass was  $100 \text{ g mol}^{-1}$  and the average carbon number was  
625 6 resulting in  $\sim 28 \pm 24$  % of the molecular fraction represented by atoms other than carbon. Adjusting the  
626  $\text{NMOG}_T$  of  $31.2 \pm 3.8 \text{ g C kg}^{-1}$  upwards by  $28 \pm 24$  % to reflect the additional molecular mass results in a  
627  $\text{NMOG}_F$  of  $39.9 \pm 5.8 \text{ g kg}^{-1}$ . The resulting estimated  $\text{NMOG}_F$  in this study of  $37.8$  to  $36.8 \pm 11.3$  to  $39.9 \pm 5.8 \text{ g}$   
628  $\text{kg}^{-1}$  lies between the estimated average of  $58.7 \text{ g kg}^{-1}$  for the BFF19 (Fig. 9a) and those estimated from  
629 the  $\Sigma$ NMOG EFs of  $25.0 \text{ g kg}^{-1}$  (LAB18) (Fig. 9b), and  $26.1 \pm 6.9 \text{ g kg}^{-1}$  (TFF21) (Fig. 9c) derived from  
630 laboratory- and field-based studies (Table A1). In contrast to the current work, previous estimates of  
631  $\text{NMOG}_T$  are likely to underestimate total NMOG emissions as they typically represent the sum of  
632 measured species only. Some studies have attempted to account for  $\text{NMOG}_T$  by including the sum of  
633 measured plus estimates of ‘unknown’ portions of NMOGs ( $\Sigma$ NMOGs) (Permar et al., 2021; Koss et al.,  
634 2018; Stockwell et al., 2015; Gilman et al., 2015). The BFF19 EF was recently doubled from  $29.3 \pm 10.1 \text{ g}$

635 kg<sup>-1</sup> to 58.7 g kg<sup>-1</sup> to account for unidentified NMOGs where the ΣNMOGs were measured by FTIR, GC  
636 and PTRMS (Andreae, 2019; Akagi et al., 2011). These results support that doubling the ΣNMOG  
637 provides a reasonable estimate the NMOG<sub>T</sub>. It is noted, however, that the average BFF19 NMOG EF is  
638 ~1.5 times higher than that derived in the present study, however, this may reflect variability in NMOG  
639 emissions even within the same boreal biome.

640  
641 Although it is known that acidic compounds are emitted from biomass burning, few studies have  
642 quantified their emissions, particularly under field conditions (Andreae, 2019; Veres et al., 2010;  
643 Yokelson et al., 2009; Goode et al.; 2000). In this study, EFs for ~~31-22~~ organic acidic compounds were  
644 derived (Table A1) representing the most detailed set of organic acid EFs from biomass burning for any  
645 ecosystem (Andreae, 2019). The largest EFs for these compounds include acetic acid, ~~C5-oxo-carboxylic~~  
646 ~~acids~~, C4 oxo-carboxylic acids, and pyruvic acid, all of which are found among the top 24 NMOGs (Fig.  
647 8c). For those measurements that are available for comparison, EFs in the present study were lower for  
648 formic acid and acetic acid ~~compared to, than in~~ BFF19, and were also lower than in LAB18, and TFF21,  
649 ranging from factors of 1.7 to 8.8 (Figs. 9a, b, c, d). ~~A total of nine O~~organic acids that were in common  
650 with TFF21 and LAB18 (Table A1) ~~had~~ve lower EFs, with the exception of pyruvic acid, which was  
651 substantially higher (> factor of 37) in the present study. ~~Differences in fuel type may be an important~~  
652 ~~factor in the variability of these comparisons. Based on laboratory experiments, Veres et al. (2010) found~~  
653 ~~a large range (factor of 5 to 13) of organic acid emissions with different fuel types suggesting that the~~  
654 ~~lignin content of the fuel could be a source of biomass burning organic acid emissions. Emissions for an~~  
655 ~~additional-1023~~ organic acids that have not previously been reported, as well as several inorganic acids  
656 including nitrous acid, isocyanic acid, and peroxyxynitric acid, are included in Table A1. These acids,  
657 representing ~~10.39~~ % of the ΣNMOGs (Fig. 5), are an important class of oxygenates as they can form  
658 additional PM (Reid et al., 2005) and influence the hygroscopicity of smoke particles (Rogers et al., 1991;  
659 Kotchenruther and Hobbs, 1998).

660 Isoprene and monoterpenes, with similar EFs  $\sim 0.410 \pm 0.190$  g kg<sup>-1</sup>, represented 167<sup>th</sup> and 1820<sup>th</sup>,  
661 respectively, of the top 24 NMOG EFs in this study. Terpenes are known to be emitted from a range of  
662 biomass burning fuels (Andreae, 2019 and references therein), but there have been few measurements in  
663 boreal forest wildfire plumes (Simpson et al., 2011; Andreae, 2019). It is noted that PTRMS  
664 measurements of IVOCs like sesquiterpenes likely represent lower limits as they tend to be easily lost to  
665 sample inlet lines due to their low volatility. The isoprene average EF of  $0.421 \pm 0.2610$  g kg<sup>-1</sup> was more  
666 than a factor of 5 higher, while the monoterpenes EF,  $0.4139 \pm 0.03419$  g kg<sup>-1</sup>, was substantially lower  
667 than the only reported EF for boreal forest wildfires (Simpson et al., 2011). The difference in EFs for  
668 isoprene would be even greater if only the NP EF ( $0.64 \pm 0.34$  g kg<sup>-1</sup>) is compared (if it is assumed that  
669 isoprene emissions were influenced by photochemical losses in the SP). As the present study and the  
670 Simpson et al. (2011) study were conducted in similar locations (i.e. boreal forest region within  $\sim 300$  km  
671 of each other), ~~with similar average MCEs,~~ and comparable background levels, these differences are  
672 likely driven by fire ~~stage sampled combustion state, despite having similar study-averaged MCEs.~~ The  
673 majority of monoterpenes are stored in plant tissues (resin stores) for long periods of time, but isoprene is  
674 synthesized and immediately released by plants, and can also be emitted as a combustion product  
675 (Ciccioli et al., 2014; Akagi et al., 2013). Hatch et al. (2019) found that a wide range of terpenoids are  
676 released across a variety of biomass types with variable emissions that were dependent on plant species,  
677 and specifically related to their fuel resin stores. In the present study, monoterpenes may have ‘boiled-  
678 off’ through distillation processes in the early stages of the fire resulting in lower monoterpene emissions  
679 at the aircraft sampling time,  $\sim 14$  hrs post-flaming. In contrast, the Simpson et al. (2011) study sampled  
680 comparatively earlier and more intense fire stages where higher monoterpene emissions were likely  
681 released from live or recently fallen trees that still contained significant resin stores. The monoterpenes  
682 EF reported by Simpson et al. (2011) was likely even higher given only two monoterpenes were speciated  
683 and emissions of other terpenes were likely (Hatch et al., 2019). Higher isoprene emissions in the present  
684 study compared to Simpson et al. (2011) could be related to the comparatively larger smoldering  
685 component. Although limited data exist on the release of isoprene as a function of fire intensity, negative

686 relationships between isoprene and MCE were observed in Australian temperate forest fires (Guérette et  
687 al., 2018) and wheat fields (Kumar et al., 2018).

688 Several furanoid compounds also exhibited significant emissions (Fig. 8c) including furfural,  
689 furan, and methyl furan ranking 12<sup>th</sup>, 19<sup>th</sup>, and 22<sup>nd</sup> of the top 24 ~~NMOG-organic~~ compounds,  
690 respectively. Emissions of furanoids have been observed for a wide range of fuel types (Hatch et al.,  
691 2017; Simpson et al., 2011). ~~Fairly good a~~Agreement ~~within uncertainties~~ was found with BFF19 for  
692 furfural, and furan (Fig 9a). The EFs for furan ( $0.39 \pm 0.1920$  g kg<sup>-1</sup>) and furfural ( $0.65 \pm 0.31$ -g kg<sup>-1</sup>) were  
693 also similar to that in LAB18 (Fig. 9b), and TFF21 (Fig. 9c), as well as other ecosystems (Andreae, 2019)  
694 suggesting their emissions were relatively insensitive to fire intensity and fuel mixture. ~~Overall, t~~The  
695 comparisons in Fig. 9 indicate that for the higher emitting species, the current results are fairly similar,  
696 but for the lower emitting species, these results are lower than previous reported values. ~~These~~  
697 ~~comparisons provide context for the emissions reported in the present study and moves towards improved~~  
698 ~~statistics to better constrain wildfire emissions. Additional factors are considered to explain variability in~~  
699 ~~emissions between this study and other reported values, as well as within this study (NP vs SP).~~  
700 ~~Differences and variability in burn conditions (e.g. fire intensity, winds, fuel density, flame dynamics,~~  
701 ~~fuel moisture) likely influence these comparisons; the Screen 1 measurements in the present study were~~  
702 ~~taken from 9-10 am LT when the fire was in a low intensity, smoldering state, while those in Permar et al.~~  
703 ~~(2021) and Simpson et al. (2011) took place during mid-day under active wildfire conditions. Aircraft~~  
704 ~~measurements in general have a higher probability of sampling variable burn conditions compared to~~  
705 ~~laboratory studies (Hodshire et al., 2019), and as such, aircraft-derived EFs are likely to reflect variability~~  
706 ~~for reactive species as speculated earlier with isoprene. Particularly for reactive species that can exhibit~~  
707 ~~complex variation across plumes, EFs (and ERs) derived by integrating across plumes can be biased low,~~  
708 ~~(Sect. 2.5; Peng et al., 2021; Decker et al., 2021). Also, EFs derived using TC in this study may result in~~  
709 ~~lower, albeit small, EFs compared to reported values that do not account for all the carbon (estimated to~~  
710 ~~be 1-2 % (Akagi et al., 2011)).~~

711

## 712 3.5 Evaluation of emissions models

### 713 3.5.1 Comparison of EFs with the model emissions speciation profile

714  
715 EFs derived in the present study are compared with those that are currently incorporated into the  
716 emissions component of the FireWork modelling system using the Forest Fire Emissions Prediction  
717 System (CFFEPS). CFFEPS uses EFs allocated for 3 combustion states (flaming, smoldering and  
718 residual) and for 8 species including lumped non-methane hydrocarbons (NMHC) based on United States  
719 vegetation data compiled in Urbanski et al. (2014) (Table 3 in Chen et al., 2019). Fig. 9d (bolded  
720 compounds) shows that the smoldering EFs in the present study were comparable for CO, ~~and CH<sub>4</sub> and~~  
721 ~~NMOG~~, but lower for PM<sub>1</sub> (PM<sub>2.5</sub>), NH<sub>3</sub>, SO<sub>2</sub> and NO<sub>x</sub> by factors of 3.4, 2.4, 6.6 and 17, respectively. ~~In~~  
722 ~~the present study, additional mass between PM<sub>1</sub> and PM<sub>2.5</sub> accounted for only an additional 10 % of~~  
723 ~~aerosol mass (SI Sect. 2.1.2).~~ The lower EFs for these species implies that the CFFEPS EFs would not  
724 adequately capture their total emissions under smoldering conditions for the boreal fuel in the current  
725 measurement study.

726 For incorporation into numerical air quality models, total organic gas (TOG=NMOG+CH<sub>4</sub>)  
727 emissions are typically split into detailed chemical components using chemical mass speciation profiles,  
728 and converted to lumped chemical mechanism species. In the FireWork modelling system, the  
729 smoldering combustion TOG is split into components based on EPA's SPECIATEv4.5 profile (#95428)  
730 (US EPA 2016, Urbanski et al.; 2014 - supplement Table A.2, Boreal Forest Duff/Organic soil). This  
731 profile is ultimately compiled using laboratory data from Yokelson et al. (2013), Bertschi et al. (2003),  
732 and Yokelson et al. (1997) based entirely on U.S. fuel types. EFs in the present study were found to be  
733 generally lower than the laboratory-based EFs for 74 species in common ranging from factors of 1.7 to  
734 8.5 including for monoterpenes, formic acid, phenol, ~~and furan (Fig. 9d) and acetonitrile (Fig. 9d).~~ ~~The~~  
735 ~~largest differences (factors of 49-57) were observed for sesquiterpenes, benzofuran, and naphthalene.~~ A  
736 few species including furfural, propane nitrile and ethyl styrene are comparable, while isoprene, ~~and~~  
737 pyruvic acid, ~~acetylene and cyclohexene~~ are notably higher by factors 2 to 5.3.

738 For a research version of the FireWork system, the component speciation is mapped to the  
739 SAPRC-11 chemical mechanism species (Carter and Heo, 2013) with detailed oxygenated compounds  
740 and aromatic species, largely to better represent SOA formation processes. For comparison with the  
741 measurement derived speciation profile in this study, EFs were first mapped to SAPRC-11 species and  
742 ~~then~~ normalized by the total identified mass species fraction without unknowns to obtain mass fractions  
743 of relevant model mechanism species (Table S9). Comparing the normalized mass fractions for similar  
744 mechanism species (Fig. S142) showed a substantially ~~much~~ lower fractions of reactive alkaenes (ALK5)  
745 ~~and aromatics (ARO2) and a slightly higher acetic acid group (CCOOH)~~ with an estimated 5 % in this  
746 study compared to 28 % in the SPECIATEv4.5 wildfire smoldering profile. Mass fractions in this study  
747 are notably higher for the ACYL, ETHE, and ISOP lumped model species by factors of 13, 7 and 51. The  
748 mass fraction of CH<sub>4</sub> is also different with ~~2413~~ % of TOG in this study compared to 4 % from the  
749 ~~SAPRC-11SPECIATE4.5~~ profile. The measurement derived chemical speciation profile is expected to be  
750 ~~slightly~~ different from the average speciation profile from EPA's SPECIATEv4.5 due to ~~differences in~~  
751 ~~chemical species identification, fuel type, fire and measurement conditions, chemical species~~  
752 ~~identification~~ and ~~uncertainties on how measured compounds are mapped to lumped mechanism mapping~~  
753 ~~schemes~~ species. The emissions profile developed in the present study ~~is considered a more~~ can be used to  
754 improve ~~representative~~ predictions of wildfire smoldering emissions ~~profile~~ specific to the ~~wildfire~~  
755 ~~characterization for the~~ Canadian boreal forest ~~fuel~~.

756

### 757 3.5.2 Linking aircraft and satellite observations to evaluate modelled emissions diurnal variability

758 Wildfires generally exhibit a diurnal cycle with fire intensities maximizing late afternoon and  
759 diminishing at night having important implications for fire emissions (Chen et al., 2019). Evaluating  
760 modelled emissions throughout the diurnal cycle with observations is a critical step in verifying smoke  
761 predictions. Emissions models mostly parameterize diurnal fire emissions with prescribed profiles that  
762 distribute daily total emissions to hourly. In CFFEPs, a diurnal profile is applied to allocate daily burn  
763 area to hourly intervals, with highest activity in the late afternoon. The actual fuel consumed, and thus,

764 hourly emissions, is then calculated with depth of burn estimates driven by hourly meteorology (Chen et  
765 al., 2019). In Fig. 10, for the wildfire in the present study, the hourly CFFEPS-predicted emissions  
766 (orange dots) for selected compounds are shown between 2018-06-24 17:00 UTC and 2018-06-25 21:00  
767 UTC, spanning the aircraft sample time (red arrow at 15:00 UTC). After 21:00 UTC, the discrepancy  
768 between the CFFEPS-predicted emissions and FRP increased as a result of rain that passed through the  
769 area that is not considered in the model bottom-up emission estimates (not shown in the figure). The  
770 burning phases are outlined in the figure where flaming (light pink background) is assumed to occur when  
771 the atmospheric conditions alongside fire behaviour and emissions model outputs infer a fireline intensity  
772  $>4,000 \text{ kW m}^{-1}$  (Forestry Canada Fire Danger Rating Group, 1992), and a smoldering fire (blue  
773 background) for intensity  $<4000 \text{ kW m}^{-1}$ . The fire intensity distinction between flaming and smoldering  
774 roughly aligns with the observed minimum for this particular fire with the fire radiative power (FRP, grey  
775 dots) retrieval from the GOES-16 satellite sensor of 500 MW where smoldering occurs  $<500 \text{ MW}$  and  
776 flaming for  $>500 \text{ MW}$ . The 500 MW threshold over the approximately 1,700 ha of actively smoldering  
777 area observed by overnight VIIRS thermal detections gives an estimated energy density of  $0.29 \text{ MW ha}^{-1}$ .  
778 This energy density threshold for smoldering  $<0.29 \text{ MW ha}^{-1}$  found in this study is in agreement with FRP  
779 ~~per unit area corresponds with observed FRP for flaming combustion of  $>0.4 \text{ MW ha}^{-1}$  from lower~~  
780 ~~intensity flaming fires by O'Brien et al. (2015) who found flaming combustion at  $>0.4 \text{ MW ha}^{-1}$  for lower~~  
781 ~~intensity flaming fires and smoldering combustion at lower energy densities.~~ The FRP represents the sum  
782 over all hotspots of this fire for each 15-min observation period. Emission rates in metric tonnes per hour  
783 ( $\text{t h}^{-1}$ ) were derived from selected aircraft measurements using a mass balance method that was designed  
784 to estimate pollutant transfer rates through virtual screens using aircraft flight data (Gordon et al., 2015)  
785 (see SI Methods). Emission rates were ~~and~~ estimated to be  $29 \pm 2.1 \text{ t h}^{-1}$  for  $\text{PM}_{10}$ ,  $433 \pm 26.7 \text{ t h}^{-1}$  for CO,  
786  $0.65 \pm 0.03 \text{ t h}^{-1}$  for  $\text{NO}_x$  (as NO), and  $2.7 \pm 0.16 \text{ t h}^{-1}$  for  $\text{NH}_3$  (red arrows). Emission rates were also  
787 derived from satellite observations (black arrows) for CO,  $\text{NO}_x$ , and  $\text{NH}_3$ . Emissions of CO were  
788 estimated using a flux method as described in Stockwell et al. (2021) using TROPOMI satellite  
789 observations yielding  $1670 \pm 670 \text{ t h}^{-1}$  at 19:06 UTC and  $4050 \pm 1620 \text{ t h}^{-1}$  at 20:48 UTC.  $\text{NO}_x$  emissions

790 (9.1±3.4; scaled to t NO h<sup>-1</sup> at 19:06 UTC (not enough high-quality observations for the 20:48 UTC  
791 overpass) were derived from the TROPOMI NO<sub>2</sub> dataset using an Exponentially Modified Gaussian  
792 approach (Griffin et al., 2021). NH<sub>3</sub> emission rates (5.6±3.9 t h<sup>-1</sup>) were derived from CRIS satellite  
793 observations at the satellite overpass time of 19:00 UTC by applying a flux method (Adams et al., 2019).

794 The aircraft measurements were taken when the FRP was low reflecting a smoldering surface  
795 fire. However, the satellite overpass occurred ~4 hrs later than the aircraft measurements close to the  
796 FRP daily maximum, after which rain passed through the area. The CFFEPS model, exhibiting a  
797 prescribed diurnal pattern, captures the increase in NO<sub>x</sub> and NH<sub>3</sub> emissions between that derived from the  
798 aircraft and satellites transitioning from a smoldering to predominantly flaming fire; NO<sub>x</sub> emissions  
799 increased by a factor >10, whereas the NH<sub>3</sub> emissions increased by a factor of approximately 2. This is in  
800 agreement with recent laboratory measurements that found that the release of NO<sub>x</sub> is favoured during the  
801 flaming stage and the release of reduced forms of nitrogen, such as NH<sub>3</sub>, is favoured during the  
802 smoldering phase (Roberts et al., 2020) (also see Fig. 4). However, the CFFEPS CO emission rates do  
803 not track the increase in CO emissions between the aircraft-derived value and the two TROPOMI values,  
804 indicating that the CO EF for flaming is low in the model. This highlights the need to validate model  
805 emission rates with measurements to adjust and update the EFs accordingly.

806 ~~Using~~ The aircraft- and satellite-derived emission rates for CO, NO<sub>x</sub> and NH<sub>3</sub> were each ratioed  
807 ~~relative~~ to FRP (in units of t h<sup>-1</sup> MW<sup>-1</sup>, referred to as R<sub>species/FRP</sub>) to represent the ~~the~~ two end burning states  
808 ie. smoldering and flaming conditions. ~~, estimates of total emissions from this fire were made for CO,~~  
809 ~~NO<sub>x</sub> and NH<sub>3</sub>. R<sub>species/FRP</sub> values were estimated for the flaming and smoldering phases of the fire and it~~  
810 ~~was assumed that flaming occurred for FRP >500 MW and smoldering for FRP < 500 MW. Total~~  
811 ~~emissions were estimated by integrating the GOES FRP over the period June 24, 2018 06:24 17:00~~  
812 ~~UTC to June 25 2018 06:25 23:00 UTC (after which no more hot spots were detected by GOES and the~~  
813 ~~fire presumably extinguished), and applying the derived smoldering and flaming emission~~  
814 ~~ratio coefficients. It was assumed that flaming occurred for FRP >500 MW and smoldering for FRP <~~  
815 ~~500 MW. Emission rates coefficients were estimated with respect to the FRP for the flaming and~~



816 ~~smoldering phases of the fire.~~ The CO  $R_{\text{species}/\text{FRP}}$  ~~emission rates coefficients are~~ values were roughly  
817 twice as large during smoldering compared to flaming. For the ~~satellite emission estimates from the~~ two  
818 ~~satellite~~ overpasses during the flaming phase of the fire, the ~~CO- $R_{\text{CO}/\text{FRP}}$  values~~ ~~emission rates are~~ were  
819 ~~very similar and well~~ within the uncertainties (19:06 UTC  ~~$R_{\text{CO}/\text{FRP}}$~~   ~~$R_{\text{CO}}$~~   $=0.47 \pm 0.25$  ~~4.7~~  $\text{t h}^{-1} \text{MW}^{-1}$ ;  
820 20:48 UTC  ~~$R_{\text{CO}/\text{FRP}}$~~   ~~$R_{\text{CO}}$~~   $= 0.43 \pm 0.23$  ~~4.3~~  $\text{t h}^{-1} \text{MW}^{-1}$ ). The  ~~$R_{\text{NO}_x/\text{FRP}}$  value~~ ~~coefficient ratio~~ for  $\text{NO}_x$  is also  
821 twice as large for flaming compared to smoldering, and for  $\text{NH}_3$ , the ~~ratio- $R_{\text{NH}_3/\text{FRP}}$  value~~ ~~coefficient~~ is ~5  
822 times larger for smoldering than flaming. ~~Total emissions were then estimated by integrating the GOES~~  
823 ~~FRP over the period 2018-06-24 17:00 UTC to 2018-06-25 23:00 UTC (after which no more hot spots~~  
824 ~~were detected by GOES and the fire presumably extinguished), and applying the derived smoldering and~~  
825 ~~flaming  $R_{\text{species}/\text{FRP}}$  values.~~ Assuming that the fire went out when GOES did not observe any hot spots,  
826 total emissions for this fire of CO,  $\text{NO}_x$  and  $\text{NH}_3$  are estimated at ~~21,808~~  $22,000 \pm 8700$ , ~~104.1~~  $104 \pm 42$ , and  
827 ~~83.74~~  $83.74 \pm 33$  tonnes, respectively. If the fire is assumed to have continued burning when GOES did not  
828 detect any fire hot spots (between 22:00 - 04:00 UTC and 07:00 - 15:00 UTC, with an FRP of 150 MW  
829 (~GOES detection limit; Roberts et al., 2015), the emissions increase to ~~24,000~~  $24,000 \pm 9600$ , ~~106.4~~  $106 \pm 43.4$  and  
830 ~~97.798~~  $97.798 \pm 39$  tonnes, respectively, providing an upper limit of emissions. The combination of aircraft and  
831 satellite-derived emission estimates for multiple species helps to obtain the diurnal variability of  
832 emissions and to obtain more complete details on the emission information across different burning  
833 stages.

#### 834 4. Summary and Implications

835 This study provides detailed emissions information for boreal forest wildfires under ~~a~~ smoldering  
836 combustion ~~process~~ conditions. ~~Consistent with previous results,~~ ~~h~~ Highly speciated airborne  
837 measurements showed a large diversity of chemical classes highlighting the complexity of emissions.  
838 Despite extensive speciation across a range of NMOG volatilities, a substantial portion of  $\text{NMOG}_T$   
839 remained unidentified (~~46.447~~  $46.447 \pm 15$  to  $50 \pm 15$  %) and is expected to be comprised of more highly  
840 functionalized VOCs and I/SVOCs. Although these compounds are challenging to measure, their  
841 characterization is necessary to more fully understand particle-gas partitioning processes related to the

842 formation of SOA. Methodological advancements to achieve higher time resolution speciated  
843 measurements of I/SIVOCs would move towards further NMOG<sub>T</sub> closure and span a more complete  
844 range of volatilities. A detailed suite of EFs that were derived in this study **builds on previous work** (e.g.  
845 **Simpson et al., 2011; Andreae 2019**) and can be used to improve chemical speciation profiles that are  
846 relevant for air quality modelling of boreal forest wildfires. Aircraft-derived emission estimates were  
847 paired with those from satellite observations demonstrating their combined usefulness in assessing  
848 modelled emissions **diurnal** variability. As satellite instrumentation and methodologies advance, linking  
849 emissions derived from aircraft (and ground) observations for additional compounds will improve the  
850 ability to simulate and predict the diurnal variation in wildfire emissions.

851 ~~Although the measurements from this study provide a detailed characterization of a wildfire, the~~  
852 results **presented here** represent only one smoldering boreal forest wildfire **with limited in-plume**  
853 **sampling times**. Additional measurements are needed under a variety of fire conditions (combustion  
854 state, fire stage, biomass mixtures, time of day, etc) in order to elucidate the major controlling factors and  
855 improve statistical representation for constraining and modelling these sources. For example,  
856 measurements are needed to assess dark chemistry reactions in biomass burning emissions which have  
857 been shown to be important in the formation of OA (Kodros et al., 2020) and brown carbon (Palm et al.;  
858 2020). In addition, reduced actinic flux associated with high particle loadings in biomass burning  
859 emissions can influence plume chemistry (e.g. Juncosa-Calahorrano et al., 2021; Parrington et al., 2013).  
860 The emissions information in this work ~~can be used for~~ **will contribute to the** evaluation and  
861 improvements of models that are essential for reliable predictions of boreal forest wildfire pollutants and  
862 their downwind chemistry.

863

864

865

866 **Acknowledgements**

867

868 The authors acknowledge the significant technical and scientific contributions towards the success of this  
869 study from the AQRD technical and data teams, the NRC team, and excellent program management by  
870 Stewart Cober. **The authors would like to thank Mark Shephard for his work on the CRIS NH<sub>3</sub> retrievals  
871 and making those available.** JCD, MH, and DRG acknowledge support from the National Science  
872 Foundation (AGS1764126) and GERSTEL for their collaboration with the thermal desorption unit used  
873 as part of this study, and MH also acknowledges the Goldwater Scholarship Foundation. S.-M.L.  
874 acknowledges the support of the Ministry of Science and Technology of China (Grant  
875 2019YFC0214700).

876

#### 877 **Author contribution**

878 KH, SML, JL, MJW, JJBW, AL, PB, RLM, CM, AS, RMS, SM, AD, and MW all contributed to the  
879 collection and analyses of the aircraft observations in the field. JCD, MH, and DRG analysed the  
880 cartridge samples. ZO contributed to the analyses and created many of the figures. DT contributed to the  
881 analyses of the physical and combustion state of the wildfire fire. DG and EE provided the satellite  
882 observations and DG wrote the satellite comparison section. JC contributed to the comparisons with the  
883 model emission speciation profile. KH wrote the paper with input from all co-authors.

884

#### 885 **Competing interests**

886 The authors declare that they have no substantive conflicts of interest, but acknowledge that  
887 DRG and JL are associate editors with Atmospheric Chemistry and Physics.

888

#### 889 **Data availability**

890 All data used in this publication are available upon request.

891

892 **References**

- 893 Adams, C., McLinden, C. A., Shephard, M. W., Dickson, N., Dammers, E., Chen, J., Makar, P., Cady-  
 894 Pereira, K. E., Tam, N., Kharol, S. K., Lamsal, L. N., and Krotkov, N. A.: Satellite-derived emissions of  
 895 carbon monoxide, ammonia, and nitrogen dioxide from the 2016 Horse River wildfire in the Fort  
 896 McMurray area, *Atmos. Chem. Phys.*, 19, 2577-2599, <https://doi.org/10.5194/acp-19-2577-2019>, 2019.  
 897
- 898 Ahern, A. T., Robinson, E. S., Tkacik, D. S., Saleh, R., Hatch, L. E., Barsanti, K. C., Stockwell, C. E.,  
 899 Yokelson, R. J., Presto, A. A., Robinson, A. L., Sullivan, R. C., and Donahue, N. M.: Production of  
 900 secondary organic aerosol during aging of biomass burning smoke from fresh fuels and its relationship to  
 901 VOC Precursors, *J. Geophys. Res.-Atmos*, 124, 3583-3606, <https://doi.org/10.1029/2018JD029068>, 2019.  
 902
- 903 Akagi, S. K., Yokelson, R. J., Wiedinmyer, C., Alvarado, M. J., Reid, J. S., Karl, T., Crounse, J. D., and  
 904 Wennberg, P. O.: Emission factors for open and domestic biomass burning for use in atmospheric models,  
 905 *Atmos. Chem. Phys.*, 11, 4039-4072, <https://doi.org/10.5194/acp-11-4039-2011>, 2011.  
 906
- 907 Akagi, S. K., Craven, J. S., Taylor, J. W., McMeeking, G. R., Yokelson, R. J., Burling, I. R., Urbanski, S.  
 908 P., Wold, C. E., Seinfeld, J. H., Coe, H., Alvarado, M. J., and Weise, D. R.: Evolution of trace gases and  
 909 particles emitted by a chaparral fire in California, *Atmos. Chem. Phys.*, 12, 1397-1421,  
 910 <https://doi.org/10.5194/acp-12-1397-2012>, 2012.  
 911
- 912 Akagi, S. K., Yokelson, R. J., Burling, I. R., Meinardi, S., Simpson, I., Blake, D. R., McMeeking, G. R.,  
 913 Sullivan, A., Lee, T., Kreidenweis, S., Urbanski, S., Reardon, J., Griffith, D. W. T., Johnson, T. J., and  
 914 Weise, D. R.: Measurements of reactive trace gases and variable O<sub>3</sub> formation rates in some South  
 915 Carolina biomass burning plumes, *Atmos. Chem. Phys.*, 13, 1141-1165, <https://doi.org/10.5194/acp-13-1141-2013>, 2013.  
 916
- 917 Alvarado, M. J., Logan, J. A., Mao, J., Apel, E., Riemer, D., Blake, D., Cohen, R. C., Min, K. E., Perring,  
 918 A. E., Browne, E. C., Wooldridge, P. J., Diskin, G. S., Sachse, G. W., Fuelberg, H., Sessions, W. R.,  
 919 Harrigan, D. L., Huey, G., Liao, J., Case-Hanks, A., Jimenez, J. L., Cubison, M. J., Vay, S. A.,  
 920 Weinheimer, A. J., Knapp, D. J., Montzka, D. D., Flocke, F. M., Pollack, I. B., Wennberg, P. O., Kurten,  
 921 A., Crounse, J., Clair, J. M. S., Wisthaler, A., Mikoviny, T., Yantosca, R. M., Carouge, C. C., and Le  
 922 Sager, P.: Nitrogen oxides and PAN in plumes from boreal fires during ARCTAS-B and their impact on  
 923 ozone: an integrated analysis of aircraft and satellite observations, *Atmos. Chem. Phys.*, 10, 9739-9760,  
 924 <https://doi.org/10.5194/acp-10-9739-2010>, 2010.  
 925
- 926
- 927 Andreae, M. O.: Emission of trace gases and aerosols from biomass burning – an updated assessment,  
 928 *Atmos. Chem. Phys.*, 19, 8523-8546, <https://doi.org/10.5194/acp-19-8523-2019>, 2019. Biomass burning  
 929 emission factors [https://edmond.mpdl.mpg.de/imeji/collection/op2vVE8m0us\\_gcGC](https://edmond.mpdl.mpg.de/imeji/collection/op2vVE8m0us_gcGC), ver 14 Apr 2021.  
 930
- 931 Andreae, M. O. and Merlet, P.: Emission of trace gases and aerosols from biomass burning, *Global*  
 932 *Biogeochem. Cy.*, 15, 955-966, <https://doi.org/10.1029/2000GB001382>, 2001.  
 933
- 934 Baumgardner, D., Kok, G., and Raga, G.: Warming of the Arctic lower stratosphere by light absorbing  
 935 particles, *Geophys. Res. Lett.*, 31, L06117, <https://doi.org/10.1029/2003GL018883>, 2004.  
 936
- 937 Bertschi, I., Yokelson, R. J., Ward, D. E., Babbitt, R. E., Susott, R. A., Goode, J. G., and Hao, W. M.:  
 938 Trace gas and particle emissions from fires in large diameter and belowground biomass fuels, *J. Geophys.*  
 939 *Res.-Atmos*, 108, 8472, <https://doi.org/10.1029/2002JD002100>, 2003.  
 940

941 Bond-Lamberty, B., Gower, S. T., Wang, C., Cyr, P., and Veldhuis, H.: Nitrogen dynamics of a boreal  
942 black spruce wildfire chronosequence, *Biogeochemistry*, 81, 1-16, [https://doi.org/10.1007/s10533-006-](https://doi.org/10.1007/s10533-006-9025-7)  
943 9025-7, 2006.  
944  
945 Bruns, E. A., El Haddad, I., Slowik, J. G., Kilic, D., Klein, F., Baltensperger, U., and Prevot, A. S. H.:  
946 Identification of significant precursor gases of secondary organic aerosols from residential wood  
947 combustion, *Sci. Rep.*, 6, <https://doi.org/10.1038/srep27881>, 2016.  
948  
949 Burling, I. R., Yokelson, R. J., Akagi, S. K., Urbanski, S. P., Wold, C. E., Griffith, D. W. T., Johnson, T.  
950 J., Reardon, J., and Weise, D. R.: Airborne and ground-based measurements of the trace gases and  
951 particles emitted by prescribed fires in the United States, *Atmos. Chem. Phys.*, 11, 12197-12216,  
952 <https://doi.org/10.5194/acp-11-12197-2011>, 2011.  
953  
954 Bush, E. and Lemmen, D. S.: Canada's changing climate report, Government of Canada, Ottawa, ON.,  
955 444 pp., [www.ChangingClimate.ca/CCCR2019](http://www.ChangingClimate.ca/CCCR2019), 2019.  
956  
957 Campos, I., Abrantes, N., Pereira, P., Micaelo, A. C., Vale, C., and Keizer, J. J.: Forest fires as potential  
958 triggers for production and mobilization of polycyclic aromatic hydrocarbons to the terrestrial ecosystem,  
959 *Land Degrad. Dev.*, 30, 2360-2370, <https://doi.org/10.1002/ldr.3427>, 2019.  
960  
961 Carter, W. P. L. and Heo, G.: Development of revised SAPRC aromatics mechanisms, *Atmos. Environ.*,  
962 77, 404-414, <https://doi.org/10.1016/j.atmosenv.2013.05.021>, 2013.  
963  
964 **Carter, M.C., and Foster, C.D., Prescribed burning and productivity in southern pine forests: a review:**  
965 ***Forest Ecol. Mgmt.*, 191, 93-109, 2004.**  
966  
967 Cascio, W. E.: Wildland fire smoke and human health, *Sci. Total Environ.*, 624, 586-595,  
968 <https://doi.org/10.1016/j.scitotenv.2017.12.086>, 2018.  
969  
970 Chen, J., Anderson, K., Pavlovic, R., Moran, M. D., Englefield, P., Thompson, D. K., Munoz-Alpizar, R.,  
971 and Landry, H.: The FireWork v2.0 air quality forecast system with biomass burning emissions from the  
972 Canadian Forest Fire Emissions Prediction System v2.03, *Geosci. Model Dev.*, 12, 3283-3310,  
973 <https://doi.org/10.5194/gmd-12-3283-2019>, 2019.  
974  
975 Cherry, N. and Haynes, W.: Effects of the Fort McMurray wildfires on the health of evacuated workers:  
976 follow-up of 2 cohorts, *Can. Med. Assoc. J.*, 5, E638-E645, <https://doi.org/10.9778/cmajo.20170047>,  
977 2017.  
978  
979 Ciccioli, P., Centritto, M., and Loreto, F.: Biogenic volatile organic compound emissions from vegetation  
980 fires, *Plant, Cell Environ.*, 37, 1810-1825, <https://doi.org/10.1111/pce.12336>, 2014.  
981  
982 Coggon, M. M., Lim, C. Y., Koss, A. R., Sekimoto, K., Yuan, B., Gilman, J. B., Hagan, D. H., Selimovic,  
983 V., Zarzana, K. J., Brown, S. S., Roberts, J. M., Müller, M., Yokelson, R., Wisthaler, A., Krechmer, J. E.,  
984 Jimenez, J. L., Cappa, C., Kroll, J. H., de Gouw, J., and Warneke, C.: OH chemistry of non-methane  
985 organic gases (NMOGs) emitted from laboratory and ambient biomass burning smoke: evaluating the  
986 influence of furans and oxygenated aromatics on ozone and secondary NMOG formation, *Atmos. Chem.*  
987 *Phys.*, 19, 14875-14899, <https://doi.org/10.5194/acp-19-14875-2019>, 2019.  
988  
989 Cole, A. S., Steffen, A., Eckley, C. S., Narayan, J., Pilote, M., Tordon, R., Graydon, J. A., St. Louis, V.  
990 L., Xu, X., and Branfireun, B. A.: A survey of mercury in air and precipitation across Canada: Patterns  
991 and trends, *Atmosphere*, 5, 635-668, <https://doi.org/10.3390/atmos5030635>, 2014.

992  
993 Cubison, M.J., Ortega, A.M., Haves, P.L., Farmer, D.K., Day, D., Lechner, M.J., Brune, W.H., Apel, E.,  
994 Diskin, G.S., Fisher, J.A., Fuelberg, H.E., Hecobian, A., Knapp, D.J., Mikoviny, T., Riemer, D., Sachse,  
995 G.W., Sessions, W., Weber, R.J., Weinheimer, A.J., Wisthaler, A., and J.L. Jimenez: Effects of aging on  
996 organic aerosol from open biomass burning smoke in aircraft and laboratory studies, *Atmos. Chem. Phys.*,  
997 11, 12049-12064, doi:10.5194/acp-11-12049-2011, 2011.  
998  
999 de Gouw, J. A., Warneke, C., Stohl, A., Wollny, A. G., Brock, C. A., Cooper, O. R., Holloway, J. S.,  
1000 Trainer, M., Fehsenfeld, F. C., Atlas, E. L., Donnelly, S. G., Stroud, V., and Lueb, A.: The VOC  
1001 composition of merged and aged forest fire plumes from Alaska and Western Canada, *J. Geophys. Res.-*  
1002 *Atmos*, 111, D10303, <https://doi.org/10.1029/2005JD006175>, 2006.  
1003  
1004 de Groot, W. J., Pritchard, J. M., and Lynham, T. J.: Forest floor fuel consumption and carbon emissions  
1005 in Canadian boreal forest fires, *Can. J. Forest Res.*, 39, 367-382, <https://doi.org/10.1139/x08-192>, 2009.  
1006  
1007 Decker, Z. C. J., Zarzana, K. J., Coggon, M., Min, K.-E., Pollack, I., Ryerson, T. B., Peischl, J., Edwards,  
1008 P., Dubé, W. P., Markovic, M. Z., Roberts, J. M., Veres, P. R., Graus, M., Warneke, C., de Gouw, J.,  
1009 Hatch, L. E., Barsanti, K. C., and Brown, S. S.: Nighttime chemical transformation in biomass burning  
1010 plumes: A box model analysis Initialized with aircraft observations, *Environ. Sci. Technol.*, 53, 2529-  
1011 2538, <https://doi.org/10.1021/acs.est.8b05359>, 2019.  
1012  
1013 Decker, Z.C., Wang, S., Novel analysis to quantify plume crosswind heterogeneity applied to biomass  
1014 burning smoke, EST, 2021.  
1015  
1016 Ditto, J. C., Joo, T., Slade, J. H., Shepson, P. B., Ng, N. L., and Gentner, D. R.: Nontargeted Tandem  
1017 Mass Spectrometry Analysis Reveals Diversity and Variability in Aerosol Functional Groups across  
1018 Multiple Sites, Seasons, and Times of Day, *Environmental Science and Technology Letters*, 7, 60-  
1019 69, <https://doi.org/10.1021/acs.estlett.9b00702>, 2020.  
1020  
1021 Ditto, J. C., He, M., Hass-Mitchell, T. N., Moussa, S. G., Hayden, K., Li, S. M., Liggio, J., Leithead, A.,  
1022 Lee, P., Wheeler, M. J., Wentzell, J. J. B., and Gentner, D. R.: Atmospheric evolution of emissions from a  
1023 boreal forest fire: the formation of highly functionalized oxygen-, nitrogen-, and sulfur-containing organic  
1024 compounds, *Atmos. Chem. Phys.*, 21, 255-267, <https://doi.org/10.5194/acp-21-255-2021>, 2021.  
1025  
1026 Ditto, J. C., Machesky, J., and Gentner, D. R.: Analysis of reduced and oxidized nitrogen-containing  
1027 organic compounds at a coastal site in summer and winter, *Atmos. Chem. Phys.*, 22, 3045-  
1028 3065, <https://doi.org/10.5194/acp-22-3045-2022>, 2022.  
1029  
1030 Donahue, N. M., Epstein, S. A., Pandis, S. N., and Robinson, A. L.: A two-dimensional volatility basis  
1031 set: 1. organic-aerosol mixing thermodynamics, *Atmos. Chem. Phys.*, 11, 3303-3318,  
1032 <https://doi.org/10.5194/acp-11-3303-2011>, 2011.  
1033  
1034 EPA: Air method, toxic organics-15 (TO-15): Compendium of methods for the determination of toxic  
1035 organic compounds in ambient air, second edition: Determination of volatile organic compounds (VOCs)  
1036 in air collected in specially-prepared canisters and analyzed by gas chromatography/mass spectrometry  
1037 (GC/MS)." EPA 625/R-96/010b, 1999.  
1038  
1039 Finlay, S. E., Moffat, A., Gazzard, R., Baker, D., and Murray, V.: Health impacts of wildfires, *PLoS*  
1040 *Curr.*, 4, e4f959951cce959952c, <https://doi.org/10.1371/4f959951cce2c>, 2012.  
1041

1042 Forestry Canada Fire Danger Rating Group: Development and structure of the Canadian Forest Fire  
1043 Behaviour Prediction System, Forestry Canada, Headquarters, Fire Danger Group and Science and  
1044 Sustainable Development Directorate, Ottawa, Information Report ST-X-3, 64 p., 992.  
1045

1046 Garofalo, L. A., Pothier, M. A., Levin, E. J. T., Campos, T., Kreidenweis, S. M., and Farmer, D. K.:  
1047 Emission and evolution of submicron organic aerosol in smoke from wildfires in the Western United  
1048 States, *ACS Earth Space Chem.*, 3, 1237-1247, <https://doi.org/10.1021/acsearthspacechem.9b00125>,  
1049 2019.  
1050

1051 Gilman, J. B., Lerner, B. M., Kuster, W. C., Goldan, P. D., Warneke, C., Veres, P. R., Roberts, J. M., de  
1052 Gouw, J. A., Burling, I. R., and Yokelson, R. J.: Biomass burning emissions and potential air quality  
1053 impacts of volatile organic compounds and other trace gases from fuels common in the US, *Atmos.*  
1054 *Chem. Phys.*, 15, 13915-13938, <https://doi.org/10.5194/acp-15-13915-2015>, 2015.  
1055

1056 Goode, J. G., Yokelson, R. J., Ward, D. E., Susott, R. A., Babbitt, R. E., Davies, M. A., and Hao, W. M.:  
1057 Measurements of excess O<sub>3</sub>, CO<sub>2</sub>, CO, CH<sub>4</sub>, C<sub>2</sub>H<sub>4</sub>, C<sub>2</sub>H<sub>2</sub>, HCN, NO, NH<sub>3</sub>, HCOOH, CH<sub>3</sub>COOH, HCHO,  
1058 and CH<sub>3</sub>OH in 1997 Alaskan biomass burning plumes by airborne fourier transform infrared spectroscopy  
1059 (AFTIR), *J. Geophys. Res.*, 105, 22147-22166, <https://doi.org/10.1029/2000JD900287>, 2000.  
1060

1061 Gordon, M., Li, S. M., Staebler, R., Darlington, A., Hayden, K., O'Brien, J., and Wolde, M.: Determining  
1062 air pollutant emission rates based on mass balance using airborne measurement data over the Alberta oil  
1063 sands operations, *Atmos. Meas. Tech.*, 8, 3745-3765, <https://doi.org/10.5194/amt-8-3745-2015>, 2015.  
1064

1065 Griffin, D., McLinden, C. A., Dammers, E., Adams, C., Stockwell, C., Warneke, C., Bourgeois, I.,  
1066 Peischl, J., Ryerson, T. B., Zarzana, K. J., Rowe, J. P., Volkamer, R., Knote, C., Kille, N., Koenig, T. K.,  
1067 Lee, C. F., Rollins, D., Rickly, P. S., Chen, J., Fehr, L., Bourassa, A., Degenstein, D., Hayden, K.,  
1068 Mihele, C., Wren, S. N., Liggio, J., Akingunola, A., and Makar, P.: Biomass burning nitrogen dioxide  
1069 emissions derived from space with TROPOMI: methodology and validation, *Atmos. Meas. Tech.*  
1070 *Discuss.* [preprint], <https://doi.org/10.5194/amt-2021-223>, in review, 2021.  
1071

1072 Griffith, D. W. T., Mankin, W. G., Coffey, M. T., Ward, D. E., and Riebau, A.: FTIR remote sensing of  
1073 biomass burning emissions of CO<sub>2</sub>, CO, CH<sub>4</sub>, CH<sub>2</sub>O, NO, NO<sub>2</sub>, NH<sub>3</sub>, and N<sub>2</sub>O, in: *Global Biomass*  
1074 *Burning: Atmospheric, Climatic, and Biospheric Implications*, edited by: Levine, J. S., MIT Press,  
1075 Cambridge, MA, United States, 230-241, 1991.  
1076

1077 Guérette, E. A., Paton-Walsh, C., Desservettaz, M., Smith, T. E. L., Volkova, L., Weston, C. J., and  
1078 Meyer, C. P.: Emissions of trace gases from Australian temperate forest fires: Emission factors and  
1079 dependence on modified combustion efficiency, *Atmos. Chem. Phys.*, 18, 3717-3735,  
1080 <https://doi.org/10.5194/acp-18-3717-2018>, 2018.  
1081

1082 Hatch, L. E., Luo, W., Pankow, J. F., Yokelson, R. J., Stockwell, C. E., and Barsanti, K. C.: Identification  
1083 and quantification of gaseous organic compounds emitted from biomass burning using two-dimensional  
1084 gas chromatography–time-of-flight mass spectrometry, *Atmos. Chem. Phys.*, 15, 1865-1899,  
1085 <https://doi.org/10.5194/acp-15-1865-2015>, 2015.  
1086

1087 Hatch, L. E., Rivas-Ubach, A., Jen, C. N., Lipton, M., Goldstein, A. H., and Barsanti, K. C.:  
1088 Measurements of I/SVOCs in biomass-burning smoke using solid-phase extraction disks and two-  
1089 dimensional gas chromatography, *Atmos. Chem. Phys.*, 18, 17801-17817, [https://doi.org/10.5194/acp-18-](https://doi.org/10.5194/acp-18-17801-2018)  
1090 [17801-2018](https://doi.org/10.5194/acp-18-17801-2018), 2018.  
1091

1092 Hatch, L. E., Yokelson, R. J., Stockwell, C. E., Veres, P. R., Simpson, I. J., Blake, D. R., Orlando, J. J.,  
1093 and Barsanti, K. C.: Multi-instrument comparison and compilation of non-methane organic gas emissions  
1094 from biomass burning and implications for smoke-derived secondary organic aerosol precursors, *Atmos.*  
1095 *Chem. Phys.*, 17, 1471-1489, <https://doi.org/10.5194/acp-17-1471-2017>, 2017.

1096  
1097 Hatch, L. E., Jen, C. N., Kreisberg, N. M., Selimovic, V., Yokelson, R. J., Stamatis, C., York, R. A.,  
1098 Foster, D., Stephens, S. L., Goldstein, A. H., and Barsanti, K. C.: Highly speciated measurements of  
1099 terpenoids emitted from laboratory and mixed-conifer forest prescribed fires, *Environ. Sci. Technol.*, 53,  
1100 9418-9428, <https://doi.org/10.1021/acs.est.9b02612>, 2019.

1101  
1102 Hecobian, A., Liu, Z., Hennigan, C. J., Huey, L. G., Jimenez, J. L., Cubison, M. J., Vay, S., Diskin, G. S.,  
1103 Sachse, G. W., Wisthaler, A., Mikoviny, T., Weinheimer, A. J., Liao, J., Knapp, D. J., Wennberg, P. O.,  
1104 Kürten, A., Crounse, J. D., Clair, J. S., Wang, Y., and Weber, R. J.: Comparison of chemical  
1105 characteristics of 495 biomass burning plumes intercepted by the NASA DC-8 aircraft during the  
1106 ARCTAS/CARB-2008 field campaign, *Atmos. Chem. Phys.*, 11, 13325-13337,  
1107 <https://doi.org/10.5194/acp-11-13325-2011>, 2011.

1108  
1109 Hodshire, A. L., Akherati, A., Alvarado, M. J., Brown-Steiner, B., Jathar, S. H., Jimenez, J. L.,  
1110 Kreidenweis, S. M., Lonsdale, C. R., Onasch, T. B., Ortega, A. M., and Pierce, J. R.: Aging effects on  
1111 biomass burning aerosol mass and composition: A critical review of field and laboratory studies, *Environ.*  
1112 *Sci. Technol.*, 53, 10007-10022, <https://doi.org/10.1021/acs.est.9b02588>, 2019.

1113  
1114 Hosseini, S., Urbanski, S., Dixit, P., Li, Q., Burling, I., Yokelson, R., Johnson, T.E., Sharivastava, M.,  
1115 Jung, H., Weise, D.R., Miller, W., and Cocker, D.: Laboratory characterization of PM emissions from  
1116 combustion of wildland biomass fuels, *J. Geophys. Res.*, 118, 9914-9929,  
1117 <https://doi.org/10.1002/jgrd.50481>, 2013.

1118  
1119 Jia, Y., Yu, G., Gao, Y., He, N., Wang, Q., Jiao, C., and Zuo, Y.: Global inorganic nitrogen dry  
1120 deposition inferred from ground- and space-based measurements, *Sci. Rep.*, 6, 19810,  
1121 <https://doi.org/10.1038/srep19810>, 2016.

1122  
1123 Johnstone, J. F., Hollingsworth, T. N., Chapin III, F. S., and Mack, M. C.: Changes in fire regime break  
1124 the legacy lock on successional trajectories in Alaskan boreal forest, *Global Change Biol.*, 16, 1281-1295,  
1125 <https://doi.org/10.1111/j.1365-2486.2009.02051.x>, 2010.

1126  
1127 Jolley, M.D., Coe, H., McFiggans, G., Taylor, J.W., O'Shea, S.J., Le Breton, M., Bauguitte, S.J.-B.,  
1128 Moller, S., Di Carlo, P., Aruffo, E., Palmer, P.I., Lee, J.D., Percival, C.J., and Gallagher, M.W.:  
1129 Properties and evolution of biomass burning organic aerosol from Canadian boreal forest fires, *Atmos.*  
1130 *Chem. Phys.*, 15, 3077-3095, doi:10.5194/acp-15-3077-2015, 2015.

1131  
1132 Juncosa Calahorrano, J. F., Lindaas, J., O'Dell, K., Palm, B. B., Peng, Q., Flocke, F., Pollack, I. B.,  
1133 Garofalo, L. A., Farmer, D. K., Pierce, J. R., Collett Jr., J. L., Weinheimer, A., Campos, T., Hornbrook,  
1134 R. S., Hall, S. R., Ullmann, K., Pothier, M. A., Apel, E. C., Permar, W., Hu, L., Hills, A. J., Montzka, D.,  
1135 Tyndall, G., Thornton, J. A., and Fischer, E. V.: Daytime oxidized reactive nitrogen partitioning in  
1136 western U.S. wildfire smoke plumes, *J. Geophys. Res.-Atmos*, 126, e2020JD033484,  
1137 <https://doi.org/10.1029/2020JD033484>, 2021.

1138  
1139 Kaiser, J. W., Heil, A., Andreae, M. O., Benedetti, A., Chubarova, N., Jones, L., Morcrette, J.-J.,  
1140 Razinger, M., Schultz, M. G., Suttie, M., and van der Werf, G. R.: Biomass burning emissions estimated  
1141 with a global fire assimilation system based on observed fire radiative power, *Biogeosciences*, 9, 527–  
1142 554, <https://doi.org/10.5194/bg-9-527-2012>, 2012.



1143  
1144 Kallenborn, R., Halsall, C., Dellong, M., and Carlsson, P.: The influence of climate change on the global  
1145 distribution and fate processes of anthropogenic persistent organic pollutants, *J. Environ. Monitor.*, 14,  
1146 2854-2869, <https://doi.org/10.1039/c2em30519d>, 2012.

1147  
1148 Khare, P., Marcotte, A., Sheu, R., Walsh, A. N., Ditto, J. C., and Gentner, D. R.: Advances in offline  
1149 approaches for trace measurements of complex organic compound mixtures via soft ionization and high-  
1150 resolution tandem mass spectrometry, *J. Chromatogr. A*, 1598, 163-  
1151 174, <https://doi.org/10.1016/j.chroma.2019.03.037>, 2019.

1152  
1153 Kodros, J. K., Papanastasiou, D. K., Paglione, M., Masiol, M., Squizzato, S., Florou, K., Skyllakou, K.,  
1154 Kaltsonoudis, C., Nenes, A., and Pandis, S. N.: Rapid dark aging of biomass burning as an overlooked  
1155 source of oxidized organic aerosol, *P. Natl. Acad. Sci. USA*, 117, 33028-33033,  
1156 <https://doi.org/10.1073/pnas.2010365117>, 2020.

1157  
1158 Kondo, Y., Sahu, L., Moteki, N., Khan, F., Takegawa, N., Liu, X., Koike, M., and Miyakawa, T.:  
1159 Consistency and traceability of black carbon measurements made by laser-induced incandescence,  
1160 thermal-optical transmittance, and filter-based photo-absorption techniques, *Aerosol Sci. Tech.*, 45, 295-  
1161 312, <https://doi.org/10.1080/02786826.2010.533215>, 2011.

1162  
1163 Koss, A. R., Sekimoto, K., Gilman, J. B., Selimovic, V., Coggon, M. M., Zarzana, K. J., Yuan, B.,  
1164 Lerner, B. M., Brown, S. S., Jimenez, J. L., Krechmer, J., Roberts, J. M., Warneke, C., Yokelson, R. J.,  
1165 and de Gouw, J.: Non-methane organic gas emissions from biomass burning: identification,  
1166 quantification, and emission factors from PTR-ToF during the FIREX 2016 laboratory experiment,  
1167 *Atmos. Chem. Phys.*, 18, 3299-3319, <https://doi.org/10.5194/acp-18-3299-2018>, 2018.

1168  
1169 Kotchenruther, R. A. and Hobbs, P. V.: Humidification factors of aerosols from biomass burning in  
1170 Brazil, *J. Geophys. Res.-Atmos*, 103, 32081-32089, <https://doi.org/10.1029/98JD00340>, 1998.

1171  
1172 Kou-Giesbrecht, S. and Menge, D.: Nitrogen-fixing trees could exacerbate climate change under elevated  
1173 nitrogen deposition, *Nat. Commun.*, 10, 1493, <https://doi.org/10.1038/s41467-019-09424-2>, 2019.

1174  
1175 Kumar, V., Chandra, B. P., and Sinha, V.: Large unexplained suite of chemically reactive compounds  
1176 present in ambient air due to biomass fires, *Sci. Rep.*, 8, 626, [https://doi.org/10.1038/s41598-017-19139-](https://doi.org/10.1038/s41598-017-19139-3)  
1177 3, 2018.

1178  
1179 Laborde, M., Mertes, P., Zieger, P., Dommen, J., Baltensperger, U., and Gysel, M.: Sensitivity of the  
1180 Single Particle Soot Photometer to different black carbon types, *Atmos. Meas. Tech.*, 5, 1031-1043,  
1181 <https://doi.org/10.5194/amt-5-1031-2012>, 2012.

1182  
1183 Landis, M. S., Edgerton, E. S., White, E. M., Wentworth, G. R., Sullivan, A. P., and Dillner, A. M.: The  
1184 impact of the 2016 Fort McMurray Horse River Wildfire on ambient air pollution levels in the Athabasca  
1185 Oil Sands Region, Alberta, Canada, *Sci. Total Environ.*, 618, 1665-1676,  
1186 <https://doi.org/10.1016/j.scitotenv.2017.10.008>, 2018.

1187  
1188 ~~Lapina, K., Honrath, R. E., Owen, R. C., Val Martin, M., Hyer, E. J., and Fialho, P.: Late summer~~  
1189 ~~changes in burning conditions in the boreal regions and their implications for NO<sub>x</sub> and CO emissions~~  
1190 ~~from boreal fires, *J. Geophys. Res.*, 113, D11304, <https://doi.org/10.1029/2007JD009421>, 2008.~~

1191  
1192 Lee, T., Sullivan, A. P., Mack, L., Jimenez, J. L., Kreidenweis, S. M., Onasch, T. B., Worsnop, D. R.,  
1193 Malm, W., Wold, C. E., Hao, W. M., and Collett Jr, J. L.: Chemical smoke marker emissions during

1194 flaming and smoldering phases of laboratory open burning of wildland fuels, *Aerosol Sci. Tech.*, 44, i-v,  
1195 <https://doi.org/10.1080/02786826.2010.499884>, 2010.  
1196  
1197 Leifer, I., Melton, C. Tratt, D.M., Buckland, K.N., Clarisse, L., Coheur, P., Frash, J., Gupta, M., Johnson,  
1198 P.D., Leen, J.B., Van Damme, M., Whitburn, S., and Yurganov, L.: Remote sensing and in situ  
1199 measurements of methane and ammonia emissions from a megacity dairy complex: Chino, CA, *Environ.*  
1200 *Poll.*, 221, 37-51, <https://doi.org/10.1016/j.envpol.2016.09.083>, 2017.  
1201  
1202 Lerner, B. M., Gilman, J. B., Aikin, K. C., Atlas, E. L., Goldan, P. D., Graus, M., Hendershot, R.,  
1203 Isaacman-VanWertz, G. A., Koss, A., Kuster, W. C., Lueb, R. A., McLaughlin, R. J., Peischl, J., Sueper,  
1204 D., Ryerson, T. B., Tokarek, T. W., Warneke, C., Yuan, B., and de Gouw, J. A.: An improved, automated  
1205 whole air sampler and gas chromatography mass spectrometry analysis system for volatile organic  
1206 compounds in the atmosphere, *Atmos. Meas. Tech.*, 10, 291-313, [https://doi.org/10.5194/amt-10-291-](https://doi.org/10.5194/amt-10-291-2017)  
1207 [2017](https://doi.org/10.5194/amt-10-291-2017), 2017.  
1208  
1209 ~~Li, K., Liggio, J., Han, C., Liu, Q., Moussa, S. G., Lee, P., and Li, S. M.: Understanding the impact of~~  
1210 ~~high NO<sub>x</sub> conditions on the formation of secondary organic aerosol in the photooxidation of oil sand-~~  
1211 ~~related precursors, *Environ. Sci. Technol.*, 53, 14420-14429, <https://doi.org/10.1021/acs.est.9b05404>,~~  
1212 ~~2019.~~  
1213  
1214 ~~Li, K., Wentzell, J. J. B., Liu, Q., Leithead, A., Moussa, S. G., Wheeler, M. J., Han, C., Lee, P., Li, S. M.,~~  
1215 ~~and Liggio, J.: Evolution of atmospheric total organic carbon from petrochemical mixtures, *Environ. Sci.*~~  
1216 ~~*Technol.*, 55, 12841-12851, <https://doi.org/10.1021/acs.est.1c02620>, 2021.~~  
1217  
1218 ~~Li, S. M., Leithead, A., Moussa, S. G., Liggio, J., Moran, M. D., Wang, D., Hayden, K., Darlington, A.,~~  
1219 ~~Gordon, M., Staebler, R., Makar, P. A., Stroud, C. A., McLaren, R., Liu, P. S. K., O'Brien, J.,~~  
1220 ~~Mittermeier, R. L., Zhang, J., Marson, G., Cober, S. G., Wolde, M., and Wentzell, J. J. B.: Differences~~  
1221 ~~between measured and reported volatile organic compound emissions from oil sands facilities in Alberta,~~  
1222 ~~Canada, *P. Natl. Acad. Sci. USA*, 114, E3756-E3765, <https://doi.org/10.1073/pnas.1617862114>, 2017.~~  
1223  
1224 Li, Y., Poschl, U., and Shiraiwa, M.: Molecular corridors and parameterizations of volatility in the  
1225 chemical evolution of organic aerosols, *Atmos. Chem. Phys.*, 16, 3327-3344, [https://doi.org/10.5194/acp-](https://doi.org/10.5194/acp-16-3327-2016)  
1226 [16-3327-2016](https://doi.org/10.5194/acp-16-3327-2016), 2016.  
1227  
1228 Lindaas, J., Pollack, I. B., Garofalo, L. A., Pothier, M. A., Farmer, D. K., Kreidenweis, S. M., Campos, T.  
1229 L., Flocke, F., Weinheimer, A. J., Montzka, D. D., Tyndall, G. S., Palm, B. B., Peng, Q., Thornton, J. A.,  
1230 Permar, W., Wielgasz, C., Hu, L., Ottmar, R. D., Restaino, J. C., Hudak, A. T., Ku, I.-T., Zhou, Y., Sive,  
1231 B. C., Sullivan, A., Collett Jr, J. L., and Fischer, E. V.: Emissions of reactive nitrogen from western U.S.  
1232 wildfires during summer 2018, *J. Geophys. Res.-Atmos*, 125, e2020JD032657,  
1233 <https://doi.org/10.1029/2020JD032657>, 2020.  
1234  
1235 ~~Liu, Y., Liggio, J., Hayden, K., Mihele, C., Wentzell, J., Darlington, A., Moussa, S., Huang, Y., Xie, C.,~~  
1236 ~~Yang, Y., Zhang, Y., Han, T., Wolde, M., and Li, S. M.: Quantifying the interplay of physical and~~  
1237 ~~chemical evolution of oxidized reactive nitrogen in a boreal forest fire plume using airborne~~  
1238 ~~measurements, in preparation for submission to *ES&T*, 2022.~~  
1239  
1240 Liu, X., Huey, L. G., Yokelson, R. J., Selimovic, V., Simpson, I. J., Müller, M., Jimenez, J. L.,  
1241 Campuzano-Jost, P., Beyersdorf, A. J., Blake, D. R., Butterfield, Z., Choi, Y., Crounse, J. D., Day, D. A.,  
1242 Diskin, G. S., Dubey, M. K., Fortner, E., Hanisco, T. F., Hu, W., King, L. E., Kleinman, L., Meinardi, S.,  
1243 Mikoviny, T., Onasch, T. B., Palm, B. B., Peischl, J., Pollack, I. B., Ryerson, T. B., Sachse, G. W.,  
1244 Sedlacek, A. J., Shilling, J. E., Springston, S., St. Clair, J. M., Tanner, D. J., Teng, A. P., Wennberg, P.

1245 O., Wisthaler, A., and Wolfe, G. M.: Airborne measurements of western U.S. wildfire emissions:  
1246 Comparison with prescribed burning and air quality implications, *J. Geophys. Res.-Atmos.*, 122, 6108-  
1247 6129, <https://doi.org/10.1002/2016JD026315>, 2017.

1248  
1249 Loehman, R. A., Reinhardt, E., and Riley, K. L.: Wildland fire emissions, carbon, and climate: Seeing the  
1250 forest and the trees – A cross-scale assessment of wildfire and carbon dynamics in fire-prone, forested  
1251 ecosystems, *For. Ecol. Manag.*, 317, 9-19, <https://doi.org/10.1016/j.foreco.2013.04.014>, 2014.

1252  
1253 Matz, C.J., Egyed, M., Xi, G., Racine, J., Pavlovic, R., Rittmaster, R., Henderson, S.B., and Stieb, D.M.:  
1254 Health impact analysis of PM<sub>2.5</sub> from wildfire smoke in Canada (2013-2015, 2017-2018), *Sci. Total*  
1255 *Environ.*, 725(10), <https://doi.org/10.1016/j.scitotenv.2020.138506>, 2020.

1256  
1257 May, A. A., McMeeking, G. R., Lee, T., Taylor, J. W., Craven, J. S., Burling, I., Sullivan, A. P., Akagi,  
1258 S., Collett Jr., J. L., Flynn, M., Coe, H., Urbanski, S. P., Seinfeld, J. H., Yokelson, R. J., and Kreidenweis,  
1259 S. M.: Aerosol emissions from prescribed fires in the United States: A synthesis of laboratory and aircraft  
1260 measurements, *J. Geophys. Res.-Atmos*, 119, 11826-11849, <https://doi.org/10.1002/2014JD021848>,  
1261 2014.

1262  
1263 McGee, T., McFarlane, B., and Tymstra, C.: Chapter 3 - Wildfire: A Canadian Perspective, in: *Wildfire*  
1264 *Hazards, Risks and Disasters*, edited by: Shroder, J. F., and Paton, D., Elsevier, Amsterdam, The  
1265 Netherlands, 35-58, <https://doi.org/10.1016/B978-0-12-410434-1.00003-8>, 2015.

1266  
1267 McLagan, D. S., Stupple, G. W., Darlington, A., Hayden, K., and Steffen, A.: Where there is smoke there  
1268 is mercury: Assessing boreal forest fire mercury emissions using aircraft and highlighting uncertainties  
1269 associated with upscaling emissions estimates, *Atmos. Chem. Phys.*, 21, 5635-5653,  
1270 <https://doi.org/10.5194/acp-21-5635-2021>, 2021.

1271  
1272 McMeeking, G. R., Kreidenweis, S. M., Baker, S., Carrico, C. M., Chow, J. C., Collett Jr., J. L., Hao, W.  
1273 M., Holden, A. S., Kirchstetter, T. W., Malm, W. C., Moosmüller, H., Sullivan, A. P., and Wold, C. E.:  
1274 Emissions of trace gases and aerosols during the open combustion of biomass in the laboratory, *J.*  
1275 *Geophys. Res.-Atmos*, 114, D19210, <https://doi.org/10.1029/2009JD011836>, 2009.

1276  
1277 Miller, D. J., Sun, K., Zondlo, M. A., Kanter, D., Dubovik, O., Welton, E. J., Winker, D. M., and Ginoux,  
1278 P.: Assessing boreal forest fire smoke aerosol impacts on U.S. air quality: A case study using multiple  
1279 data sets, *J. Geophys. Res.-Atmos*, 116, D22209, <https://doi.org/10.1029/2011JD016170>, 2011.

1280  
1281 Moteki, N. and Kondo, Y.: Dependence of laser-induced incandescence on physical properties of black  
1282 carbon aerosols: Measurements and theoretical interpretation, *Aerosol Sci. Tech.*, 44, 663-675,  
1283 <https://doi.org/10.1080/02786826.2010.484450>, 2010.

1284  
1285 Moussa, S. G., Leithead, A., Li, S. M., Chan, T. W., Wentzell, J. J. B., Stroud, C., Zhang, J. H., Lee, P.,  
1286 Lu, G., Brook, J. R., Hayden, K., Narayan, J., and Liggió, J.: Emissions of hydrogen cyanide from on-  
1287 road gasoline and diesel vehicles, *Atmos. Environ.*, 131, 185-195,  
1288 <https://doi.org/10.1016/j.atmosenv.2016.01.050>, 2016.

1289  
1290 NRCan, Blueprint for wildland fire science in Canada (2019-2029), Sankey, S., Technical  
1291 Coordinator. Canadian Forest Service, Northern Forestry Centre, Edmonton, AB, 45p,  
1292 <https://cfs.nrcan.gc.ca/publications?id=39429>, 2018.

1293

1294 O'Brien, J. J., Loudermilk, E. L., Hornsby, B. S., Hudak, A. T., Bright, B. C., Dickinson, M. B., Hiers, J.  
1295 K., Teske, C., and Ottmar, R. D.: High-resolution infrared thermography for capturing wildland fire  
1296 behaviour: RxCADRE 2012, *Int. J. Wildland Fire*, 25, 62-75, <https://doi.org/10.1071/WF14165>, 2015.  
1297

1298 Palm, B. B., Peng, Q., Fredrickson, C. D., Lee, B. H., Garofalo, L. A., Pothier, M. A., Kreidenweis, S.  
1299 M., Farmer, D. K., Pokhrel, R. P., Shen, Y., Murphy, S. M., Permar, W., Hu, L., Campos, T. L., Hall, S.  
1300 R., Ullmann, K., Zhang, X., Flocke, F., Fischer, E. V., and Thornton, J. A.: Quantification of organic  
1301 aerosol and brown carbon evolution in fresh wildfire plumes, *P. Natl. Acad. Sci. USA*, 117, 29469-29477,  
1302 <https://doi.org/10.1073/pnas.2012218117>, 2020.  
1303

1304 Peng, Q., Palm, B. B., Melander, K. E., Lee, B. H., Hall, S. R., Ullmann, K., Campos, T., Weinheimer, A.  
1305 J., Apel, E. C., Hornbrook, R. S., Hills, A. J., Montzka, D. D., Flocke, F., Hu, L., Permar, W., Wielgasz,  
1306 C., Lindaas, J., Pollack, I. B., Fischer, E. V., Bertram, T. H., and Thornton, J. A.: HONO Emissions from  
1307 Western U.S. Wildfires Provide Dominant Radical Source in Fresh Wildfire Smoke, *Environ. Sci.*  
1308 *Technol.*, 54, 5954-5963, <https://doi.org/10.1021/acs.est.0c00126>, 2020.  
1309

1310 Permar, W., Wang, Q., Selimovic, V., Wielgasz, C., Yokelson, R. J., Hornbrook, R. S., Hills, A. J., Apel,  
1311 E. C., Ku, I.-T., Zhou, Y., Sive, B. C., Sullivan, A. P., Collett Jr, J. L., Campos, T. L., Palm, B. B., Peng,  
1312 Q., Thornton, J. A., Garofalo, L. A., Farmer, D. K., Kreidenweis, S. M., Levin, E. J. T., DeMott, P. J.,  
1313 Flocke, F., Fischer, E. V., and Hu, L.: Emissions of trace organic gases from western U.S. wildfires based  
1314 on WE-CAN aircraft measurements, *J. Geophys. Res.-Atmos*, 126, e2020JD033838,  
1315 <https://doi.org/10.1029/2020JD033838>, 2021.  
1316

1317 Randerson, J. T., Liu, H., Flanner, M. G., Chambers, S. D., Jin, Y., Hess, P. G., Pfister, G., Mack, M. C.,  
1318 Treseder, K. K., Welp, L. R., Chapin, F. S., Harden, J. W., Goulden, M. L., Lyons, E., Neff, J. C., Schuur,  
1319 E. A., and Zender, C. S.: The impact of boreal forest fire on climate warming, *Science*, 314, 1130-1132,  
1320 <https://doi.org/10.1126/science.1132075>, 2006.  
1321

1322 Reid, C. E., Brauer, M., Johnston, F. H., Jerrett, M., Balmes, J. R., and Elliott, C. T.: Critical review of  
1323 health impacts of wildfire smoke exposure, *Environ. Health Persp.*, 124, 1334-1343,  
1324 <https://doi.org/10.1289/ehp.1409277>, 2016.  
1325

1326 Reid, J. S., Koppmann, R., Eck, T. F., and Eleuterio, D. P.: A review of biomass burning emissions part  
1327 II: intensive physical properties of biomass burning particles, *Atmos. Chem. Phys.*, 5, 799-825,  
1328 <https://doi.org/10.5194/acp-5-799-2005>, 2005.  
1329

1330 Roberts, J. M., Stockwell, C. E., Yokelson, R. J., de Gouw, J., Liu, Y., Selimovic, V., Koss, A. R.,  
1331 Sekimoto, K., Coggon, M. M., Yuan, B., Zarzana, K. J., Brown, S. S., Santin, C., Doerr, S. H., and  
1332 Warneke, C.: The nitrogen budget of laboratory-simulated western US wildfires during the FIREX 2016  
1333 Fire Lab study, *Atmos. Chem. Phys.*, 20, 8807-8826, <https://doi.org/10.5194/acp-20-8807-2020>, 2020.  
1334

1335 Roberts, G., Wooster, M. J., Xu, W., Freeborn, P. H., Morcrette, J. J., Jones, L., Benedetti, A., Jiangping,  
1336 H., Fisher, D., and Kaiser, J. W.: LSA SAF Meteosat FRP products – Part 2: Evaluation and  
1337 demonstration for use in the Copernicus Atmosphere Monitoring Service (CAMS), *Atmos. Chem. Phys.*,  
1338 15, 13241-13267, <https://doi.org/10.5194/acp-15-13241-2015>, 2015.  
1339

1340 Rogers, C. F., Hudson, J. G., Hallett, J., and Penner, J. E.: Cloud Droplet Nucleation by Crude-Oil Smoke  
1341 and Coagulated Crude-Oil Wood Smoke Particles, *Atmos. Environ. a-Gen*, 25, 2571-2580,  
1342 [https://doi.org/10.1016/0960-1686\(91\)90174-6](https://doi.org/10.1016/0960-1686(91)90174-6), 1991.  
1343

1344 Rogers, H. M., Ditto, J. C., and Gentner, D. R.: Evidence for impacts on surface-level air quality in the  
1345 northeastern US from long-distance transport of smoke from North American fires during the Long Island  
1346 Sound Tropospheric Ozone Study (LISTOS) 2018, *Atmos. Chem. Phys.*, 20, 671-  
1347 682, <https://doi.org/10.5194/acp-20-671-2020>, 2020.

1348  
1349 Schwarz, J. P., Gao, R. S., Fahey, D. W., Thomson, D. S., Watts, L. A., Wilson, J. C., Reeves, J. M.,  
1350 Darbeheshti, M., Baumgardner, D. G., Kok, G. L., Chung, S. H., Schulz, M., Hendricks, J., Lauer, A.,  
1351 Kärcher, B., Slowik, J. G., Rosenlof, K. H., Thompson, T. L., Langford, A. O., Loewenstein, M., and  
1352 Aikin, K. C.: Single-particle measurements of midlatitude black carbon and light-scattering aerosols from  
1353 the boundary layer to the lower stratosphere, *J. Geophys. Res.-Atmos*, 111, D16207,  
1354 <https://doi.org/10.1029/2006JD007076>, 2006.

1355  
1356 Seidl, R., Thom, D., Kautz, M., Martin-Benito, D., Peltoniemi, M., Vacchiano, G., Wild, J., Ascoli, D.,  
1357 Petr, M., Honkaniemi, J., Lexer, M. J., Trotsiuk, V., Mairota, P., Svoboda, M., Fabrika, M., Nagel, T. A.,  
1358 and Reyer, C. P. O.: Forest disturbances under climate change, *Nat. Clim. Change*, 7, 395-402,  
1359 <https://doi.org/10.1038/nclimate3303>, 2017.

1360  
1361 Seinfeld, J. H. and Pandis, S. N.: *Atmospheric chemistry and physics: from air pollution to climate*  
1362 *change*, John Wiley & Sons, New York, 1998.

1363  
1364 Sekimoto, K., Li, S.-M., Yuan, B., Koss, A., Coggon, M., Warneke, C., and de Gouw, J.: Calculation of  
1365 the sensitivity of proton-transfer-reaction mass spectrometry (PTR-MS) for organic trace gases using  
1366 molecular properties, *Int. J. Mass Spectrom.*, 421, 71-94, <https://doi.org/10.1016/j.ijms.2017.04.006>,  
1367 2017.

1368  
1369 Sheu, R., Marcotte, A., Khare, P., Charan, S., Ditto, J. C., and Gentner, D. R.: Advances in offline  
1370 approaches for chemically speciated measurements of trace gas-phase organic compounds via adsorbent  
1371 tubes in an integrated sampling-to-analysis system, *J. Chromatogr. A*, 1575, 80-  
1372 90, <https://doi.org/10.1016/j.chroma.2018.09.014>, 2018.

1373  
1374 Simoneit, B. R. T., Schauer, J. J., Nolte, C. G., Oros, D. R., Elias, V. O., Fraser, M. P., Rogge, W. F., and  
1375 Cass, G. R.: Levoglucosan, a tracer for cellulose in biomass burning and atmospheric particles, *Atmos.*  
1376 *Environ.*, 33, 173-182, [https://doi.org/10.1016/S1352-2310\(98\)00145-9](https://doi.org/10.1016/S1352-2310(98)00145-9), 1999.

1377  
1378 Simpson, I. J., Akagi, S. K., Barletta, B., Blake, N. J., Choi, Y., Diskin, G. S., Fried, A., Fuelberg, H. E.,  
1379 Meinardi, S., Rowland, F. S., Vay, S. A., Weinheimer, A. J., Wennberg, P. O., Wiebring, P., Wisthaler,  
1380 A., Yang, M., Yokelson, R. J., and Blake, D. R.: Boreal forest fire emissions in fresh Canadian smoke  
1381 plumes: C<sub>1</sub>-C<sub>10</sub> volatile organic compounds (VOCs), CO<sub>2</sub>, CO, NO<sub>2</sub>, NO, HCN and CH<sub>3</sub>CN, *Atmos.*  
1382 *Chem. Phys.*, 11, 6445-6463, <https://doi.org/10.5194/acp-11-6445-2011>, 2011.

1383  
1384 Singh, H. B., Anderson, B. E., Brune, W. H., Cai, C., Cohen, R. C., Crawford, J. H., Cubison, M. J.,  
1385 Czech, E. P., Emmons, L., Fuelberg, H. E., Huey, G., Jacob, D. J., Jimenez, J. L., Kaduwela, A., Kondo,  
1386 Y., Mao, J., Olson, J. R., Sachse, G. W., Vay, S. A., Weinheimer, A., Wennberg, P. O., and Wisthaler, A.:  
1387 Pollution influences on atmospheric composition and chemistry at high northern latitudes: Boreal and  
1388 California forest fire emissions, *Atmos. Environ.*, 44, 4553-4564,  
1389 <https://doi.org/10.1016/j.atmosenv.2010.08.026>, 2010.

1390  
1391 Stephens, M., Turner, N., and Sandberg, J.: Particle identification by laser-induced incandescence in a  
1392 solid-state laser cavity, *Appl. Optics*, 42, 3726-3736, <https://doi.org/10.1364/ao.42.003726>, 2003.

1393

1394 Stockwell, C. E., Veres, P. R., Williams, J., and Yokelson, R. J.: Characterization of biomass burning  
1395 emissions from cooking fires, peat, crop residue, and other fuels with high-resolution proton-transfer-  
1396 reaction time-of-flight mass spectrometry, *Atmos. Chem. Phys.*, 15, 845-865, [https://doi.org/10.5194/acp-](https://doi.org/10.5194/acp-15-845-2015)  
1397 15-845-2015, 2015.

1398  
1399 Stockwell, C. E., Kupc, A., Witkowski, B., Talukdar, R. K., Liu, Y., Selimovic, V., Zarzana, K. J.,  
1400 Sekimoto, K., Warneke, C., Washenfelder, R. A., Yokelson, R. J., Middlebrook, A. M., and Roberts, J.  
1401 M.: Characterization of a catalyst-based conversion technique to measure total particulate nitrogen and  
1402 organic carbon and comparison to a particle mass measurement instrument, *Atmos. Meas. Tech.*, 11,  
1403 2749-2768, <https://doi.org/10.5194/amt-11-2749-2018>, 2018.

1404  
1405 Stockwell, C. E., Bela, M., Coggon, M. M., Gkatzelis, G. I., Wiggins, E. B., Gargulinski, E. M., Shingler,  
1406 T., Fenn, M., Griffin, D., Holmes, C. D., Ye, X., Saide, P. E., Bourgeois, I., Peischl, J., Womack, C. C.,  
1407 Washenfelder, R. A., Veres, P. R., Neuman, J. A., Gilman, J. B., Lamplugh, A., Schwantes, R. H.,  
1408 McKeen, S. A., Wisthaler, A., Piel, F., Guo, H., Campuzano-Jost, P., Jimenez, J. L., Fried, A., Hanisco,  
1409 T. F., Huey, L. G., Kondragunta, S., Zhang, X., Perring, A., Katich, J. M., Diskin, G. S., Nowak, J. B.,  
1410 Bui, T. P., Halliday, H. S., Pereira, G., James, E. P., Ahmadov, R., McLinden, C. A., Soja, A. J., Moore,  
1411 R. H., Hair, J. W., and Warneke, C.: Airborne emission rate measurements validate remote sensing  
1412 observations and emission inventories of western U.S. wildfires, submitted to *ES&T*, in review, 2021.

1413  
1414 Urbanski, S.: Wildland fire emissions, carbon, and climate: Emission factors, *For. Ecol. Manag.*, 317, 51-  
1415 60, <https://doi.org/10.1016/j.foreco.2013.05.045>, 2014.

1416  
1417 Urbanski, S. P.: Combustion efficiency and emission factors for wildfire-season fires in mixed conifer  
1418 forests of the Northern Rocky Mountains, US, *Atmos. Chem. Phys.*, 13, 7241-7262,  
1419 <https://doi.org/10.5194/acp-13-7241-2013>, 2013.

1420  
1421 Urbanski, S. P., Hao, W. M., and Baker, S.: Chapter 4 Chemical Composition of Wildland Fire  
1422 Emissions, in: *Developments in Environmental Science*, edited by: Bytnerowicz, A., Arbaugh, M. J.,  
1423 Riebau, A. R., and Andersen, C., Elsevier, Amsterdam, The Netherlands, 79-107,  
1424 [https://doi.org/10.1016/S1474-8177\(08\)00004-1](https://doi.org/10.1016/S1474-8177(08)00004-1), 2009.

1425  
1426 Uresk, D. W., Cline, J. F., and Rickard, W. H.: Growth rates of a cheatgrass community and some  
1427 associated factors, *J. Range Manage.*, 32, 168-170, <https://doi.org/10.2307/3897114>, 1979.

1428  
1429 US EPA, SPECIATE Version 4.5 Database Development Documentation, Final Report EPA/600/R-  
1430 16/294, September 2016. Available <https://www.epa.gov/air-emissions-modeling/speciate>.

1431  
1432 van der Werf, G. R., Randerson, J. T., Giglio, L., Collatz, G. J., Kasibhatla, P. S., and Arellano Jr, A. F.:  
1433 Interannual variability in global biomass burning emissions from 1997 to 2004, *Atmos. Chem. Phys.*, 6,  
1434 3423-3441, <https://doi.org/10.5194/acp-6-3423-2006>, 2006.

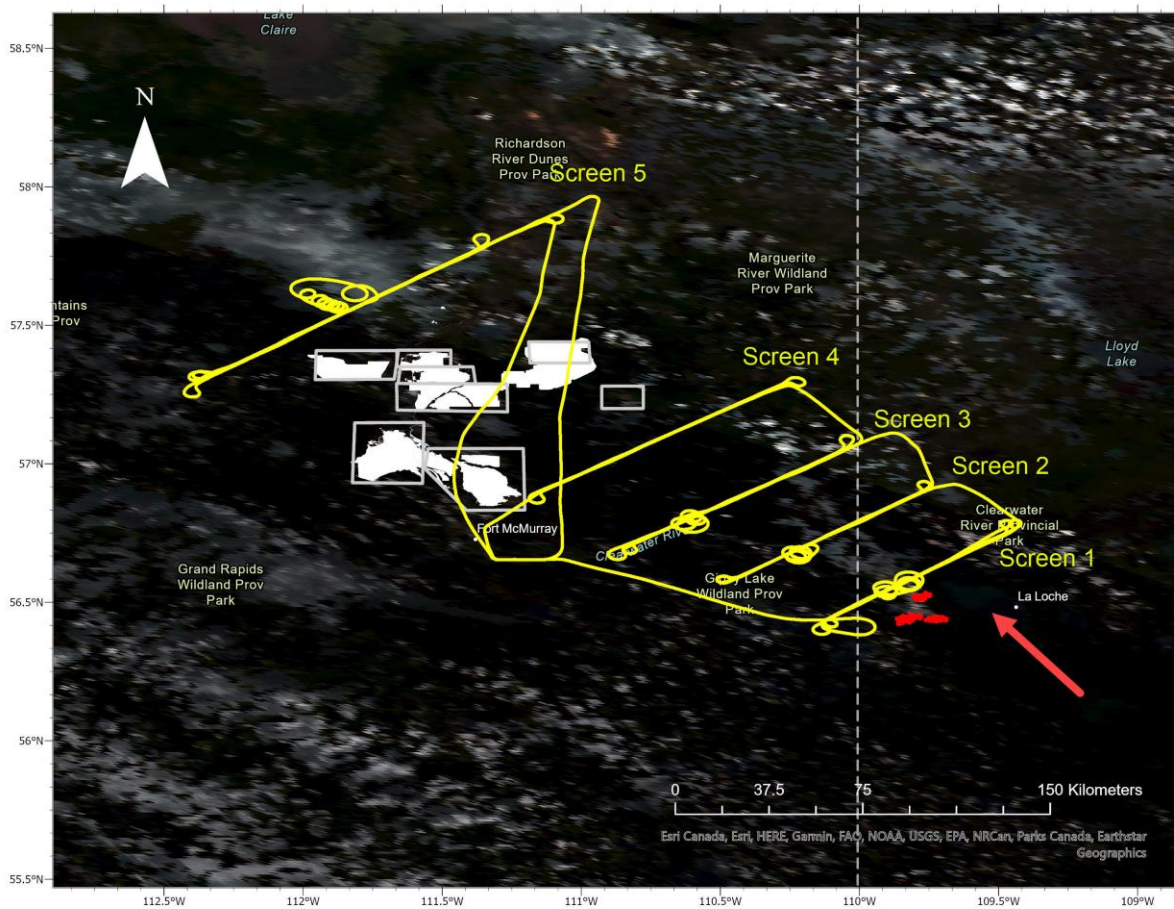
1435  
1436 van der Werf, G. R., Randerson, J. T., Giglio, L., van Leeuwen, T. T., Chen, Y., Rogers, B. M., Mu, M.,  
1437 van Marle, M. J. E., Morton, D. C., Collatz, G. J., Yokelson, R. J., and Kasibhatla, P. S.: Global fire  
1438 emissions estimates during 1997–2016, *Earth Syst. Sci. Data*, 9, 697–720, [https://doi.org/10.5194/essd-9-](https://doi.org/10.5194/essd-9-697-2017)  
1439 697-2017, 2017.

1440  
1441 Veres, P., Roberts, J. M., Burling, I. R., Warneke, C., de Gouw, J., and Yokelson, R. J.: Measurements of  
1442 gas-phase inorganic and organic acids from biomass fires by negative-ion proton-transfer chemical-  
1443 ionization mass spectrometry, *J. Geophys. Res.-Atmos.*, 115, D23302,  
1444 <https://doi.org/10.1029/2010JD014033>, 2010.

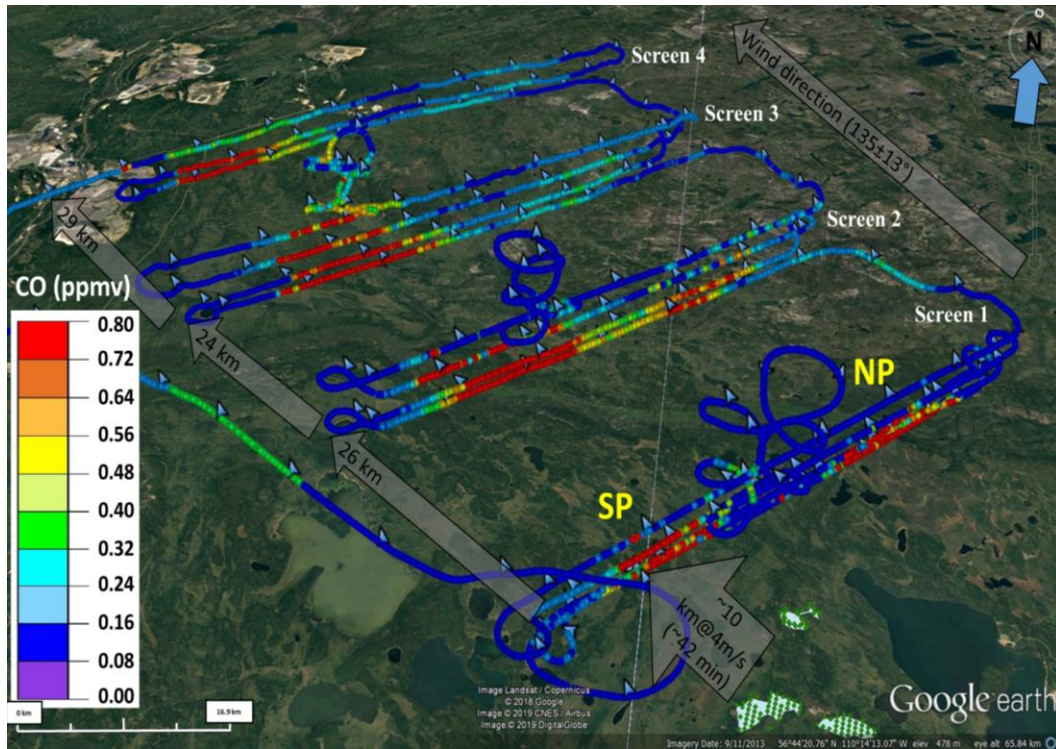
1445  
1446 Ward, D. E. and Radke, L. F.: Emissions measurements from vegetation fires: A comparative evaluation  
1447 of methods and results, in: *Fire in the Environment: The Ecological, Atmospheric, and Climatic*  
1448 *Importance of Vegetation Fires*. Dahlem Workshop Reports: Environmental Sciences Research Report  
1449 13, edited by: Crutzen, P. J., and Goldammer, J. G., John Wiley & Sons, Chichester, England, 53-76,  
1450 1993.  
1451  
1452 Whitman, E., Parisien, M. A., Thompson, D. K., and Flannigan, M. D.: Short-interval wildfire and  
1453 drought overwhelm boreal forest resilience, *Sci. Rep.*, 9, 18796, [https://doi.org/10.1038/s41598-019-](https://doi.org/10.1038/s41598-019-55036-7)  
1454 [55036-7](https://doi.org/10.1038/s41598-019-55036-7), 2019.  
1455  
1456 Wiggins, E. B., Andrews, A., Sweeney, C., Miller, J. B., Miller, C. E., Veraverbeke, S., Commane, R.,  
1457 Wofsy, S., Henderson, J. M., and Randerson, J. T.: Boreal forest fire CO and CH<sub>4</sub> emission factors  
1458 derived from tower observations in Alaska during the extreme fire season of 2015, *Atmos. Chem. Phys.*,  
1459 21, 8557-8574, <https://doi.org/10.5194/acp-21-8557-2021>, 2021.  
1460  
1461 Wiggins, E. B., Soja, A. J., Gargulinski, E., Halliday, H. S., Pierce, R. B., Schmidt, C. C., Nowak, J. B.,  
1462 DiGangi, J. P., Diskin, G. S., Katich, J. M., Perring, A. E., Schwarz, J. P., Anderson, B. E., Chen, G.,  
1463 Crosbie, E. C., Jordan, C., Robinson, C. E., Sanchez, K. J., Shingler, T. J., Shook, M., Thornhill, K. L.,  
1464 Winstead, E. L., Ziemba, L. D., and Moore, R. H.: High Temporal Resolution Satellite Observations of  
1465 Fire Radiative Power Reveal Link Between Fire Behavior and Aerosol and Gas Emissions, *Geophys. Res.*  
1466 *Let.*, 47, <https://doi.org/10.1029/2020GL090707>, 2020.  
1467  
1468 Wotton, B. M., Nock, C. A., and Flannigan, M. D.: Forest fire occurrence and climate change in Canada,  
1469 *Int. J. Wildland Fire*, 19, 253-271, <https://doi.org/10.1071/WF09002>, 2010.  
1470  
1471 Yokelson, R. J., Bertschi, I. T., Christian, T. J., Hobbs, P. V., Ward, D. E., and Hao, W. M.: Trace gas  
1472 measurements in nascent, aged, and cloud-processed smoke from African savanna fires by airborne  
1473 Fourier transform infrared spectroscopy (AFTIR), *J. Geophys. Res.-Atmos*, 108, 8478,  
1474 <https://doi.org/10.1029/2002JD002322>, 2003.  
1475  
1476 Yokelson, R. J., Burling, I. R., Gilman, J. B., Warneke, C., Stockwell, C. E., de Gouw, J., Akagi, S. K.,  
1477 Urbanski, S. P., Veres, P., Roberts, J. M., Kuster, W. C., Reardon, J., Griffith, D. W. T., Johnson, T. J.,  
1478 Hosseini, S., Miller, J. W., Cocker, D. R., Jung, H., and Weise, D. R.: Coupling field and laboratory  
1479 measurements to estimate the emission factors of identified and unidentified trace gases for prescribed  
1480 fires, *Atmos. Chem. Phys.*, 13, 89-116, <https://doi.org/10.5194/acp-13-89-2013>, 2013.  
1481  
1482 Yokelson, R. J., Crouse, J. D., DeCarlo, P. F., Karl, T., Urbanski, S., Atlas, E., Campos, T., Shinozuka,  
1483 Y., Kapustin, V., Clarke, A. D., Weinheimer, A., Knapp, D. J., Montzka, D. D., Holloway, J., Weibring,  
1484 P., Flocke, F., Zheng, W., Toohey, D., Wennberg, P. O., Wiedinmyer, C., Mauldin, L., Fried, A., Richter,  
1485 D., Walega, J., Jimenez, J. L., Adachi, K., Buseck, P. R., Hall, S. R., and Shetter, R.: Emissions from  
1486 biomass burning in the Yucatan, *Atmos. Chem. Phys.*, 9, 5785-5812, [https://doi.org/10.5194/acp-9-5785-](https://doi.org/10.5194/acp-9-5785-2009)  
1487 [2009](https://doi.org/10.5194/acp-9-5785-2009), 2009.  
1488  
1489 Yokelson, R. J., Goode, J. G., Ward, D. E., Susott, R. A., Babbitt, R. E., Wade, D. D., Bertschi, I.,  
1490 Griffith, D. W. T., and Hao, W. M.: Emissions of formaldehyde, acetic acid, methanol, and other trace  
1491 gases from biomass fires in North Carolina measured by airborne Fourier transform infrared  
1492 spectroscopy, *J. Geophys. Res.-Atmos*, 104, 30109-30125, <https://doi.org/10.1029/1999JD900817>, 1999.  
1493

1494 Yokelson, R. J., Griffith, D. W. T., and Ward, D. E.: Open-path Fourier transform infrared studies of  
1495 large-scale laboratory biomass fires, *J. Geophys. Res.-Atmos*, 101, 21067-21080,  
1496 <https://doi.org/10.1029/96JD01800>, 1996.  
1497  
1498 Yokelson, R. J., Karl, T., Artaxo, P., Blake, D. R., Christian, T. J., Griffith, D. W. T., Guenther, A., and  
1499 Hao, W. M.: The tropical forest and fire emissions experiment: Overview and airborne fire emission  
1500 factor measurements, *Atmos. Chem. Phys.*, 7, 5175-5196, <https://doi.org/10.5194/acp-7-5175-2007>, 2007.  
1501  
1502 Yokelson, R. J., Susott, R., Ward, D. E., Reardon, J., and Griffith, D. W. T.: Emissions from smoldering  
1503 combustion of biomass measured by open-path Fourier transform infrared spectroscopy, *J. Geophys.*  
1504 *Res.-Atmos*, 102, 18865-18877, <https://doi.org/10.1029/97JD00852>, 1997.  
1505  
1506 Yu, S.: Role of organic acids (formic, acetic, pyruvic and oxalic) in the formation of cloud condensation  
1507 nuclei (CCN): a review, *Atmos. Res.*, 53, 185-217, [https://doi.org/10.1016/S0169-8095\(00\)00037-5](https://doi.org/10.1016/S0169-8095(00)00037-5),  
1508 2000.  
1509  
1510 Yu, P., Toon, O. B., Bardeen, C. G., Zhu, Y., Rosenlof, K. H., Portmann, R. W., Thornberry, T. D., Gao,  
1511 R.-S., Davis, S. M., Wolf, E. T., Gouw, J. d., Peterson, D. A., Fromm, M. D., and Robock, A.: Black  
1512 carbon lofts wildfire smoke high into the stratosphere to form a persistent plume, *Science*, 365, 587-590,  
1513 <https://doi.org/10.1126/science.aax1748>, 2019.  
1514  
1515 Zhang, R., Suh, I., Zhao, J., Zhang, D., Fortner, E. C., Tie, X., Molina, L. T., and Molina, M. J.:  
1516 Atmospheric new particle formation enhanced by organic acids, *Science*, 304, 1487-1490,  
1517 <https://doi.org/10.1126/science.1095139>, 2004.  
1518



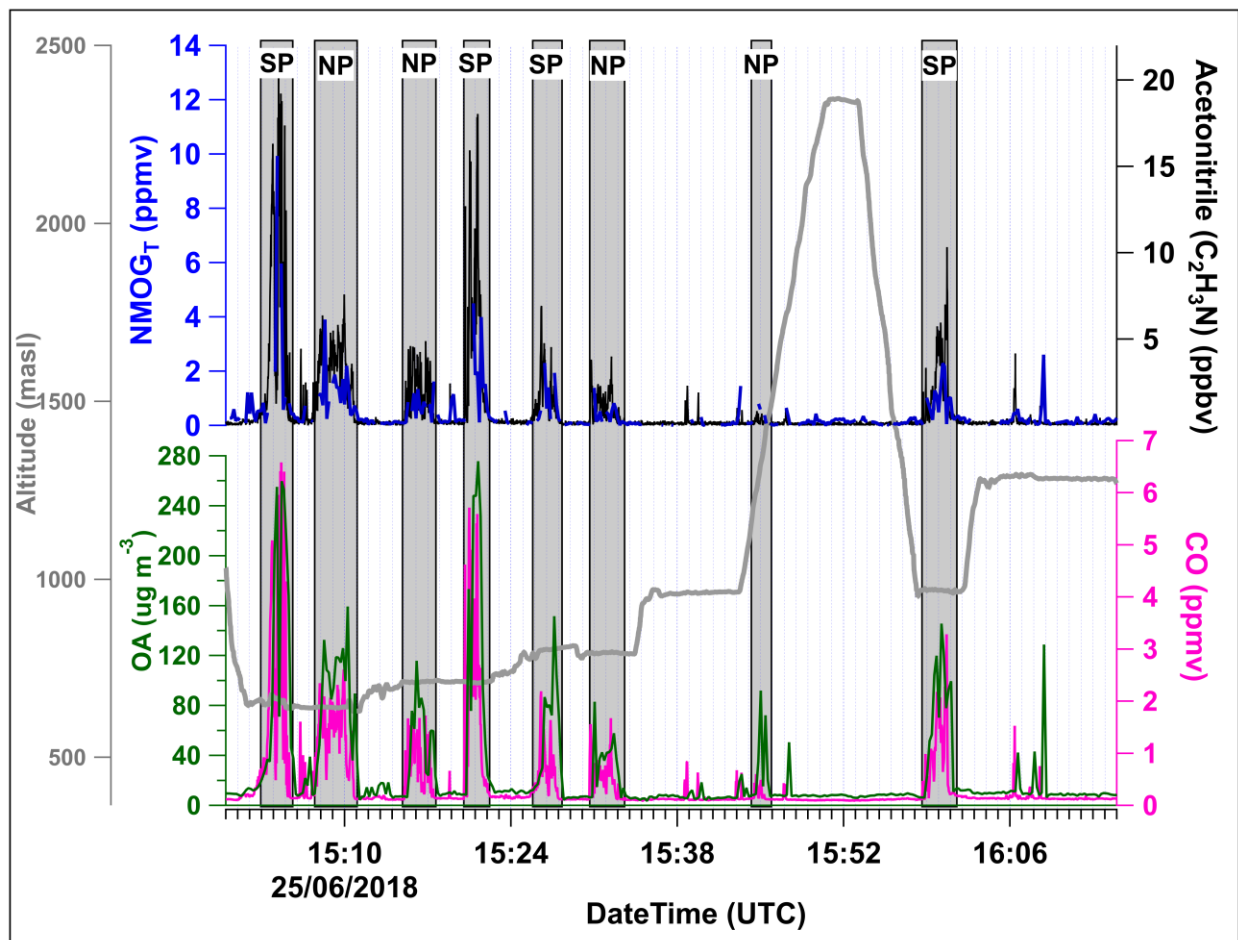


1519  
 1520 Figure 1. Corrected reflectance satellite image from the VIIRS spectroradiometer on the Suomi  
 1521 NPP and NOAA-20 satellites taken on June 25, 2018. The fire hot spots for the wildfire of  
 1522 interest are indicated by the red dots. Flight tracks were flown at Lagrangian distances  
 1523 downwind of the wildfire. Multiple transects at varying altitudes perpendicular to the plume  
 1524 direction formed 5 virtual screens. Plume direction of travel is indicated by the large red  
 1525 arrow. The location of the Alberta oil sands mining facilities are shown in white.  
 1526

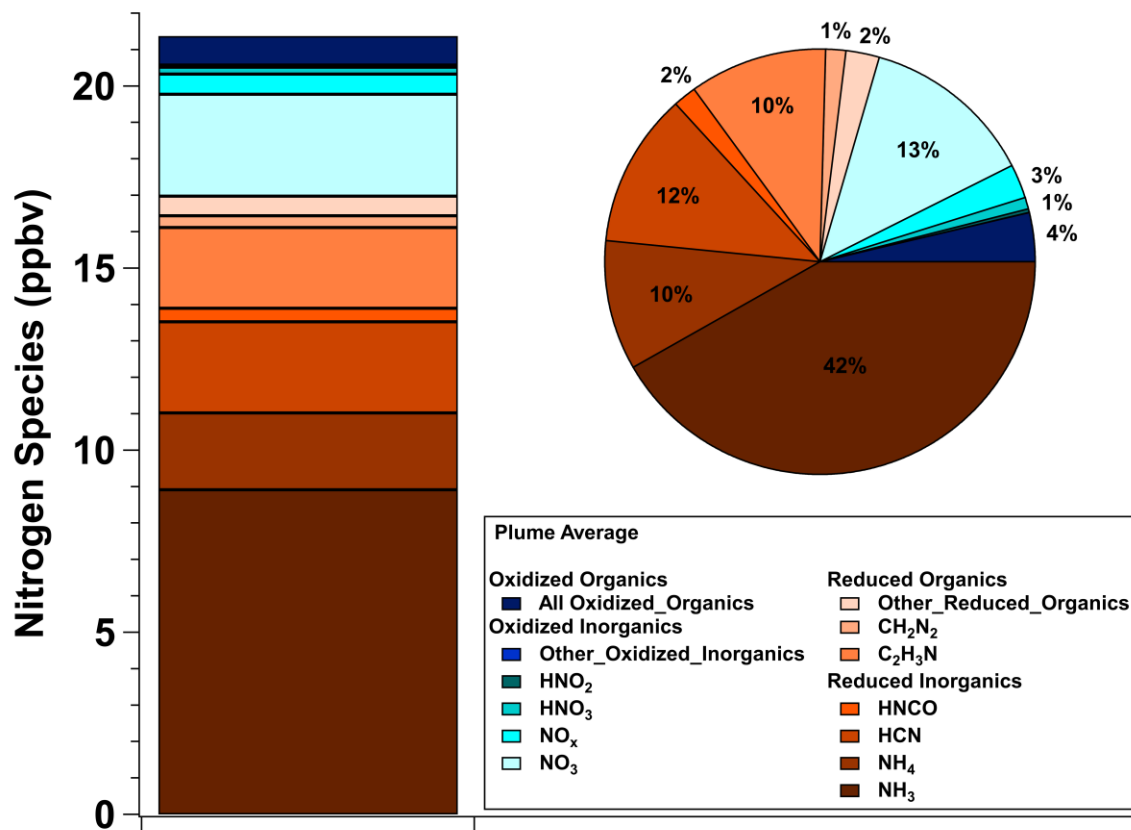


1527  
 1528  
 1529  
 1530  
 1531  
 1532  
 1533  
 1534  
 1535  
 1536

Figure 2. Flight tracks coloured by CO mixing ratio (ppmv) for Screens 1 to 4. The two plumes are identified as south plume (SP) and north plume (NP). The fire perimeter surrounding the detected MODIS-derived ‘hot spots’ on June 25, 2018 is shown in the green hatched area. The source of the NP is expected to be the same hot spots as the SP but ~ 30 min older; see [SI Sect. 2.2](#). The small blue arrows along the flight tracks indicate the aircraft measured wind direction with the average wind direction depicted with the large gray arrow. Distances between screens are shown in the grey arrows.

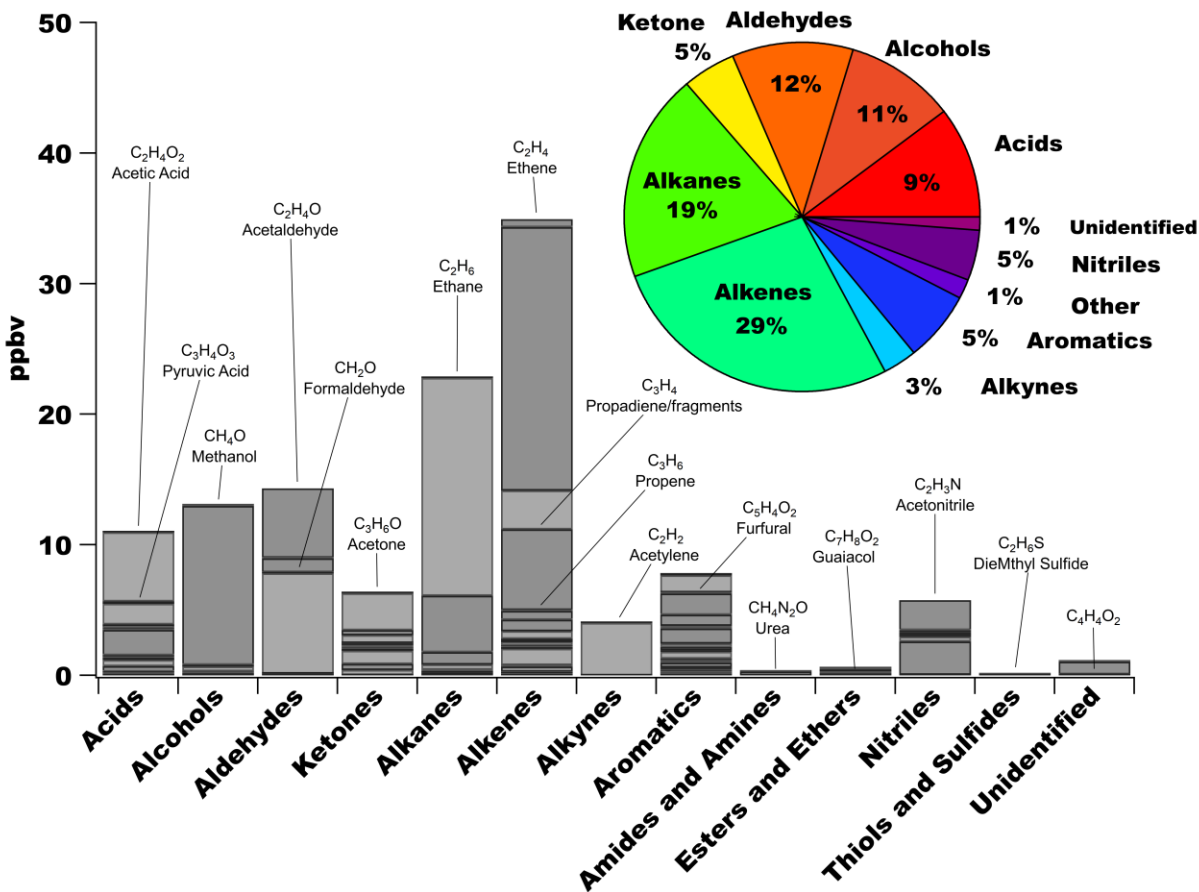


1537  
 1538 Figure 3. Time series of NMOGs (ppmv), acetonitrile (C<sub>2</sub>H<sub>3</sub>N; ppbv) and CO (ppmv), as well as  
 1539 OA concentrations (μg m<sup>-3</sup>) and altitude for Screen 1. The in-plume portions are indicated by the  
 1540 vertical grey bars. The aircraft flew back and forth across the plumes at increasing altitudes to  
 1541 complete five transects; a transect represents one pass across the SP and NP at the same altitude.  
 1542  
 1543

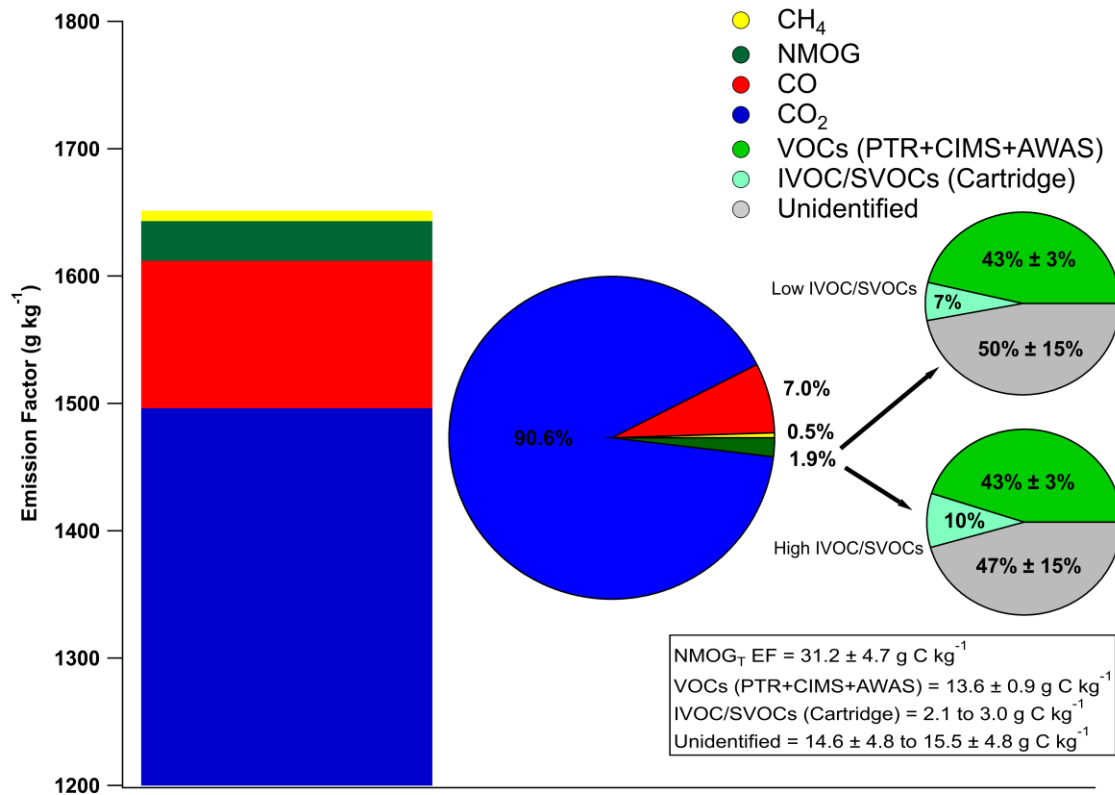


1544 Figure 4. Background-subtracted average Screen 1 in-plume mixing ratios of measured gas- and  
 1545 particle-phase N-containing species (N<sub>r</sub>) and their fractional contribution to the total summed N<sub>r</sub>  
 1546 species. The N<sub>r</sub> species are grouped into categories of reduced inorganics, reduced organics,  
 1547 oxidized inorganics and oxidized organics with reduced species in shades of red and oxidized  
 1548 species in shades of blue.  
 1549

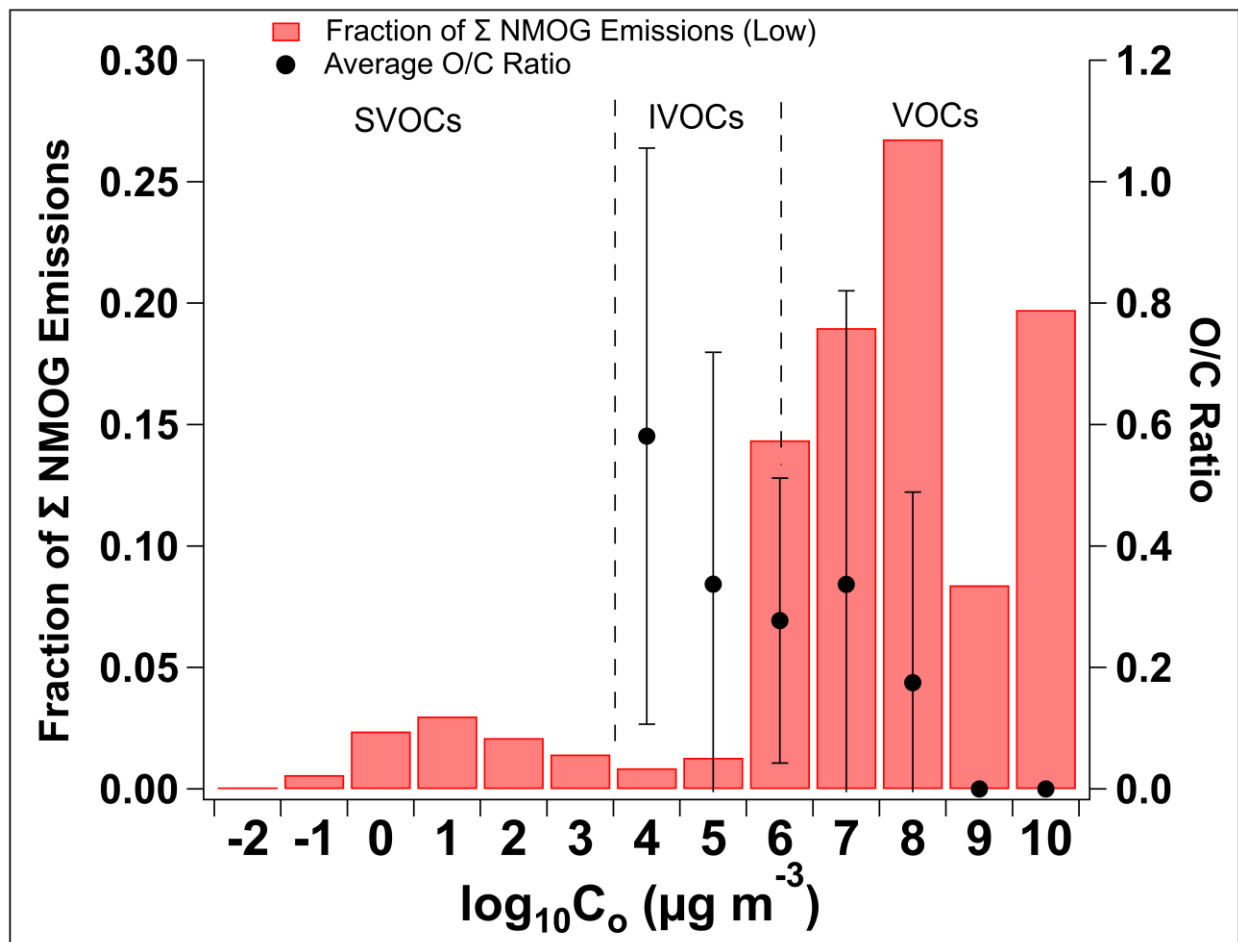
1550  
 1551  
 1552  
 1553  
 1554  
 1555  
 1556  
 1557



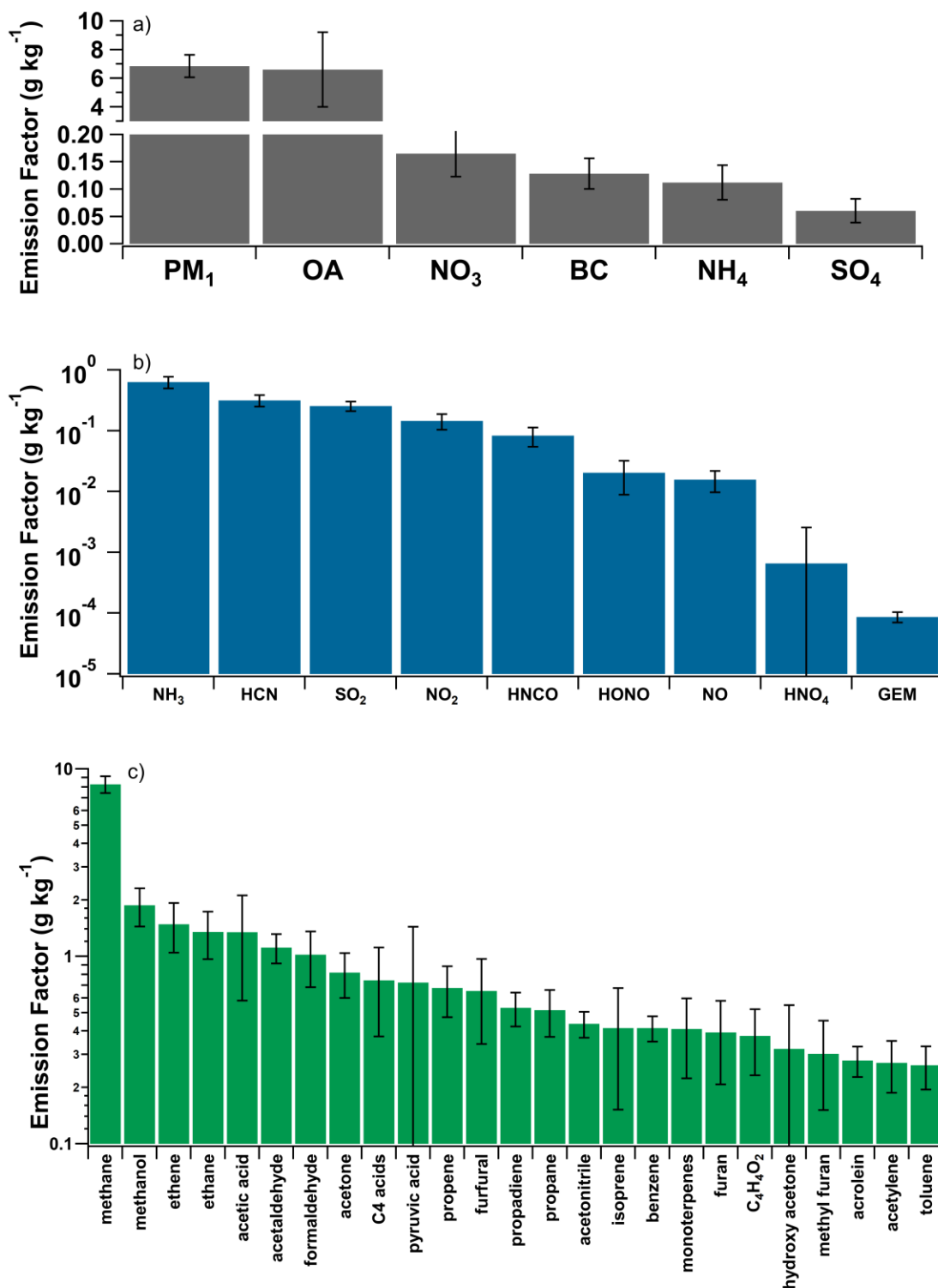
1558  
 1559 Figure 5. Background-subtracted average mixing ratios of individually measured NMOGs  
 1560 shown for thirteen chemical classes. In some cases, compounds are double- (or triple-) counted if  
 1561 they can be identified in more than one category. For example, phenol is an alcohol + an  
 1562 aromatic; guaiacol is an alcohol + an ether + an aromatic. In the pie chart, the *Other* category  
 1563 includes amides, amines, ethers, thiols and sulfides. The unidentified category contains  
 1564 molecular formulas detected, but the compound(s) could not be identified.



1565 Figure 6. Total carbon (TC) partitioning based on EFs (carbon fraction). The bar chart shows  
 1566 the stacked EFs for carbon-containing compounds with the middle pie chart showing their  
 1567 percent contributions to the TC. The two magnified pie charts (right side), representing the low and  
 1568 high I/SVOC EF estimates, show the percent breakdown of the measured NMOGs and the  
 1569 remaining unidentified portion. The EF values (g C kg<sup>-1</sup>) are provided in the box. The pie chart on  
 1570 the right show the percent breakdown of the measured NMOGs with the remaining unidentified  
 1571 portion in terms of g C kg<sup>-1</sup>. Note that all the EFs shown in Table A1 were converted to g C kg<sup>-1</sup>  
 1572 for this breakdown.  
 1573  
 1574  
 1575  
 1576

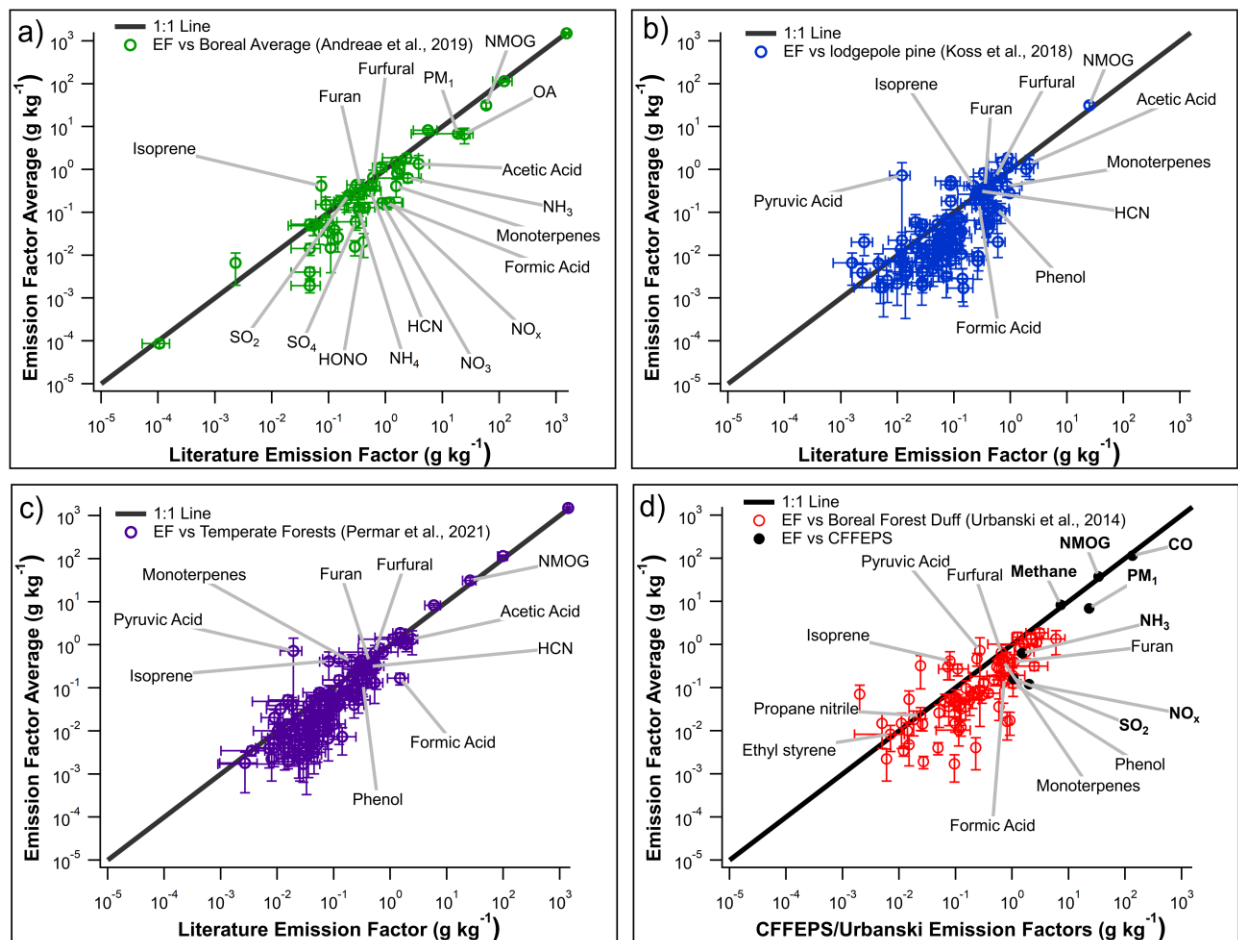


1577  
 1578 Figure 7. Fraction of total  $\Sigma$ NMOG emissions in each volatility bin, as well as the bin-averaged  
 1579 O/C ratio spanning VOCs, IVOCs and SVOCs. Data is included from PTRMS, CIMS, AWAS  
 1580 and cartridge measurements. The O/C ratio is derived for only the PTRMS, CIMS and AWAS  
 1581 measurements and the errors bars indicate the standard deviation of the average O/C ratio.  
 1582



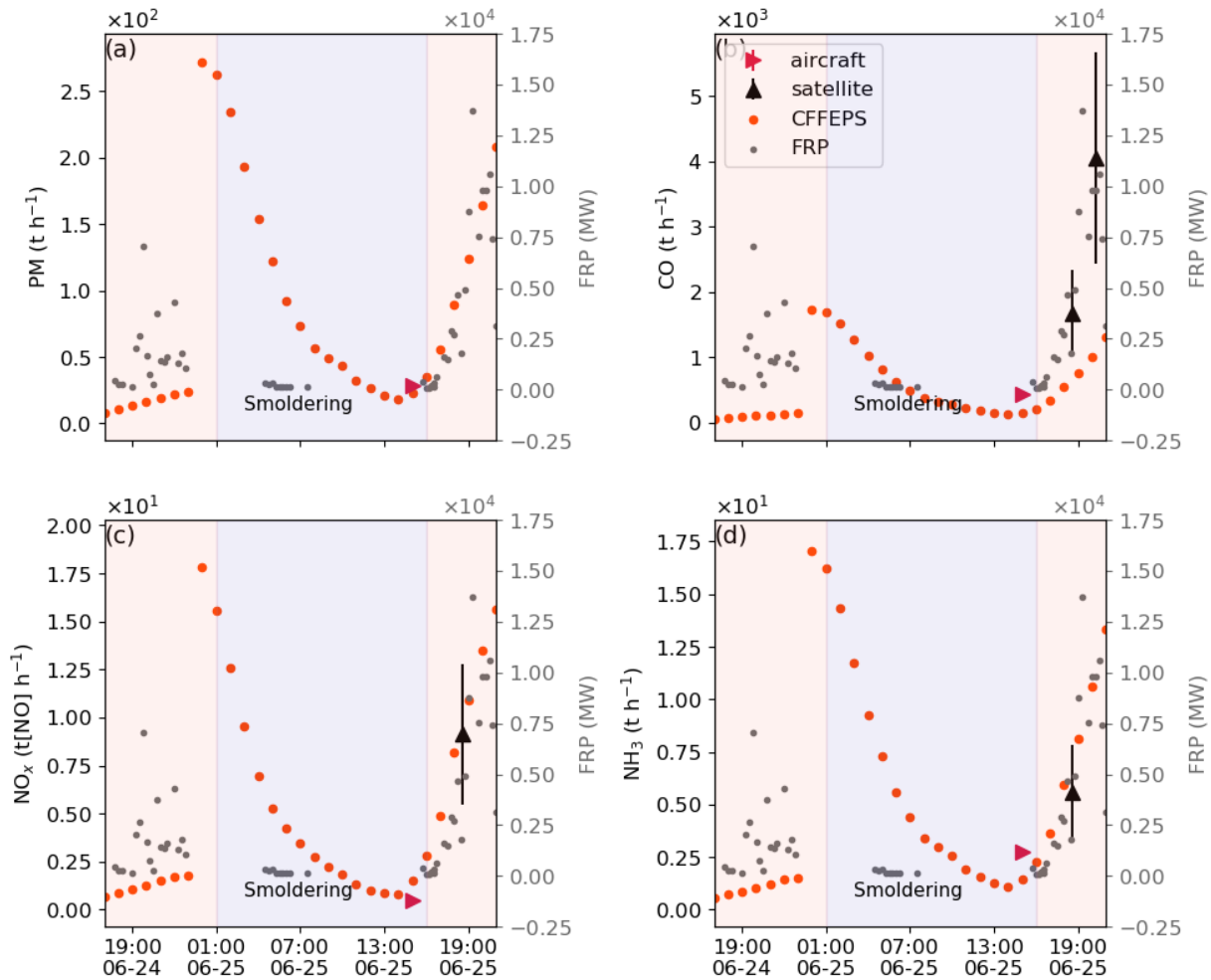
1584  
 1585 Figure 8. Average emission factors ( $\text{g kg}^{-1}$ ) of a) particle species; b) inorganic gas-phase species, and c)  
 1586 the top 25 measured gas-phase organic species. ~~C5 acids = C5 oxo-carboxylic acids~~; C4 acids = C4 oxo-  
 1587 carboxylic acids; propadiene = fragments/propadiene; hydroxy acetone = hydroxy acetone/ ethyl formate.  
 1588 Organic species measurements are from the PTRMS, CIMS and AWAS.





1589  
 1590 Figure 9. Comparison of averaged emission factors with a) boreal forest field-based  
 1591 measurements (Andreae, 2019; Akagi et al., 2011; Liu et al., 2017), b) laboratory-based  
 1592 measurements of lodgepole pine (Koss et al., 2018), c) temperate forest field-based  
 1593 measurements (Permar et al., 2021), and d) those used in CFFEPS (Urbanski et al., 2014). See  
 1594 Table S8 for compound comparisons that don't have exact matches.

1595  
 1596  
 1597  
 1598  
 1599



1600  
 1601  
 1602  
 1603  
 1604  
 1605  
 1606  
 1607  
 1608  
 1609  
 1610

Figure 10. Fire radiative power (FRP; in MW) from GOES-R (grey dots) and emissions from the CFFEPS model (orange dots) from 2018-06-24 17:00 UTC to 2018-06-25 21:00 UTC. **Local time = UTC - 6 hrs.** Aircraft-derived emission rates are shown for a)  $PM_{10}$ , b) CO, c)  $NO_x$  (as NO) and d)  $NH_3$  (in  $t\ h^{-1}$ ; red arrow) at 15:00 UTC when the aircraft flew closest to the fire. The corresponding TROPOMI satellite-derived emission rates are also shown (in  $t\ h^{-1}$ ; black arrows). Note, the aircraft flight time occurred when the fire intensity reflected a surface, smoldering fire and the satellite overpass time took place when the fire had transitioned to a crown (flaming) fire. The smoldering and flaming time periods are coloured in blue and pink, respectively.

1611 **Table A1**

1612

1613 **Table S7.** Summary of in-plume and background average mixing ratios (or concentrations),  
 1614 emission factors ( $\text{g kg}^{-1}$ ) (EF) and emission ratios ( $\text{ppbv ppmv}^{-1}$  except  $\text{CO}_2$  which is in units of  
 1615  $\text{ppmv ppmv}^{-1}$ ; particulates in  $\mu\text{g m}^{-3} \text{ppm}^{-1}$  and TGM-GEM in  $\text{ng m}^{-3} \text{ppmv}^{-1}$ ) (ER) for the SP,  
 1616 NP, and the EF average of the two plumes. In-plume and background averages are in units of  $\mu\text{g}$   
 1617  $\text{m}^{-3}$  for particulates, ppbv for gas-phase compounds, except GEM which is  $\text{ng m}^{-3}$ , and  $\text{CO}_2$  is  
 1618 ppmv. Compounds are grouped by particulate species, and inorganic and organic gas-phase  
 1619 species and (sorted by increasing molecular weight).  $\text{PM}_1$  is the sum of all the AMS-derived  
 1620 particulate species. The CE was  $0.84 \pm 0.04$  and  $0.82 \pm 0.01$  for the SP and NP, respectively. For  
 1621 comparison, EFs are also included from previously published literature including: Andreae  
 1622 (2019)<sup>1</sup>, Liu et al. (2017)<sup>a</sup>, Akagi et al. (2011)<sup>b</sup>, and Simpson et al. (2011)<sup>e</sup>, Koss et al. (2018)<sup>2</sup>,  
 1623 and Permar et al. (2021)<sup>3</sup>, and Liu et al. (2017)<sup>4</sup>. The Andreae (2019) PM EF represents  
 1624  $\text{PM}_{2.5}$ . See Table S8 for compounds that did not have exact matches for comparison to literature  
 1625 values. To derive the EF for species measured in mass concentration units, Eq. 32 was  
 1626 modified by converting TC to mass concentrations using the measured temperature and pressure,  
 1627 and removing the molar mass ratio term. \* Indicates that the compound was ‘calculated’ (SI Sect  
 1628 12.1.1) while the remaining compounds were calibrated. \*\*Estimated, see text in Sect. 3.4.3.  
 1629 Uncertainties reflect the standard deviation of the calibration were estimated by summing in  
 1630 quadrature the standard error of the average EF (or ER) and the measurement uncertainties (see  
 1631 Sect. 2.5).

1632  
1633

Molecular Weight	Compound	Compound Name	Instrument	SP Average	NP Average	Background	Average EF ( $\text{g kg}^{-1}$ )	NP EF ( $\text{g kg}^{-1}$ )	SP EF ( $\text{g kg}^{-1}$ )	Literature EF ( $\text{g kg}^{-1}$ )	NP ER	SP ER
Particulates												
	$\text{PM}_1$	particulate matter (<1 $\mu\text{m}$ )	AMS	112±35	75.5±29.3	13.2±0.9	6.8±0.8	7.1±0.3	6.6±1.1	18.7±15.9 <sup>1</sup> 26.0±6.2 <sup>4</sup>	58.8±1.0	65.1±7.3
	BC	black carbon	SP2	1.3±0.4	0.74±0.30	0.11±0.06	0.13±0.03	0.11±0.02	0.14±0.04	0.43±0.21 <sup>1</sup> 0.39±0.17 <sup>3</sup>	0.55±0.08	0.58±0.19
	$\text{NH}_4$	p-ammonium	AMS	2.3±1.0	1.2±0.4	0.21±0.03	0.11±0.03	0.11±0.03	0.12±0.04	0.34±0.15 <sup>4</sup>	1.1±0.3	1.9±0.6
	$\text{NO}_3$	p-nitrate	AMS	3.2±1.5	1.4±0.5	0.078±0.017	0.17±0.04	0.14±0.03	0.19±0.05	0.87±0.13 <sup>4</sup>	0.90±0.16	1.2±0.3
	$\text{SO}_4$	p-sulphate	AMS	1.7±0.7	0.98±0.31	0.39±0.03	0.060±0.022	0.066±0.020	0.055±0.023	0.30±0.16 <sup>4</sup>	0.035±0.011	0.054±0.020
	OA	p-total organics	AMS	101±34	72.6±27.0	12.5±0.83	6.6±2.6	6.9±2.4	6.3±2.8	24.3±0.21 <sup>4</sup>	57.5±1.94	61.7±27.1
Gas												
Inorganic												
17.031	$\text{NH}_3$	ammonia	LGR	15.4±9.6	5.2±2.1	-0.039±2.2	0.63±0.14	0.45±0.04	0.82±0.19	2.5±1.8 <sup>1</sup> 0.68±0.19 <sup>2</sup>	5.8±0.6	12.6±2.5
27.026	HCN	hydrogen cyanide	CIMS	3.2±1.6	2.3±1.0	0.18±0.07	0.31±0.07	0.34±0.06	0.29±0.07	0.53±0.30 <sup>1</sup> 0.28±0.060 <sup>2</sup> 0.43±0.17 <sup>3</sup>	2.8±0.5	2.9±0.7
28.01	CO	carbon monoxide	Picarro	991±443	819±327	119±5	116±6	127±4	104±7	121±47 <sup>1</sup> 99.3±19.7 <sup>3</sup>	108±39	126±52
30.006	NO	nitric oxide	TECOs	0.14±0.05		0.0014±0.086	0.016±0.006	0.016±0.006	0.14±0.05	0.29 <sup>1</sup>		0.14±0.046

Molecular Weight	Compound	Compound Name	Instrument	SP Average	NP Average	Background	Average EF (g kg <sup>-1</sup> )	NP EF (g kg <sup>-1</sup> )	SP EF (g kg <sup>-1</sup> )	Literature EF (g kg <sup>-1</sup> )	NP ER	SP ER
43.025	HNCO	isocyanic acid	CIMS	0.52±0.17	0.44±0.13	0.068±0.024	0.083±0.029	0.091±0.027	0.076±0.031	0.57±0.24 <sup>2</sup> 0.16±0.04 <sup>3</sup>	0.46±0.13	0.47±0.92
44.009	CO <sub>2</sub>	carbon dioxide	Picarro	414±0.4	411±0.2	405±0.4	1496±92	1481±103	1511±80	1529±135 <sup>1</sup> 1413±61 <sup>3</sup>	7.4±0.5	9.4±0.45
46.005	NO <sub>2</sub>	nitrogen dioxide	TECOs	0.88±0.17		0.39±0.19	0.15±0.04	0.15±0.04	0.88±0.17	1.0 <sup>1</sup>		0.83±0.21
46.005	NO <sub>x</sub>	sum (NO+NO <sub>2</sub> )	TECOs	1.0±0.2		0.39±0.20	0.17±0.04	0.17±0.04	1.0±0.2	1.2±0.9 <sup>1</sup>		0.97±0.58
47.013	HONO	nitrous acid	CIMS	0.22±0.04		0.098±0.038	0.020±0.012	0.020±0.012	0.22±0.04	0.60±0.20 <sup>2</sup>		0.11±0.061
64.064	SO <sub>2</sub>	sulphur dioxide	TECOs	1.3±0.3		0.19±0.46	0.26±0.05	0.26±0.05	1.3±0.3	0.22±0.31 <sup>1</sup>		1.1±0.16
79.011	HNO <sub>4</sub>	pernitric acid	CIMS	0.036±0.0049	0.032±0.0043	0.020±0.007	0.0010±0.0019	0.00047±0.0025	0.00085±0.0001		0.00089±0.0068	0.0028±0.0033
200.59	GEM	gaseous elemental mercury	Tekran	1.6±0.2	1.4±0.1	1.2±0.03	0.000087±0.000017	0.000082±0.000017	0.000092±0.000016	0.00023±0.00030 <sup>1</sup>	0.00068±0.00014	0.00091±0.00014
Gas Organic												
	ΣNMOG	non methane organic gases	PTRMS +CIMS +AWAS + cartridges				24.5±1.6 to 25.6±1.6	26.2±2.1	25.4±5.8			
	Estim. NMOG <sub>T</sub> (see Sect 3.4.3)	non methane organic gases	PTRMS +CIMS +AWAS + cartridges				36.8±11.3 to 39.9±5.8			58.7 <sup>1</sup> 25.0 <sup>2</sup> 26.1 <sup>3</sup>		
	NMOG <sub>T</sub>	carbon fraction of NMOG	Picarro	936±341	649±225	375±85	31.2±3.8	36.8±5.1	25.5±5.6		680±111	580±92
16.043	CH <sub>4</sub>	methane	Picarro	2026±54	1982±35	1911±8	8.3±0.9	7.8±0.4	8.7±1.1	5.5±2.5 <sup>1</sup> 5.9±1.8 <sup>3</sup>	107±5	146±16
26.038	C <sub>2</sub> H <sub>2</sub>	acetylene	AWAS	6.9±2.5	1.8±0.7	0.34±0.041	0.27±0.08	0.20±0.05	0.34±0.11	0.31±0.17 <sup>3</sup>	2.2±0.9	4.0±1.1
28.054	C <sub>2</sub> H <sub>4</sub>	ethene	AWAS	32.4±14.0	9.3±3.8	0.64±0.01	1.5±0.4	1.3±0.3	1.7±0.5	1.5±1.0 <sup>3</sup>	12.9±3.5	18.3±5.0
30.026	CH <sub>2</sub> O	formaldehyde	PTR	13.9±4.9	10.1±2.8	4.4±2.0	1.0±0.3	1.1±0.3	0.93±0.36	1.8±0.4 <sup>1</sup> 1.9±0.7 <sup>2</sup> 1.9±0.4 <sup>3</sup>	8.1±2.2	8.9±3.2
30.07	C <sub>2</sub> H <sub>6</sub>	ethane	AWAS	27.1±12.4	10.1±3.4	1.9±0.016	1.3±0.4	1.3±0.3	1.4±0.5	1.1±0.84 <sup>3</sup>	12.5±2.7	13.8±3.8
32.042	CH <sub>4</sub> O	methanol	PTR	21.9±7.9	15.9±4.9	6.8±0.9	1.9±0.4	2.2±0.4	1.6±0.4	2.3±1.0 <sup>1</sup> 0.90±0.35 <sup>2</sup> 1.5±0.4 <sup>3</sup>	14.9±2.9	13.4±3.6
40.065	C <sub>3</sub> H <sub>4</sub>	fragments/propadiene*	PTR	3.7±1.6	3.0±1.3	0.39±0.05	0.53±0.11	0.64±0.11	0.42±0.11	0.060±0.030 <sup>1</sup> 0.088±0.041 <sup>2</sup>	3.5±0.6	2.8±0.7
41.053	C <sub>2</sub> H <sub>3</sub> N	acetonitrile	PTR	2.8±1.4	2.0±0.8	0.10±0.06	0.44±0.07	0.48±0.06	0.40±0.08	0.31±0.10 <sup>1</sup> 0.086±0.027 <sup>2</sup>	2.6±0.3	2.6±0.5
42.041	CH <sub>2</sub> N <sub>2</sub>	cyanamide*	PTR	0.55±0.22	0.40±0.12	0.10±0.20	0.064±0.042	0.067±0.042	0.061±0.042		1.4±0.9	1.3±0.9

Molecular Weight	Compound	Compound Name	Instrument	SP Average	NP Average	Background	Average EF (g kg <sup>-1</sup> )	NP EF (g kg <sup>-1</sup> )	SP EF (g kg <sup>-1</sup> )	Literature EF (g kg <sup>-1</sup> )	NP ER	SP ER
42.081	C <sub>3</sub> H <sub>6</sub>	propene	AWAS	9.7±4.8	2.9±1.3	0.12±0.01	0.68±0.21	0.62±0.15	0.73±0.25	0.74±0.62 <sup>3</sup>	4.2±1.0	5.2±1.5
44.053	C <sub>2</sub> H <sub>4</sub> O	acetaldehyde	PTR	7.3±3.2	5.2±2.0	0.96±0.20	1.1±0.2	1.2±0.2	1.0±0.2	0.81±0.23 <sup>1</sup> 0.92±0.32 <sup>2</sup> 1.7±0.4 <sup>3</sup>	6.3±0.9	6.3±1.2
44.097	C <sub>3</sub> H <sub>8</sub>	propane	AWAS	6.7±3.2	2.5±1.0	0.28±0.03	0.52±0.14	0.53±0.12	0.50±0.16	0.46±0.18 <sup>3</sup>	3.4±0.7	3.4±1.0
46.025	CH <sub>2</sub> O <sub>2</sub>	formic acid	CIMS	3.0±1.2	2.8±0.9	2.4±0.1	0.17±0.05	0.17±0.04	0.17±0.06	1.0±0.9 <sup>1</sup> 0.28±0.14 <sup>2</sup> 1.5±0.6 <sup>3</sup>	1.2±2.6	0.56±1.3
48.103	CH <sub>4</sub> S	methane thiol*	PTR	0.074±0.039	0.049±0.022	0.0024±0.028	0.014±0.0086	0.015±0.009	0.013±0.008	0.011±0.006 <sup>2</sup>	0.068±0.043	0.073±0.043
50.057	CH <sub>6</sub> O <sub>2</sub>	methanol hydrate*	PTR	0.25±0.10	0.16±0.06	0.062±0.057	0.028±0.020	0.034±0.023	0.022±0.017		0.15±0.10	0.12±0.09
52.076	C <sub>4</sub> H <sub>4</sub>	butenyne/fragments*	PTR	0.11±0.05	0.080±0.034	0.011±0.044	0.018±0.010	0.020±0.011	0.016±0.010	0.052±0.018 <sup>3</sup>	0.086±0.046	0.081±0.050
53.064	C <sub>3</sub> H <sub>3</sub> N	acrylonitrile*	PTR	0.17±0.08	0.12±0.06	0.0024±0.013	0.036±0.018	0.040±0.018	0.032±0.018	0.025±0.012 <sup>2</sup> 0.044±0.015 <sup>3</sup>	0.17±0.07	0.16±0.09
54.048	C <sub>3</sub> H <sub>2</sub> O	propynal*	PTR	0.053±0.033	0.023±0.0054	0.013±0.019	0.0087±0.0053	0.0045±0.0031	0.013±0.007	0.034±0.014 <sup>2</sup> 0.037±0.015 <sup>3</sup>	0.018±0.013	0.062±0.032
54.092	C <sub>4</sub> H <sub>6</sub>	butadiene/fragments*	PTR	0.74±0.38	0.47±0.24	0.070±0.017	0.15±0.08	0.15±0.08	0.15±0.08	0.089±0.030 <sup>1</sup> 0.34±0.18 <sup>2</sup> 0.27±0.10 <sup>3</sup>	0.62±0.30	0.73±0.37
54.092	C <sub>4</sub> H <sub>6</sub>	1,3-butadiene	AWAS	0.74±0.38	0.20±0.09	0.0041±0.0006	0.065±0.022	0.055±0.016	0.075±0.026	0.089±0.030 <sup>1</sup> 0.34±0.18 <sup>2</sup> 0.27±0.10 <sup>3</sup>	0.29±0.09	0.41±0.12
55.08	C <sub>3</sub> H <sub>5</sub> N	propane nitrile*	PTR	0.11±0.05	0.080±0.032	0.0097±0.019	0.022±0.012	0.025±0.012	0.019±0.012	0.012±0.005 <sup>2</sup> 0.037±0.018 <sup>3</sup>	0.10±0.05	0.094±0.057
56.064	C <sub>3</sub> H <sub>4</sub> O	acrolein	PTR	1.5±0.6	1.0±0.4	0.17±0.09	0.28±0.05	0.29±0.04	0.26±0.06	0.34 <sup>1</sup> 0.97±0.50 <sup>2</sup> 0.40±0.18 <sup>3</sup>	0.82±0.12	0.83±0.15
56.108	C <sub>4</sub> H <sub>8</sub>	cis-2-butene	AWAS	0.16±0.08		0.016±0.008	0.015±0.006		0.015±0.006			0.078±0.023
56.108	C <sub>4</sub> H <sub>8</sub>	isobutene	AWAS	0.94±0.49	0.34±0.12	0.062±0.022	0.084±0.023	0.082±0.008	0.086±0.032		0.41±0.03	0.45±0.13
56.108	C <sub>4</sub> H <sub>8</sub>	t-2-butene	AWAS	0.13±0.07		0.010±0.003	0.012±0.005		0.012±0.005			0.063±0.018
56.108	C <sub>4</sub> H <sub>8</sub>	1-butene	AWAS	1.4±0.7	0.41±0.17	0.014±0.005	0.13±0.03	0.12±0.01	0.14±0.04		0.60±0.05	0.74±0.12
57.052	C <sub>2</sub> H <sub>3</sub> NO	hydroxy acetonitrile	CIMS	0.021±0.029	0.0078±0.014	0.00035±0.00014	0.0035±0.0031	0.0025±0.0028	0.0044±0.0034	0.033±0.009 <sup>3</sup>	0.0095±0.011	0.021±0.016
57.052	C <sub>2</sub> H <sub>3</sub> NO	methyl isocyanate*	PTR	0.074±0.029		0.0067±0.06	0.0052±0.0032		0.0052±0.0032	0.033±0.009 <sup>3</sup>		0.024±0.015
58.08	C <sub>3</sub> H <sub>6</sub> O	acetone	PTR	6.0±1.8	4.7±1.2	2.5±0.3	0.82±0.22	0.99±0.25	0.65±0.19	1.6±1.6 <sup>1</sup> 0.34±0.12 <sup>2</sup> 0.84±0.22 <sup>3</sup>	0.065±0.018	0.072±0.028
58.124	C <sub>4</sub> H <sub>10</sub>	n-butane	AWAS	1.5±0.7	0.62±0.22	0.098±0.013	0.15±0.04	0.16±0.04	0.14±0.05	0.11±0.06 <sup>1</sup> 0.12±0.06 <sup>3</sup>	0.79±0.17	0.73±0.20

Molecular Weight	Compound	Compound Name	Instrument	SP Average	NP Average	Background	Average EF (g kg <sup>-1</sup> )	NP EF (g kg <sup>-1</sup> )	SP EF (g kg <sup>-1</sup> )	Literature EF (g kg <sup>-1</sup> )	NP ER	SP ER
60.052	C <sub>2</sub> H <sub>4</sub> O <sub>2</sub>	acetic acid	CIMS	8.8±7.5	6.0±3.9	2.1±0.8	1.3±0.8	1.1±0.5	1.6±0.9	3.8±2.0 <sup>1</sup> 2.4±0.6 <sup>3</sup>	7.4±3.5	8.9±5.2
60.056	CH <sub>4</sub> N <sub>2</sub> O	Urea*	PTR	0.44±0.18	0.28±0.08	0.067±0.13	0.078±0.052	0.079±0.054	0.076±0.049		0.29±0.20	0.34±0.21
61.04	CH <sub>3</sub> NO <sub>2</sub>	nitromethane*	PTR	0.055±0.023	0.038±0.020	0.0051±0.023	0.011±0.007	0.010±0.007	0.011±0.007	0.074±0.030 <sup>2</sup> 0.078±0.009 <sup>3</sup>	0.036±0.024	0.048±0.030
62.068	C <sub>2</sub> H <sub>6</sub> O <sub>2</sub>	ethylene glycol*	PTR	0.023±0.0077		0.0036±0.018	0.0036±0.0023		0.0036±0.0023			0.015±0.010
62.13	C <sub>2</sub> H <sub>6</sub> S	dimethyl sulfide	PTR	0.051±0.022		0.011±0.034	0.0067±0.0047		0.0067±0.0047	0.0016±0.0008 <sup>2</sup> 0.080±0.083 <sup>3</sup> 0.0047 <sup>4</sup>		0.029±0.020
66.103	C <sub>5</sub> H <sub>6</sub>	cyclopentadiene*	PTR	0.13±0.05	0.12±0.04	0.025±0.039	0.032±0.019	0.041±0.022	0.023±0.016	0.011±0.005 <sup>3</sup>	0.14±0.07	0.096±0.064
67.091	C <sub>4</sub> H <sub>5</sub> N	pyrrole*	PTR	0.10±0.06	0.067±0.033	0.00073±0.013	0.026±0.014	0.027±0.014	0.025±0.014	0.054±0.029 <sup>2</sup> 0.039±0.021 <sup>3</sup>	0.090±0.046	0.098±0.055
68.075	C <sub>4</sub> H <sub>4</sub> O	furan*	PTR	1.5±0.8	1.1±0.5	0.0083±0.035	0.39±0.19	0.43±0.17	0.35±0.20	0.36±0.44 <sup>1</sup> 0.36±0.11 <sup>2</sup> 0.43±0.19 <sup>3</sup>	1.4±0.6	1.4±0.8
68.119	C <sub>5</sub> H <sub>8</sub>	isoprene	PTR	1.7±0.7	1.8±0.8	0.52±0.25	0.42±0.26	0.64±0.34	0.19±0.15	0.074 <sup>1</sup> 0.22±0.11 <sup>2</sup> 0.082±0.095 <sup>3</sup>	2.1±1.1	0.47±0.47
68.119	C <sub>5</sub> H <sub>8</sub>	isoprene	AWAS	0.82±0.46	0.35±1.65	1.3±0.4	0.30±0.18	0.40±0.17	0.20±0.19	0.074 <sup>1</sup> 0.22±0.11 <sup>2</sup> 0.082±0.095 <sup>3</sup>	2.0±1.0	0.18±0.18
69.083	C <sub>4</sub> H <sub>5</sub> O	*	PTR	0.017±0.0064	0.013±0.0063	0.00079±0.01	0.0043±0.0025	0.0047±0.0028	0.0038±0.0022		0.015±0.009	0.015±0.008
69.107	C <sub>4</sub> H <sub>7</sub> N	butane nitrile*	PTR	0.030±0.014	0.022±0.009	0.0041±0.011	0.0077±0.0051	0.0088±0.0059	0.0065±0.0042	0.011±0.005 <sup>2</sup> 0.020±0.010 <sup>3</sup>	0.028±0.019	0.025±0.016
70.091	C <sub>4</sub> H <sub>6</sub> O	MVK, methacrolein, crotonaldehyde	PTR	1.3±0.3	1.3±0.3	0.91±0.17	0.19±0.09	0.20±0.08	0.18±0.11	0.11±0.12 <sup>1</sup> 0.34±0.15 <sup>2</sup> 0.39±0.15 <sup>3</sup>	0.66±0.26	0.68±0.38
70.135	C <sub>5</sub> H <sub>10</sub>	c-2-pentene	AWAS	0.040±0.017	0.013±0.0034	0.0040±0.0006	0.0040±0.0012	0.0033±0.0007	0.0048±0.0016	0.046±0.025 <sup>1</sup> 0.015±0.008 <sup>3</sup>	0.013±0.004	0.021±0.0057
70.135	C <sub>5</sub> H <sub>10</sub>	cyclopentane	AWAS	0.031±0.013	0.015±0.0022	0.0052±0.0003	0.0035±0.0009	0.0038±0.0009	0.0031±0.0009	0.046±0.025 <sup>1</sup> 0.015±0.008 <sup>3</sup>	0.016±0.004	0.014±0.005
70.135	C <sub>5</sub> H <sub>10</sub>	1-pentene	AWAS	0.42±0.21	0.15±0.06	0.0053±0.0012	0.052±0.015	0.053±0.013	0.052±0.018	0.046±0.025 <sup>1</sup> 0.015±0.008 <sup>3</sup>	0.21±0.05	0.22±0.06
70.135	C <sub>5</sub> H <sub>10</sub>	t-2-pentene	AWAS	0.13±0.12	0.068±0.020	0.0094±0.0058	0.018±0.013	0.0049±0.0040	0.031±0.018	0.046±0.025 <sup>1</sup> 0.015±0.008 <sup>3</sup>	0.013±0.010	0.063±0.035

Molecular Weight	Compound	Compound Name	Instrument	SP Average	NP Average	Background	Average EF (g kg <sup>-1</sup> )	NP EF (g kg <sup>-1</sup> )	SP EF (g kg <sup>-1</sup> )	Literature EF (g kg <sup>-1</sup> )	NP ER	SP ER
70.135	C <sub>5</sub> H <sub>10</sub>	2-me-1-butene	AWAS	0.12±0.061	0.047±0.018	0.0088±0.0017	0.014±0.005	0.014±0.004	0.015±0.005	0.046±0.025 <sup>1</sup> 0.015±0.008 <sup>3</sup>	0.056±0.013	0.062±0.018
70.135	C <sub>5</sub> H <sub>10</sub>	2-me-2-butene	AWAS	0.019±0.0071	0.0077±0.0016	0.0034±0.0006	0.0019±0.0006	0.0017±0.0004	0.0022±0.0008	0.046±0.025 <sup>1</sup> 0.015±0.008 <sup>3</sup>	0.0068±0.0030	0.0095±0.0027
70.135	C <sub>5</sub> H <sub>10</sub>	3-me-1-butene	AWAS	0.10±0.10	0.045±0.032	0.029±0.012	0.016±0.010	0.0078±0.0037	0.025±0.013	0.046±0.025 <sup>1</sup> 0.015±0.008 <sup>3</sup>	0.045±0.018	0.058±0.028
72.063	C <sub>3</sub> H <sub>4</sub> O <sub>2</sub>	acrylic acid	CIMS	0.28±0.24	0.21±0.15	0.060±0.046	0.096±0.048	0.13±0.06	0.062±0.035	0.22±0.08 <sup>3</sup>	0.25±0.11	0.35±0.20
72.107	C <sub>4</sub> H <sub>8</sub> O	MEK, 2-methyl acetate, ethyl formate	PTR	0.80±0.35	0.57±0.23	0.097±0.051	0.18±0.07	0.22±0.08	0.14±0.06		0.67±0.23	0.54±0.20
72.151	C <sub>5</sub> H <sub>12</sub>	n-pentane	AWAS	0.59±0.28	0.26±0.09	0.035±0.005	0.078±0.021	0.086±0.019	0.070±0.023	0.057±0.028 <sup>3</sup>	0.34±0.07	0.29±0.08
72.151	C <sub>5</sub> H <sub>12</sub>	2-methylbutane	AWAS	0.21±0.08	0.11±0.01	0.051±0.001	0.022±0.006	0.024±0.0049	0.021±0.007	0.057±0.028 <sup>3</sup>	0.097±0.019	0.086±0.027
74.079	C <sub>3</sub> H <sub>6</sub> O <sub>2</sub>	propanoic acid	CIMS	0.81±0.24	0.70±0.15	0.49±0.17	0.13±0.08	0.12±0.08	0.14±0.09	0.57±0.20 <sup>3</sup>	0.35±0.24	0.51±0.30
74.079	C <sub>3</sub> H <sub>6</sub> O <sub>2</sub>	hydroxy acetone/ ethyl formate *	PTR	1.5±0.62	1.1±0.4	0.30±0.11	0.32±0.23	0.35±0.25	0.30±0.20		1.0±0.8	1.1±0.7
78.114	C <sub>6</sub> H <sub>6</sub>	benzene	PTR	1.4±0.69	1.0±0.5	0.054±0.045	0.41±0.06	0.47±0.06	0.36±0.07	0.57±0.21 <sup>1</sup> 0.42±0.25 <sup>2</sup> 0.50±0.14 <sup>3</sup>	1.3±0.2	1.2±0.2
80.086	C <sub>5</sub> H <sub>4</sub> O	cyclopentadienone/isomers*	PTR	0.049±0.026	0.024±0.012	0.00054±0.0061	0.011±0.006	0.0093±0.0047	0.012±0.007	0.027±0.017 <sup>3</sup>	0.026±0.013	0.040±0.023
80.13	C <sub>6</sub> H <sub>8</sub>	cyclohexadiene/monoterpene fragment *	PTR	0.45±0.18	0.40±0.20	0.040±0.040	0.14±0.07	0.17±0.07	0.10±0.06		0.48±0.19	0.34±0.20
81.118	C <sub>5</sub> H <sub>7</sub> N	pentene nitriles/ methyl pyrrole*	PTR	0.018±0.0093	0.013±0.0053	0.0015±0.0055	0.0047±0.0032	0.0050±0.0036	0.0044±0.0028	0.020±0.011 <sup>3</sup>	0.014±0.010	0.015±0.009
82.102	C <sub>5</sub> H <sub>6</sub> O	methyl furan*	PTR	1.1±0.5	0.69±0.32	0.042±0.065	0.30±0.15	0.31±0.13	0.29±0.17	0.32±0.11 <sup>2</sup> 0.28±0.13 <sup>3</sup>	0.84±0.34	0.96±0.55
82.146	C <sub>6</sub> H <sub>10</sub>	cyclohexene*	PTR	0.14±0.06	0.093±0.044	0.015±0.035	0.054±0.030	0.075±0.038	0.033±0.020	0.015±0.011 <sup>3</sup>	0.20±0.10	0.11±0.07
83.09	C <sub>4</sub> H <sub>5</sub> NO	methyloxazole*	PTR	0.0096±0.0044		0.00012±0.0083	0.0020±0.0011		0.0020±0.0011			0.0066±0.0037
83.134	C <sub>5</sub> H <sub>9</sub> N	pentanenitriles*	PTR	0.049±0.025	0.037±0.017	0.0024±0.0088	0.016±0.008	0.019±0.009	0.013±0.008	0.021±0.011 <sup>3</sup>	0.049±0.024	0.042±0.025
84.074	C <sub>4</sub> H <sub>4</sub> O <sub>2</sub>	*	CIMS	1.7±0.7	0.79±0.24	0.29±0.13	0.38±0.14	0.23±0.04	0.52±0.20	0.32±0.11 <sup>3</sup>	0.61±0.20	1.3±0.6

Molecular Weight	Compound	Compound Name	Instrument	SP Average	NP Average	Background	Average EF (g kg <sup>-1</sup> )	NP EF (g kg <sup>-1</sup> )	SP EF (g kg <sup>-1</sup> )	Literature EF (g kg <sup>-1</sup> )	NP ER	SP ER
84.074	C <sub>4</sub> H <sub>4</sub> O <sub>2</sub>	furanone*	ptr	0.54±0.25	0.37±0.16	0.0030±0.041	0.16±0.09	0.16±0.09	0.15±0.08		0.42±0.23	0.48±0.26
84.118	C <sub>5</sub> H <sub>8</sub> O	cyclopentanone/isomers*	PTR	0.23±0.11	0.16±0.07	0.017±0.026	0.069±0.036	0.073±0.032	0.065±0.039	0.087±0.038 <sup>3</sup>	0.19±0.09	0.21±0.12
84.162	C <sub>6</sub> H <sub>12</sub>	hexene*	PTR	0.029±0.013	0.021±0.0065	0.0013±0.015	0.015±0.011	0.020±0.014	0.0098±0.0065	0.008±0.014 <sup>3</sup>	0.052±0.037	0.031±0.019
84.162	C <sub>6</sub> H <sub>12</sub>	c-2-hexene	AWAS	0.019±0.012	0.0079±0.0024	0.0031±0.0002	0.0020±0.0014	0.0021±0.0016	0.0020±0.0011	0.008±0.014 <sup>3</sup>	0.0069±0.0044	0.0064±0.0055
84.162	C <sub>6</sub> H <sub>12</sub>	cyclohexane	AWAS	0.022±0.0077	0.0089±0.0010	0.0051±0.0008	0.0022±0.0016	0.0019±0.0015	0.0026±0.0016	0.008±0.014 <sup>3</sup>	0.0064±0.0053	0.0097±0.0058
86.09	C <sub>4</sub> H <sub>6</sub> O <sub>2</sub>	butanediol/isomers	ptr	0.57±0.23	0.39±0.14	0.089±0.077	0.13±0.09	0.13±0.09	0.13±0.09		0.33±0.23	0.41±0.26
86.134	C <sub>5</sub> H <sub>10</sub> O	pentanone	PTR	0.14±0.07	0.11±0.04	0.013±0.020	0.046±0.025	0.053±0.026	0.038±0.024	0.062±0.023 <sup>3</sup>	0.0095±0.0046	0.0080±0.0049
86.178	C <sub>6</sub> H <sub>14</sub>	n-hexane	AWAS	0.31±0.14	0.13±0.05	0.013±0.0012	0.049±0.020	0.053±0.019	0.044±0.021	0.050±0.036 <sup>3</sup>	0.17±0.06	0.16±0.07
86.178	C <sub>6</sub> H <sub>14</sub>	2,3-DMB	AWAS	0.017±0.0091	0.013±0.001	0.0048±0.0001	0.0031±0.0012	0.004±0.0012	0.0022±0.0013	0.050±0.036 <sup>3</sup>	0.014±0.004	0.0066±0.0039
86.178	C <sub>6</sub> H <sub>14</sub>	2,3-methylpentane	AWAS	0.090±0.047	0.026±0.004	0.011±0.0003	0.010±0.005	0.0089±0.0041	0.011±0.006	0.050±0.036 <sup>3</sup>	0.032±0.011	0.039±0.021
88.062	C <sub>3</sub> H <sub>4</sub> O <sub>3</sub>	pyruvic acid	CIMS	4.4±2.4	3.4±1.0	2.3±0.3	0.72±0.71	0.56±0.54	0.89±0.85	0.012±0.005 <sup>2</sup> 0.019±0.008 <sup>3</sup>	0.022±0.022	- 0.0025±0.010
88.106	C <sub>4</sub> H <sub>8</sub> O <sub>2</sub>	methyl propanoate*	ptr	0.24±0.11	0.17±0.07	0.021±0.040	0.070±0.043	0.075±0.047	0.065±0.040		0.19±0.12	0.20±0.12
88.168	C <sub>4</sub> H <sub>8</sub> OS	oxathiane*	PTR	0.012±0.0049	0.0090±0.0030	0.00061±0.0073	0.0031±0.0024	0.0023±0.0021	0.0040±0.0026		0.0058±0.0053	0.012±0.008
90.125	C <sub>7</sub> H <sub>6</sub>	*	PTR	0.026±0.014		0.0012±0.018	0.0074±0.0011		0.0074±0.0011			0.022±0.013
90.184	C <sub>4</sub> H <sub>10</sub> S	diethyl sulfide, butanethiol	PTR	0.31±0.13	0.22±0.10	0.036±0.012	0.077±0.015	0.083±0.014	0.071±0.015		0.20±0.04	0.21±0.05
92.141	C <sub>7</sub> H <sub>8</sub>	toluene	PTR	0.62±0.30	0.48±0.21	0.034±0.037	0.26±0.07	0.26±0.04	0.26±0.09	0.35±0.11 <sup>1</sup> 0.25±0.13 <sup>2</sup> 0.42±0.16 <sup>3</sup>	0.63±0.08	0.71±0.23
93.082	C <sub>2</sub> H <sub>7</sub> N O <sub>3</sub>	*	PTR	0.0071±0.0034		0.0012±0.0046	0.0025±0.0012		0.0025±0.0012			0.0070±0.0048
93.085	C <sub>5</sub> H <sub>3</sub> N O	furancarbo-nitrile*	PTR	0.056±0.031	0.038±0.017	0.00022±0.0040	0.020±0.011	0.022±0.010	0.018±0.011	0.0026±0.010 <sup>2</sup> 0.0088±0.037 <sup>3</sup>	0.053±0.025	0.053±0.030
94.113	C <sub>6</sub> H <sub>6</sub> O	phenol*	PTR	0.42±0.22	0.27±0.13	0.0026±0.030	0.12±0.06	0.12±0.05	0.12±0.07	3.0 <sup>1</sup> 0.57±0.36 <sup>2</sup> 0.33±0.13 <sup>3</sup>	0.28±0.11	0.35±0.20
94.157	C <sub>7</sub> H <sub>10</sub>	cycloheptadiene*	PTR	0.080±0.035	0.061±0.028	0.005±0.020	0.021±0.011	0.023±0.011	0.020±0.012		0.053±0.025	0.056±0.033
94.19	C <sub>2</sub> H <sub>6</sub> S <sub>2</sub>	dimethyl disulfide*	PTR	0.012±0.0071		0.0012±0.012	0.0039±0.0022		0.0039±0.0022	0.0024±0.009 <sup>2</sup>		0.011±0.006



Molecular Weight	Compound	Compound Name	Instrument	SP Average	NP Average	Background	Average EF (g kg <sup>-1</sup> )	NP EF (g kg <sup>-1</sup> )	SP EF (g kg <sup>-1</sup> )	Literature EF (g kg <sup>-1</sup> )	NP ER	SP ER
95.077	C <sub>5</sub> H <sub>3</sub> O <sub>2</sub>	*	PTR	0.014±0.0085	0.0094±0.0043	0.0012±0.0070	0.0030±0.0021	0.0043±0.0028	0.0038±0.0012		0.0099±0.0063	0.011±0.007
95.101	C <sub>5</sub> H <sub>5</sub> N O	pyridinol*	PTR	0.0066±0.0026	0.0045±0.0026	- 0.00087±0.0041	0.0022±0.0015	0.0021±0.0017	0.0023±0.0012	0.0099±0.0054 <sup>2</sup>	0.0048±0.0041	0.0063±0.0032
95.145	C <sub>6</sub> H <sub>9</sub> N	C2 pyrrole*	PTR	0.0068±0.0034		- 0.000091±0.0054	0.0021±0.0012		0.0021±0.0012			0.0060±0.0033
96.085	C <sub>5</sub> H <sub>4</sub> O <sub>2</sub>	furfural*	PTR	2.0±1.0	1.3±0.6	- 0.0040±0.029	0.65±0.31	0.67±0.26	0.64±0.36	0.61 <sup>1</sup> 0.54±0.17 <sup>2</sup> 0.53±0.21 <sup>3</sup>	1.5±0.6	1.8±1.0
96.129	C <sub>6</sub> H <sub>8</sub> O	C2-furan*	PTR	0.32±0.16	0.20±0.09	0.00016±0.024	0.087±0.044	0.086±0.037	0.087±0.050	0.20±0.10 <sup>3</sup>	0.20±0.09	0.24±0.14
96.173	C <sub>7</sub> H <sub>12</sub>	cycloheptene*	PTR	0.042±0.02	0.035±0.013	0.0049±0.017	0.022±0.015	0.033±0.020	0.011±0.007		0.076±0.047	0.031±0.020
97.073	C <sub>4</sub> H <sub>3</sub> N O <sub>2</sub>	*	PTR	0.010±0.005	0.0093±0.0026	0.0012±0.0075	0.0030±0.0021	0.0044±0.0027	0.0036±0.0012		0.0098±0.0073	0.0096±0.0071
97.161	C <sub>6</sub> H <sub>11</sub> N	hexanenitrile*	PTR	0.011±0.0053	0.0077±0.0041	0.00031±0.0040	0.0040±0.0026	0.0041±0.0028	0.0040±0.0023	0.0088±0.0047 <sup>3</sup>	0.0093±0.0063	0.011±0.006
98.057	C <sub>4</sub> H <sub>2</sub> O <sub>3</sub>	maleic anhydride*	PTR	0.21±0.08	0.16±0.05	0.011±0.032	0.070±0.036	0.072±0.031	0.068±0.040	0.14±0.07 <sup>3</sup>	0.16±0.07	0.18±0.11
98.101	C <sub>5</sub> H <sub>6</sub> O <sub>2</sub>	furan methanol isomers*	PTR	0.28±0.13	0.20±0.08	0.021±0.047	0.058±0.030	0.061±0.025	0.054±0.034	0.38±0.15 <sup>2</sup> 0.090±0.043 <sup>3</sup>	0.14±0.06	0.15±0.09
98.145	C <sub>6</sub> H <sub>10</sub> O	methyl cyclopentanone/isomers*	PTR	0.052±0.023	0.036±0.015	0.0027±0.015	0.015±0.008	0.017±0.009	0.013±0.008	0.022±0.009 <sup>2</sup> 0.034±0.015 <sup>2</sup>	0.038±0.019	0.035±0.020
100.117	C <sub>5</sub> H <sub>8</sub> O <sub>2</sub>	unsaturated C5 carboxylic acids	CIMS	0.20±0.03	0.25±0.07	0.078±0.043	0.072±0.027	0.10±0.03	0.045±0.021	0.11±0.04 <sup>3</sup>	0.22±0.07	0.13±0.06
100.117	C <sub>5</sub> H <sub>8</sub> O <sub>2</sub>	methyl methacrylate/isomers*	ptr	0.15±0.06	0.12±0.04	0.017±0.041	0.036±0.023	0.035±0.022	0.037±0.024		0.078±0.049	0.098±0.062
100.161	C <sub>6</sub> H <sub>12</sub> O	hexanal/hexanone*	PTR	0.022±0.0077	0.018±0.008	0.003±0.010	0.0065±0.0043	0.0074±0.0049	0.0057±0.0035	0.0046±0.0029 <sup>2</sup> 0.013±0.006 <sup>3</sup>	0.016±0.011	0.015±0.009
102.089	C <sub>4</sub> H <sub>6</sub> O <sub>3</sub>	C4 oxocarboxylic acids	CIMS	4.7±1.2	3.8±0.7	2.3±0.2	0.74±0.37	0.57±0.30	0.92±0.43	0.044±0.020 <sup>3</sup>	1.2±0.7	2.4±1.1
102.089	C <sub>4</sub> H <sub>6</sub> O <sub>3</sub>	acetic anhydride*	ptr	0.033±0.016	0.022±0.008	0.0020±0.018	0.0075±0.0046	0.0078±0.0046	0.0072±0.0045		0.017±0.010	0.019±0.012
102.133	C <sub>5</sub> H <sub>10</sub> O <sub>2</sub>	valeric acid*	ptr	0.083±0.042	0.057±0.025	0.0037±0.016	0.024±0.014	0.027±0.016	0.020±0.012		0.059±0.035	0.052±0.031
103.121	C <sub>4</sub> H <sub>9</sub> N O <sub>2</sub>	*	PTR	0.017±0.0063	0.013±0.005	0.0012±0.0032	0.0030±0.0020	0.0074±0.0026	0.0064±0.0011		0.016±0.009	0.016±0.010
103.124	C <sub>7</sub> H <sub>5</sub> N	benzonitrile*	PTR	0.15±0.08	0.11±0.05	0.00028±0.0051	0.060±0.029	0.065±0.026	0.054±0.031	0.021±0.004 <sup>2</sup> 0.055±0.022 <sup>3</sup>	0.14±0.06	0.14±0.08

Molecular Weight	Compound	Compound Name	Instrument	SP Average	NP Average	Background	Average EF (g kg <sup>-1</sup> )	NP EF (g kg <sup>-1</sup> )	SP EF (g kg <sup>-1</sup> )	Literature EF (g kg <sup>-1</sup> )	NP ER	SP ER
104.149	C <sub>5</sub> H <sub>12</sub> O <sub>2</sub>	pentanediol*	PTR	0.0073±0.0034	0.0052±0.0016	- 0.00087±0.0057	0.0029±0.0025	0.0033±0.0033	0.0024±0.0013		0.0069±0.0069	0.0060±0.0032
104.152	C <sub>8</sub> H <sub>8</sub>	styrene*	PTR	0.053±0.027	0.041±0.020	0.000051±0.0092	0.039±0.021	0.056±0.026	0.022±0.013	0.088±0.056 <sup>2</sup> 0.018±0.012 <sup>3</sup>	0.12±0.06	0.058±0.033
106.121	C <sub>4</sub> H <sub>10</sub> O <sub>3</sub>	Diethylene glycol*	PTR	0.014±0.0035		0.0016±0.011	0.0036±0.0026		0.0036±0.0026			0.0088±0.0061
106.124	C <sub>7</sub> H <sub>6</sub> O	benzaldehyde*	PTR	0.10±0.05	0.079±0.037	0.011±0.015	0.036±0.019	0.042±0.018	0.030±0.019	0.095±0.053 <sup>2</sup> 0.084±0.026 <sup>3</sup>	0.087±0.038	0.077±0.047
106.168	C <sub>8</sub> H <sub>10</sub>	C8 aromatic s	PTR	0.19±0.09	0.13±0.06	0.0082±0.020	0.075±0.012	0.082±0.012	0.068±0.013	0.21±0.08 <sup>3</sup>	0.17±0.02	0.17±0.03
107.112	C <sub>6</sub> H <sub>5</sub> N O	pyridine aldehyde*	PTR	0.0035±0.0021		- 0.00051±0.0036	0.0015±0.0008		0.0015±0.0008			0.0038±0.0020
107.156	C <sub>7</sub> H <sub>9</sub> N	dimethyl pyridine/heptyl nitriles*	PTR	0.0048±0.0014		0.000012±0.0040	0.0018±0.001		0.0018±0.0010	0.0050±0.0033 <sup>2</sup>		0.0043±0.0024
108.096	C <sub>6</sub> H <sub>4</sub> O <sub>2</sub>	benzoquinone/quinone*	PTR	0.093±0.043	0.061±0.023	0.0025±0.019	0.025±0.013	0.024±0.011	0.025±0.015	0.084±0.024 <sup>2</sup> 0.077±0.020 <sup>3</sup>	0.049±0.022	0.062±0.035
108.14	C <sub>7</sub> H <sub>8</sub> O	methyl phenol/anisol/cresol*	PTR	0.13±0.07	0.083±0.043	0.00068±0.0094	0.040±0.020	0.040±0.017	0.040±0.023	0.41±0.17 <sup>2</sup> 0.23±0.11 <sup>3</sup>	0.083±0.035	0.099±0.057
108.184	C <sub>8</sub> H <sub>12</sub>	cyclooctadiene*	PTR	0.036±0.016	0.029±0.013	0.0038±0.017	0.015±0.0089	0.017±0.010	0.013±0.008		0.034±0.020	0.032±0.020
109.104	C <sub>6</sub> H <sub>5</sub> O <sub>2</sub>	*	PTR	0.019±0.0095	0.013±0.005	0.0012±0.0058	0.0030±0.0020	0.0055±0.0026	0.0055±0.0011		0.011±0.007	0.014±0.008
110.112	C <sub>6</sub> H <sub>6</sub> O <sub>2</sub>	benzene diol/methyl furfural*	PTR	0.34±0.17	0.22±0.11	- 0.00028±0.016	0.11±0.05	0.11±0.04	0.11±0.06	0.68±0.29 <sup>2</sup> 0.25±0.12 <sup>3</sup>	0.21±0.08	0.27±0.15
110.156	C <sub>7</sub> H <sub>10</sub> O	norcamphor/C3 furan*	PTR	0.096±0.049	0.062±0.030	0.0014±0.016	0.032±0.018	0.030±0.015	0.034±0.020	0.079±0.032 <sup>2</sup> 0.046±0.024 <sup>3</sup>	0.059±0.029	0.083±0.048
110.2	C <sub>8</sub> H <sub>14</sub>	cyclooctene*	PTR	0.017±0.0083	0.012±0.004	0.0011±0.0085	0.0088±0.0071	0.012±0.009	0.0053±0.0034		0.024±0.019	0.014±0.009
111.1	C <sub>5</sub> H <sub>5</sub> N O <sub>2</sub>	dihydroxypyridine/methyl maleimide*	PTR	0.0074±0.0031	0.0062±0.0021	0.00025±0.0040	0.0026±0.0018	0.0031±0.0022	0.0022±0.0015	0.024±0.008 <sup>3</sup>	0.0061±0.0043	0.0051±0.0034
112.084	C <sub>5</sub> H <sub>4</sub> O <sub>3</sub>	furoic acid/hydroxy furfural*	PTR	0.18±0.06	0.14±0.04	0.071±0.058	0.041±0.036	0.044±0.038	0.038±0.035	0.12±0.03 <sup>3</sup>	0.087±0.074	0.089±0.080
112.128	C <sub>6</sub> H <sub>8</sub> O <sub>2</sub>	cyclohexanedione*	PTR	0.057±0.027	0.044±0.021	- 0.0017±0.017	0.014±0.0072	0.014±0.007	0.014±0.007	0.12±0.06 <sup>3</sup>	0.028±0.014	0.033±0.018
112.172	C <sub>7</sub> H <sub>12</sub> O	ethylcycloheptanone*	PTR	0.019±0.0074		0.0019±0.0087	0.0070±0.0045		0.0070±0.0045	0.014±0.007 <sup>3</sup>		0.016±0.010

Molecular Weight	Compound	Compound Name	Instrument	SP Average	NP Average	Background	Average EF (g kg <sup>-1</sup> )	NP EF (g kg <sup>-1</sup> )	SP EF (g kg <sup>-1</sup> )	Literature EF (g kg <sup>-1</sup> )	NP ER	SP ER
114.144	C <sub>6</sub> H <sub>10</sub> O <sub>2</sub>	sum of cyclic saturated and n-unsaturated C5 carboxylic acids	CIMS		0.19±0.07	0.074±0.086	0.12±0.04	0.12±0.044		0.039±0.017 <sup>3</sup>	0.11±0.04	
114.144	C <sub>6</sub> H <sub>10</sub> O <sub>2</sub>	Caprolactone/c6 esters/c6 diketone isomers*	ptr	0.033±0.011	0.029±0.011	0.0065±0.019	0.0068±0.0048	0.0082±0.0057	0.0053±0.0037		0.016±0.011	0.013±0.009
114.188	C <sub>7</sub> H <sub>14</sub> O	heptanone/heptanal/isomers*	PTR	0.010±0.006		0.00080±0.0078	0.0039±0.0025		0.0039±0.0025	0.0072±0.025 <sup>3</sup>		0.0090±0.0057
116.116	C <sub>5</sub> H <sub>8</sub> O <sub>3</sub>	C5 oxo-carboxylic acids	CIMS	0.18±0.04	0.15±0.03	0.10±0.01	0.031±0.017	0.026±0.013	0.037±0.020	0.034±0.019 <sup>3</sup>	0.050±0.025	0.083±0.045
116.16	C <sub>6</sub> H <sub>12</sub> O <sub>2</sub>	butyl acetate/c6 esters*	ptr	0.023±0.010	0.019±0.009	0.00086±0.0081	0.0073±0.0045	0.0094±0.0054	0.0052±0.0033		0.018±0.010	0.012±0.007
116.222	C <sub>6</sub> H <sub>12</sub> S	cyclohexanethiol*	PTR	0.0094±0.0037	0.0073±0.0017	- 0.00048±0.0064	0.0032±0.0028	0.0040±0.0037	0.0025±0.0016		0.0075±0.0069	0.0056±0.0036
118.088	C <sub>4</sub> H <sub>6</sub> O <sub>4</sub>	succinic acid*	PTR	0.0026±0.0011	0.0025±0.0011	- 0.0012±0.0031	0.0017±0.0007	0.0026±0.0009	0.00081±0.00034		0.0048±0.0016	0.0018±0.0007
118.135	C <sub>8</sub> H <sub>6</sub> O	benzofuran*	PTR	0.039±0.022	0.025±0.016	- 0.0018±0.0060	0.017±0.009	0.018±0.010	0.017±0.009	0.037±0.020 <sup>2</sup> 0.041±0.015 <sup>3</sup>	0.034±0.018	0.038±0.021
118.179	C <sub>9</sub> H <sub>10</sub>	methylstyrene/propenyl benzenes*	PTR	0.022±0.010	0.016±0.007	0.0021±0.0079	0.018±0.012	0.024±0.016	0.011±0.007	0.037±0.020 <sup>3</sup>	0.046±0.030	0.025±0.015
119.167	C <sub>8</sub> H <sub>9</sub> N	*	PTR	0.0039±0.0022		0.0012±0.0017	0.0016±0.0015		0.0016±0.0015			0.0035±0.0029
120.151	C <sub>8</sub> H <sub>8</sub> O	methylbenzaldehyde/tolualdehyde*	PTR	0.064±0.031	0.039±0.019	0.0026±0.013	0.025±0.014	0.024±0.012	0.026±0.016	0.13±0.08 <sup>2</sup> 0.082±0.030 <sup>3</sup>	0.044±0.022	0.058±0.034
120.195	C <sub>9</sub> H <sub>12</sub>	trimethylbenzene/C9 aromatic*	PTR	0.070±0.031	0.056±0.022	0.0078±0.017	0.052±0.029	0.075±0.037	0.029±0.018	0.051 <sup>1</sup> 0.051±0.02 <sup>2</sup> 0.069±0.031 <sup>3</sup>	0.14±0.07	0.064±0.039
122.123	C <sub>7</sub> H <sub>6</sub> O <sub>2</sub>	benzoic acid/hydroxybenzaldehyde*	PTR	0.068±0.025	0.053±0.016	0.0092±0.018	0.020±0.011	0.021±0.010	0.019±0.012	0.079±0.035 <sup>2</sup> 0.065±0.023 <sup>3</sup>	0.037±0.018	0.040±0.026
122.167	C <sub>8</sub> H <sub>10</sub> O	xyleneol/C2 phenol/methylanisole*	PTR	0.033±0.019	0.025±0.014	0.00069±0.0081	0.015±0.0082	0.016±0.009	0.013±0.008	0.11±0.04 <sup>2</sup> 0.10±0.06 <sup>3</sup>	0.029±0.015	0.029±0.017

Molecular Weight	Compound	Compound Name	Instrument	SP Average	NP Average	Background	Average EF (g kg <sup>-1</sup> )	NP EF (g kg <sup>-1</sup> )	SP EF (g kg <sup>-1</sup> )	Literature EF (g kg <sup>-1</sup> )	NP ER	SP ER
122.211	C <sub>9</sub> H <sub>14</sub>	cyclohexylallene*	PTR	0.019±0.0074	0.014±0.005	0.0027±0.0083	0.0076±0.0051	0.0083±0.0059	0.0068±0.0043		0.015±0.011	0.015±0.009
124.095	C <sub>6</sub> H <sub>4</sub> O <sub>3</sub>	hydroxybenzoquinone*	PTR	0.014±0.008	0.011±0.005	- 0.00040±0.0051	0.0032±0.0022	0.0029±0.0021	0.0035±0.0023	0.073±0.018 <sup>2</sup> 0.045±0.026 <sup>3</sup>	0.0051±0.0037	0.0075±0.0047
124.139	C <sub>7</sub> H <sub>8</sub> O <sub>2</sub>	guaiacol*	PTR	0.15±0.09	0.093±0.054	0.0013±0.0073	0.052±0.026	0.051±0.020	0.053±0.031	0.37±0.12 <sup>2</sup> 0.27±0.17 <sup>3</sup>	0.091±0.037	0.12±0.07
124.183	C <sub>8</sub> H <sub>12</sub> O	acetylcyclohexene*	PTR	0.018±0.009	0.013±0.005	0.00032±0.0056	0.0078±0.0045	0.0087±0.0051	0.0068±0.0039		0.015±0.009	0.015±0.008
126.111	C <sub>6</sub> H <sub>6</sub> O <sub>3</sub>	hydroxymethylfurfural*	PTR	0.033±0.014	0.025±0.010	0.00066±0.0087	0.0096±0.0053	0.0094±0.0049	0.0098±0.0056	0.27±0.10 <sup>2</sup> 0.064±0.026 <sup>3</sup>	0.016±0.009	0.021±0.012
126.155	C <sub>7</sub> H <sub>10</sub> O <sub>2</sub>	unsaturated C6 cyclic carboxylic acid*	CIMS	0.052±0.005	0.043±0.011	0.0088±0.0096	0.012±0.005	0.015±0.0057	0.0087±0.0044		0.026±0.010	0.019±0.009
126.155	C <sub>7</sub> H <sub>10</sub> O <sub>2</sub>	cyclohexene carboxylic acid*	ptr	0.015±0.006	0.013±0.003	0.0026±0.0091	0.0064±0.0045	0.0080±0.0056	0.0048±0.0032		0.014±0.010	0.010±0.007
126.199	C <sub>8</sub> H <sub>14</sub> O	octenone*	PTR	0.0064±0.0029		0.00012±0.0051	0.0027±0.0016		0.0027±0.0016			0.0057±0.0033
126.217	C <sub>7</sub> H <sub>10</sub> S	trimethylthiophene*	PTR	0.013±0.004	0.011±0.005	0.00044±0.0084	0.011±0.011	0.016±0.015	0.0054±0.0030		0.028±0.026	0.012±0.007
128.127	C <sub>6</sub> H <sub>8</sub> O <sub>3</sub>	di hydroxymethylfuran*	PTR	0.024±0.013	0.020±0.007	- 0.0017±0.0087	0.0044±0.0026	0.0059±0.0032	0.0029±0.0017		0.010±0.006	0.0063±0.0036
128.171	C <sub>7</sub> H <sub>12</sub> O <sub>2</sub>	cyclohexanoic acid*	ptr	0.014±0.004		0.0028±0.011	0.0050±0.0034		0.0050±0.0034			0.010±0.007
128.174	C <sub>10</sub> H <sub>8</sub>	naphthalene*	PTR	0.033±0.013	0.025±0.011	0.00075±0.0086	0.017±0.011	0.018±0.012	0.015±0.009	0.078±0.056 <sup>2</sup>	0.031±0.021	0.031±0.018
128.215	C <sub>8</sub> H <sub>16</sub> O	octanone*	PTR	0.0072±0.0035		0.0014±0.0055	0.0028±0.0020		0.0028±0.0020			0.006±0.0042
130.187	C <sub>7</sub> H <sub>14</sub> O <sub>2</sub>	amyl acetate*	ptr	0.0074±0.0046	0.0056±0.0021	0.00025±0.0046	0.0031±0.0019	0.0034±0.0020	0.0028±0.0018		0.0056±0.0033	0.0058±0.0036
132.159	C <sub>6</sub> H <sub>12</sub> O <sub>3</sub>	C6 hydroxycarboxylic acids	CIMS	0.0090±0.0006	0.010±0.002	0.0062±0.0014	0.0017±0.0008	0.0027±0.0011	0.00075±0.00034		0.0045±0.0018	0.0016±0.0010
132.162	C <sub>9</sub> H <sub>8</sub> O	methylbenzofurans*	PTR	0.023±0.012	0.016±0.0085	0.00018±0.0050	0.010±0.006	0.010±0.006	0.011±0.006	0.055±0.030 <sup>2</sup> 0.046±0.021 <sup>3</sup>	0.017±0.009	0.021±0.012
132.206	C <sub>10</sub> H <sub>12</sub>	ethylstyrene/methylpropenylbenzene*	PTR	0.019±0.009	0.014±0.007	0.0013±0.0063	0.0083±0.0050	0.0083±0.0050	0.0083±0.0050	0.041±0.019 <sup>2</sup> 0.040±0.026 <sup>3</sup>	0.014±0.008	0.017±0.010
134.134	C <sub>8</sub> H <sub>6</sub> O <sub>2</sub>	phthalic acid*	PTR	0.0074±0.0028	0.0071±0.0025	0.0011±0.0051	0.0039±0.0029	0.0044±0.0035	0.0033±0.0022		0.0071±0.0057	0.0065±0.0042

Molecular Weight	Compound	Compound Name	Instrument	SP Average	NP Average	Background	Average EF (g kg <sup>-1</sup> )	NP EF (g kg <sup>-1</sup> )	SP EF (g kg <sup>-1</sup> )	Literature EF (g kg <sup>-1</sup> )	NP ER	SP ER
134.178	C <sub>9</sub> H <sub>10</sub> O	methylacetophenone*	PTR	0.012±0.007	0.0085±0.0041	- 0.00032±0.004	0.0059±0.0035	0.0062±0.0036	0.0056±0.0033	0.053±0.031 <sup>2</sup> 0.045±0.019 <sup>3</sup>	0.010±0.006	0.011±0.006
134.222	C <sub>10</sub> H <sub>14</sub>	C10 Aromatic s*	PTR	0.030±0.013	0.024±0.010	0.0024±0.0095	0.024±0.014	0.035±0.019	0.013±0.008	0.040±0.021 <sup>3</sup>	0.058±0.031	0.026±0.016
136.15	C <sub>8</sub> H <sub>8</sub> O <sub>2</sub>	methylbenzoic acid*	PTR	0.027±0.015	0.018±0.009	0.00058±0.007	0.013±0.007	0.014±0.0069	0.012±0.007	0.081±0.030 <sup>2</sup> 0.066±0.029 <sup>3</sup>	0.022±0.011	0.023±0.014
136.238	C <sub>10</sub> H <sub>16</sub>	monoterpenes*	PTR	0.68±0.28	0.65±0.31	0.057±0.055	0.41±0.19	0.49±0.20	0.33±0.17	0.41±0.06 <sup>1</sup> 0.87±0.72 <sup>2</sup> 0.21±0.15 <sup>3</sup>	0.80±0.32	0.65±0.38
138.122	C <sub>7</sub> H <sub>6</sub> O <sub>3</sub>	hydroxybenzoic acid*	PTR	0.0080±0.0030	0.0076±0.0033	- 0.000093±0.0050	0.0026±0.0017	0.0039±0.0023	0.0014±0.0008		0.0061±0.0036	0.0028±0.0015
138.166	C <sub>8</sub> H <sub>10</sub> O <sub>2</sub>	creosol/methylguaiacol*	PTR	0.016±0.0093	0.012±0.006	0.0000038±0.0069	0.0073±0.0046	0.0077±0.0049	0.0069±0.0042	0.14±0.11 <sup>3</sup>	0.012±0.008	0.013±0.008
138.21	C <sub>9</sub> H <sub>14</sub> O	isophorone*	PTR	0.027±0.0075	0.025±0.009	0.0079±0.01	0.0092±0.0064	0.0086±0.0053	0.0098±0.0074		0.014±0.009	0.019±0.014
146.189	C <sub>10</sub> H <sub>10</sub> O	dimethylbenzofuran/ethylbenzofuran*	PTR	0.0098±0.0044	0.0072±0.0033	- 0.00041±0.0037	0.0048±0.0029	0.0052±0.0034	0.0045±0.0024	0.043±0.018 <sup>2</sup> 0.051±0.028 <sup>3</sup>	0.0078±0.0051	0.0083±0.0044
146.233	C <sub>11</sub> H <sub>14</sub>	*	PTR	0.0064±0.0035		0.0012±0.0041	0.0034±0.0013		0.0034±0.0013			0.0061±0.0044
148.161	C <sub>9</sub> H <sub>8</sub> O <sub>2</sub>	cinnamic acid*	PTR	0.0040±0.0033		- 0.00094±0.0048	0.0021±0.0013		0.0021±0.0013			0.0037±0.0022
148.205	C <sub>10</sub> H <sub>12</sub> O	benzylacetone/estragole*	PTR	0.0047±0.0021	0.0043±0.0019	0.00045±0.0030	0.0023±0.0016	0.0022±0.0017	0.0024±0.0015	0.027±0.012 <sup>2</sup> 0.025±0.015 <sup>3</sup>	0.0033±0.0026	0.0044±0.0027
148.249	C <sub>11</sub> H <sub>16</sub>	C11 aromatic s/pentamethylbenzene*	PTR	0.0074±0.0032	0.0054±0.0027	0.00054±0.0047	0.0041±0.0028	0.0043±0.0032	0.0038±0.0023	0.014±0.008 <sup>2</sup> 0.014±0.007 <sup>3</sup>	0.0064±0.0048	0.0069±0.0041
150.177	C <sub>9</sub> H <sub>10</sub> O <sub>2</sub>	ethylbenzoate/vinylguaiacol*	PTR	0.0059±0.0029	0.0044±0.0020	0.00039±0.0034	0.0028±0.0020	0.0029±0.0023	0.0028±0.0017	0.14±0.08 <sup>2</sup> 0.036±0.025 <sup>3</sup>	0.0043±0.0034	0.0049±0.0030
150.221	C <sub>10</sub> H <sub>14</sub> O	carvone*	PTR	0.0040±0.0022	0.0039±0.0017	0.00055±0.0028	0.0021±0.0016	0.0027±0.0021	0.0015±0.0009		0.0039±0.0030	0.0027±0.0016
152.237	C <sub>10</sub> H <sub>16</sub> O	camphor/isomers*	PTR	0.022±0.0074	0.023±0.010	0.0063±0.0086	0.011±0.007	0.013±0.008	0.0087±0.0066	0.027±0.017 <sup>2</sup> 0.025±0.014 <sup>3</sup>	0.020±0.011	0.015±0.011
154.209	C <sub>9</sub> H <sub>14</sub> O <sub>2</sub>	norbornaneacetic acid*	PTR	0.0036±0.0015		- 0.00050±0.0041	0.0022±0.0012		0.0022±0.0012			0.0038±0.0020
154.212	C <sub>12</sub> H <sub>10</sub>	acenaphthene*	PTR	0.0054±0.0020	0.0040±0.0015	- 0.00026±0.0031	0.0029±0.0022	0.0033±0.0028	0.0025±0.0013		0.0046±0.0040	0.0042±0.0023

Molecular Weight	Compound	Compound Name	Instrument	SP Average	NP Average	Background	Average EF (g kg <sup>-1</sup> )	NP EF (g kg <sup>-1</sup> )	SP EF (g kg <sup>-1</sup> )	Literature EF (g kg <sup>-1</sup> )	NP ER	SP ER
154.253	C <sub>10</sub> H <sub>18</sub> O	terpine-4-ol/cineole/isomers*	PTR	0.0024 ±0.0009	0.0020±0.00068	- 0.00044±0.0022	0.0018±0.0014	0.0019±0.0018	0.0017±0.0009	0.0056±0.0021 <sup>2</sup> 0.0027±0.0017 <sup>3</sup>	0.0029 ±0.0028	0.0028±0.0015
204.357	C <sub>15</sub> H <sub>24</sub>	sesquiterpenes*	PTR	0.0027 ±0.0011		0.00030±0.0021	0.0017±0.0011		0.0017±0.0011	0.15±0.07 <sup>2</sup> 0.029±0.028 <sup>3</sup>		0.0022±0.0014
239±61	C <sub>11</sub> to C <sub>25</sub>	I/SVOCs - CH	cartridge			5.2	1.4±0.037 to 2.4±0.063					
255±61	C <sub>11</sub> to C <sub>25</sub>	I/SVOCs - CHO <sub>1</sub>	cartridge			4.6	0.81±0.078 to 0.81±0.079					
271±61	C <sub>11</sub> to C <sub>25</sub>	I/SVOCs - CHS <sub>1</sub>	cartridge			0.2	0.21±0.033 to 0.22±0.060					

1634